Slovak Biophysical Society

Biomedical Research Center
Slovak Academy of Sciences

Book of Contributions

10th Slovak Biophysical Symposium

May 3 – 5, 2022
Smolenice, Slovakia

ISBN: 978-80-973719-4-4

Book of Contributions, 10th Slovak Biophysical Symposium, May 3 – 5, 2022, Smolenice, Slovakia

Editors: M. Cagalinec, A. Zahradniková, B. Iaparov
Reviewers: A. Zahradniková, M. Gaburjáková, D. Jancura, Z. Gažová, J. Jakuš
Number of pages: 126

ORGANIZATION

SCIENTIFIC COMMITTEE

Michal Cagalinec (BMC SAV Bratislava)
Marta Gaburjáková (UMFG SAV Bratislava)
Zuzana Gažová (UEF SAV Košice)
Ján Jakuš (JLF UK Bratislava)
Daniel Jancura (PF UPJŠ Košice)
Alžbeta Marček Chorvátová (UCM FPV Trnava)
Alexandra Zahradníková (BMC SAV Bratislava)

ORGANIZING COMMITTEE

from the Department of Cellular Biophysics, Institute of Experimental Endocrinology, Biomedical Research Center or Slovak Academy of Sciences, Bratislava

Michal Cagalinec
Alexandra Zahradníková ml.
Alexandra Zahradníková.
Jana Pavelková
Bogdan Iaparov
Iuliia Baglaeva

ACKNOWLEDGEMENTS

The Organizing Committee of the 10th Slovak Biophysical Symposium would like to express appreciation and thanks to the following companies for their generous support.

NanoTemper Technologies GmbH
Flößergasse 4
81369 München Germany
https://nanotempertech.com/

Pragolab s.r.o.
Drieňová 1712/34
821 02 Bratislava
https://www.pragolab.sk/

Caffe del Doge
Bajkalská 19/B
821 01 Bratislava
https://caffedeldoge.sk/

SPECION, s.r.o.
Budějovická 1998
140 00 Praha 4 Czech Republic
http://www.specion.biz/

SAFTRA Photonics, s.r.o.
Moldavská cesta 51
040 11 Košice, Slovakia
https://www.saftra-photonics.org/

KVANT spol. s.r.o.
FMFI UK, Mlynská dolina
842 48 Bratislava
https://www.kvant.sk/

Lambda Life a.s.
Levočská 3
851 01 Bratislava
https://www.lambda.sk/

Carl Zeiss Slovakia, s.r.o.
Račianska 12481/77/A
831 02 Bratislava
https://www.zeiss.com/

CONTENTS

Milí kolegovia a kolegyne,

Srdečne Vás vítame na jubilejnom 10. ročníku Sympózia Slovenskej biofyzikálnej spoločnosti. Výbor SKBS poveril organizáciou tohto jubilejného ročníka Michala Cagalinca a jeho tím z Biomedicínskeho centra SAV, v.v.i. Organizátori pre nás vybrali Kongresové centrum SAV - Smolenický zámok. Veríme, že toto miesto svojím vedeckým a historickým espritom podčiarkne kvalitu práce našej vedeckej spoločnosti a poskytne nám uvoľnenie potrebné pre tvorivú diskusiu.

Biofyzika sa za posledné desaťročia stala modernou vedou a program jubilejného sympózia reprezentuje svojim rozsahom a kvalitou súčasný dynamický stav biofyzikálneho výskumu v našej krajine. Veríme, že tento zborník abstraktov zachová svedectvo našej práce pre budúce generácie. Prezentuje abstrakty 27 vedeckých prednášok a 26 posterov. Témy vedeckých prezentácii pokrývajú široké oblasti nášho výskumu od neurofyziológie, cez vápnikovú signalizáciu až po interakcie proteínov s malými molekulami, lipidmi, nanoštruktúrami a inými proteínmi a to tak experimentálne, teoretické, ako aj metodické štúdie. Jazyk zborníka abstraktov je angličtina, aby nám rozumeli aj kolegovia zo zahraničia. Rokovacím jazykom je však slovenčina, aby sme rozvíjali našu odbornú slovesnosť aj pre pedagógov a študentov.

V mene výboru a organizátorov Vám všetkým želáme podnetné diskusie a veľa elánu do ďalšej práce.

Alžbeta Marček Chorvátová
Predsedníčka SkBS

Michal Cagalinec
Výkonný predseda SkBS

Dear colleagues,

We warmly welcome you to the jubilee 10th annual Symposium of the Slovak Biophysical Society. The Committee of the Slovak Biophysical Society appointed Michal Cagalinec and his team from the Biomedical Research Center of the Slovak Academy of Sciences to organize this jubilee installment. The organizers chose the SAS Congress Center - Smolenice Castle. We believe that this place, with its scientific and historical esprit, will emphasize the quality of the work of our scientific society and provide the relaxation we need for creative discussion.

Biophysics has become a modern science in recent decades and the Jubilee Symposium program represents, with its scope and quality, the current dynamic state of biophysical research in our country. We believe that this collection of abstracts will preserve the testimony of our work for future generations. It presents abstracts of 27 scientific lectures and 26 posters. The topics of scientific presentations cover a wide range of our research, from neurophysiology, through calcium signalling, to the interactions of proteins with small molecules, lipids, nanostructures and other proteins, including experimental, theoretical and methodological studies. The language of the collection of abstracts is English, so that colleagues from abroad can also understand us. However, the working language is Slovak, so that we can develop our professional literature for teachers and students as well.

On behalf of the committee and the organizers, we wish you stimulating discussions and a lot of enthusiasm for further work.

Alžbeta Marček Chorvátová
President of the SkBS

Michal Cagalinec
President Elect of the SkBS

SCIENTIFIC PROGRAM

PROGRAM

Tuesday, May 3, 2022

12:10 - 13:30 Lunch / Registration

13:30 - 13:40 Opening of the conference

13:40 - 14:30 **Plenary Lecture- Neuroscience**

Chair Ľ. Lacinová

PL1 A. Dhoundiyal, V. Goeschl, S. Boehm, H. Kubista and **M. Hotka**
Coupling between neuronal electrical activity and metabolism.

14:30 - 15:10 **Neuroscience**

Chair M. Hotka

14:30 - 14:50

SC1 L. Hoppanová, B. Jurkovičová-Tarabová, A. Idunková, M. Tomko, M. Dubovický, **Ľ. Lacinová**
Alteration of hippocampal excitability by prenatally applied antidepressant

14:50 - 15:10

SC2 **M. Šimera**, M. Veterník, L. Martvoň, K. F. Morris, T. Pitts, D.C. Bolser, I. Poliacek
Cough modulation by changes in afferent inputs at low temperature

15:10 - 15:30 **Company presentation - NanoTemper**

Chair M. Cagalinec

CP1 **P. Kania**
Newest solutions for biophysical characterization of challenging interactions, and protein samples

15:30 - 16:00 Coffee break

16:00 - 17:00 **Singlet oxygen & Photodynamic Therapy**

Chair A. Marček Chorvátová

16:00 - 16:20

SC3 S. Tomkova, S. Kolesarova and **K. Stroffekova**
Effects of photobiomodulation on rotenone challenged human glioma cells

16:20 - 16:40

SC4 **A. Hovan**, D. Sedláková, M. Berta, G. Bánó and E. Sedlák
Singlet oxygen deactivation as a probe of heme availability in heme proteins

16:40 - 17:00

SC5 **E.Sedlák**
Flavoproteins as singlet oxygen producers

17:00 - 17:20 **Methods - Biophysics of Sequenation**

Chair E. Sedlák

M1 **M. Karhanek**, A. Zahradníková
Electrical detection of DNA synthesis

17:20 - 17:45 **Company presentation - SAFTRA photonics**

Chair M. Cagalinec

CP2 **P. Miškovský**, G. Bánó
Be always in control of water quality - PickMol™ technology, SAFTRA Photonics Ltd

17:45 - 18:00 Welcome drink

18:00 - 19:00 Dinner

19:00 - 21:30 **Poster Session I** (all posters)

Wednesday, May 4, 2022

	7:30 - 8:30	Breakfast
	8:30 -9:30	**Directed evolution**
Chair	D. Jancura	
	8:30 - 8:50	
SC6	**G. Žoldák**	
	Mechanics and evolution of Hsp70	
	8:50 - 9:10	
SC7	**M. Tomková**, V. Dzurillová, E. Sedlák	
	Directed evolution of a staphylokinase, a thrombolytic agent, by ribosome display technology	
	9:10 - 9:30	
SC8	**V. Dzurillová**, E. Sedlák	
	Utilisation of HaloTag technology in directed evolution of haloalkane dehalogenase DhaA	
	9:30 - 9:50	**Methods - Bioimaging**
Chair	G. Bánó	
M2	P. Vagovič, **J. Uličný**	
	Bioimaging opportunities using X-FEL MHz tomoscopy	
	9:50 - 10:20	Coffee break
	10:20 - 11:10	**Plenary Lecture - Calcium Transport**
Chair	M. Gaburjáková	
PL2	**A. Zahradníková,** B. Iaparov and I. Zahradník	
	Structure-function relationships of the ryanodine receptor	
	11:10 - 12:10	**Calcium transport**
Chair	A. Zahradníková Jr.	
	11:10 - 11:30	
SC9	**B. Iaparov**, I. Baglaeva, I. Zahradník and A. Zahradníková	
	Mg^{2+} binding to RyRs moderates spontaneous calcium sparks	
	11:30 - 11:50	
SC10	J. Gaburjáková and **M. Gaburjáková**	
	The cardiac ryanodine receptor provides a suitable pathway for the rapid transport of zinc (Zn^{2+})	
	11:50 - 12:10	
SC11	**M. Májeková**, V. Heger, L. Kissová and Y. Rodríguez	
	Interaction of ligands and calcium pump	
	12:10 - 13:15	Lunch
	13:15- 14:30	**SkBS Awards Ceremony**
Chair	A. Marček Chorvátová	
	13:15 - 13:30	
	A. Marček Chorvátová – introduction of candidates	
	13:30 - 14:10	
AW1	**I. Zahradník**	
	Pohyb obzoru na ceste za pochopením štruktúry a funkcie srdcovej svalovej bunky	
	14:10 - 14:30	
AW2	**V. Subjakova**, M. Tatarko , S. Mikulicova , S. Melikishvili and T. Hianik	
	Application of nanoparticles modified by DNA aptamers in biosensing and targeted drug delivery	

14:30 - 15:10 **Aptamers & Nanostructures**

Chair Z. Gažová

14:30 - 14:50

SC12 **M. Tatarko**, V. Šubjaková, M. Csiba, V. Oravczová, S. Spagnolo, J. Süle and T. Hianik
Application of QCM-D for analysis of molecular interactions at surfaces

14:50 - 15:10

SC13 **A. Marček Chorvátová**, M. Uherek , A. Mateašík and D. Chorvát
Evaluation of the interaction of nano/microplastics with living organisms by microscopy methods

15:10 - 15:30

SC14 **V. Talafová**, M. Humenik, G. Žoldák, T. Scheibel and E. Sedlák
On the pH effect on self-assembly of the recombinant spider silk protein eADF4(C16) into nanofibrils

15:30 - 16:45 Coffee break served at Poster Session
Poster Session II (all posters)

16:45 - 17:45 **General Assembly of the SkBS**

Chair A. Marček Chorvátová

- *Opening of the GA*
- *Report on the activities of the SKBS Committee (A. Marček Chorvátová)*
- *Management report (G. Bánó)*
- *Report of the Audit Committee (D. Fedunová)*
- *Changing the statute of the SKBS Prize for a Young Scientist (A. Marček Chorvátová)*
- *Information on the preparation of elections to the SKBS bodies (A. Marček Chorvátová)*
- *Discussion*
- *Miscellaneous*
- *Concluding remarks*

16:45 - 18:00 Departure for dinner

18:00 - 22:00 **Conference dinner**

Thursday, May 5, 2022

7:30 - 8:50 Breakfast

8:50 - 9:30 **Protein-lipid interactions** (Uličný) - Kučerka, Klacsová"

Chair J. Uličný

8:50 - 9:10

SC15 O. Ivankov, T. Murugova, T. Kondela, S. Kurakin, E. Ermakova, E. Dushanov, D. Badreeva, D. Soloviov, Kh. Kholmurodov, A. Kuklin and **N. Kučerka**
Interactions within the lipid membranes mimicking preclinical conformational diseases

9:10 - 9:30

SC16 **M. Klacsová**, B. Košáňová, J.C. Martínez and D. Uhríková
SARS-CoV-2 antivirals inhibition effect on membrane fusion models

Company presentation - Specion

Chair M. Cagalinec

9:30 - 9:50

CP3 **J. Golda** and J. Tkáč
Introducing the Next Generation in Protein Structure Determination - Microfluidic Modulation Spectroscopy

	9:50 - 10:20 Coffee break
	10:20 - 11:10 **Protein aggregation** (Štroffeková) - Cehlár, Škrabana, Dzupponová, Gancár"
Chair	K. Štroffeková 9:50 - 10:10
SC17	**O. Cehlár**, L. Horňáková, J. Šinský, S. Slušná, J. Galba, J. Piešťanský, A. Kováč, J. Hanes and R. Škrabana *Interaction kinetics reveal distinct properties of conformational ensembles of three-repeat and four-repeat tau proteins* 10:10 - 10:30
SC18	**R. Skrabana**, K. Rafajova, I. Jahodova, N. Zemanova, O. Cehlar, O. Bagarova *Structural clues to different aggregation propensities of tau protein isoforms* 10:30 - 10:50
SC19	**V. Džupponová** and G. Žoldák *Aggregation mechanism and morphologies of myelomatic human light chain* 10:50 - 11:10
SC20	*M. Gancar*, E. Kurin, Z. Bednarikova, J. Marek, P. Mucaji, M. Nagy and Z. Gazova *Influence of herbal extracts' constituents on the amyloid aggregation of proteins*
	11:40 - 11:50 **Concluding remarks**
	11:50 - 13:30 Lunch

LIST OF PLENARY LECTURES

PL1 **Coupling between neuronal electrical activity and metabolism**

A. Dhoundiyal, V. Goeschl, S. Boehm, H. Kubista and M. Hotka

Center of Physiology and Pharmacology, Department of Neurophysiology and Neuropharmacology, Medical University of Vienna, Waehringerstrasse 13a, 1090, Vienna, Austria.

PL2 **Structure-function relationships of the ryanodine receptor**

A. Zahradníková[1], B. Iaparov[1] and I. Zahradník[1]

[1] *Department of Cellular Biophysics, Institute of Experimental Endocrinology, Biomedical Research Center, Slovak Academy of Sciences, Dúbravská cesta 9, 845 05 Bratislava, Slovakia.*

LIST OF METHODS LECTURES

M1 **Electrical detection of DNA synthesis**

Miloslav Karhanek[1], Alexandra Zahradníková[2]

[1] *Specialized Bioinformatics Laboratory, Biomedical Research Center SAS, Dubravska 9, 84505 Bratislava*

[2] Institute of Experimental Endocrinology, Biomedical Research Center SAS, Dubravska 9, 84505 Bratislava.

M2 **Bioimaging opportunities using X-FEL MHz tomoscopy**

P. Vagovič[1], J. Uličný[2]

[1] *Center for Free-Electron Laser, Notkestraße 85, 22607 Hamburg, Germany*

[2] *Faculty of Science, Department of Biophysics, Institute of Physics, P. J. Šafárik University, Jesenná 5, 04154 Košice, Slovakia*

LIST OF COMPANY PRESENTATIONS

CP1 **Newest solutions for biophysical characterization of challenging interactions, and protein samples**

P. Kania

NanoTemper Technologies GmbH, Flößergasse 4, 81369 München, Germany

CP2 **Be always in control of water quality PickMol™ technology SAFTRA Photonics Ltd**

P. Miškovský[1,2] and G. Bánó[3]

[1] *SAFTRA photonics Ltd., Moldavská 51, 04011 Košice.*

[2] *Cassovia New Industry Cluster, Tr. SNP 1, 04001 Košice.*

[3] *KBF PF UPJŠ, Jesenná 5, 04154 Košice.*

CP3 **Introducing the Next Generation in Protein Structure Determination - Microfluidic Modulation Spectroscopy**

J. Golda[1] and J. Tkáč[1]

[1] *Specion Ltd., Budějovická 55, 140 00 Praha 4, Czech Republic.*

LIST OF SHORT COMMUNICATIONS

SC1 **Alteration of hippocampal excitability by prenatally applied antidepressant.**

L. Hoppanová[1], B. Jurkovičová-Tarabová[1], A. Idunková[1], M. Tomko[1], M. Dubovický[2], Ľ. Lacinová[1]

[1]*Institute of Molecular Physiology and Genetics, Center of Bioscience*

[2]*Institute of Experimental Pharmacology and Toxicology, Center of Experimental Medicine, Dúbravská cesta 9, Bratislava, Slovakia*

SC2 **Cough modulation by changes in afferent inputs at low temperature**

M. Šimera[1], M. Veterník[1], L. Martvoň[1], K. F. Morris[2], T. Pitts[3], D.C. Bolser[4], I. Poliacek[1]

[1] *Department of Medical Biophysics, Jessenius Faculty of Medicine in Martin, Comenius University in Bratislava, Slovakia*

[2] *Department of Molecular Pharmacology and Physiology, College of Medicine, University of South Florida, Tampa, FL, USA.*

[3] *Department of Neurological Surgery, Kentucky Spinal Cord Injury Research Center, University of Louisville, Louisville, KY, USA.*

[4]*Dept. of Physiological Sciences, College of Veterinary Medicine, University of Florida, Gainesville, FL, USA*

SC3 **Effects of photobiomodulation on rotenone challenged human glioma cells.**

S. Tomkova[1], S. Kolesarova[1,2] and K. Stroffekova[1]

[1]*Department of Biophysics, Faculty of Sciences, PJ Safarik University, Jesenna 5, Kosice, Slovakia.*

[2]*Department of Biochemistry, Faculty of Sciences, PJ Safarik University, Moyzesova 15, Kosice, Slovakia*

SC4 **Singlet oxygen deactivation as a probe of heme availability in heme proteins**

A. Hovan[1], D. Sedláková[2], M. Berta[1], G. Bánó[1] and E. Sedlák[3]

[1]*Department of Biophysics, Faculty of Science, P.J. Šafárik University in Košice, Jesenná 5, 041 54 Košice, Slovakia.*

[2]*Department of Biophysics, Institute of Experimental Physics, Slovak Academy of Sciences, Watsonova 47, 040 01 Košice, Slovakia.*

[3]*Center for Interdisciplinary Biosciences, Technology and Innovation Park, P.J. Šafárik University in Košice, Jesenná 5, 041 54 Košice, Slovakia.*

SC5 **Flavoproteins as singlet oxygen producers**

E.Sedlák[1]

[1]*Center for Interdisciplinary Biosciences, Technology and Innovation Park, Jesenná 5, Slovakia and Department of Biochemistry, Faculty of Science at P.J. Šafárik University, 041 54 Košice*

SC6 **Mechanics and evolution of Hsp70**

G. Žoldák[2]

[1] *Department of Biophysics, Faculty of Science, Pavol Jozef Šafárik University, Jesenná 5, 040 01 Košice, Slovakia.*

SC7 **Directed evolution of a staphylokinase, a thrombolytic agent, by ribosome display technology**

M. Tomková[1], V. Dzurillová[2], E. Sedlák[1]

[1]*Center for Interdisciplinary Biosciences, Technology and Innovation Park, P. J. Šafárik University, Jesenná 5, 041 51 Košice, Slovakia*

[2]*Department of Biophysics, Faculty of Science, P. J. Šafárik University, Jesenná 5, 041 51 Košice, Slovakia*

SC8 **Utilisation of HaloTag technology in directed evolution of haloalkane dehalogenase DhaA**

V. Dzurillová[1], E. Sedlák[2]

[1] *Department of Biophysics, Faculty of Science, P.J. Šafárik University, Jesenná 5, 041 54 Košice, Slovakia*

[2] *Center for Interdisciplinary Biosciences, Technology and Innovation Park, P.J. Šafárik University, Jesenná 5, 041 54 Košice, Slovakia.*

SC9 **Mg^{2+} binding to RyRs moderates spontaneous calcium sparks**

B. Iaparov[1], I. Baglaeva[1], I. Zahradník[1] and A. Zahradníková[1]

[1]*Department of Cellular Cardiology, Institute of Experimental Endocrinology, Biomedical Research Center, Slovak Academy of Sciences, Dúbravská cesta 9, 845 05 Bratislava, Slovak Republic.*

SC10 **The cardiac ryanodine receptor provides a suitable pathway for the rapid transport of zinc (Zn^{2+})**

J. Gaburjakova[1] and M. Gaburjakova[1]

[1]*Institute of Molecular Physiology and Genetics, Centre of Biosciences, Slovak Academy of Sciences, Dubravska cesta 9, 840 05 Bratislava, Slovak Republic.*

SC11 **Interaction of ligands and calcium pump**

M. Májeková[1], V. Heger[1], L. Kissová[1] and Y. Rodríguez[2,3]

[1]*Centre of Experimental Medicine SAS, Institute of Experimental Pharmacology and Toxicology,Dubravska 9, 841 04, Bratislava, Slovakia.*

[2]*Department of Natural Sciences, CUNY's Hostos Community College, 475 Grand Concourse, Bronx, 10451, New York, United States of America.*

[3]*Department of Pharmacological Sciences, Icahn School of Medicine at Mount Sinai, 1425 Madison Avenue, New York, NY 10029, USA.*

SC12 **Application of QCM-D for analysis of molecular interactions at surfaces**

M. Tatarko[1], V. Šubjaková[1], M. Csiba[1], V. Oravczová[1], S. Spagnolo[1], J. Süle[2] and T. Hianik[1]

[1]Department of Nuclear Physics and Biophysics, Faculty of Mathematics, Physics and Informatics, Comenius University, Mlynská dolina F1, 842 48 Bratislava, Slovakia

[2]Hungarian Dairy Research Institute Ltd., -HDRI Ltd., Lucsony u. 24, 9200 Mosonmagyaróvár, Hungary.

SC13 **Evaluation of the interaction of nano/microplastics with living organisms by microscopy methods**

A. Marček Chorvátová[1,2], M. Uherek[1], A. Mateašík[1] and D. Chorvát[1]

[1]Department of Biophotonics, International Laser Center, Slovak Centre of Scientific and Technical Information, Ilkovičova 3, 814 04 Bratislava, Slovakia.

[2]Department of Biophysics, FNS, Univ. Ss Cyril and Methodius, J Herdu 1, 917 02 Trnava, Slovakia.

SC14 **On the pH effect on self-assembly of the recombinant spider silk protein eADF4(C16) into nanofibrils**

V. Talafová[1], M. Humenik[2], G. Žoldák[3], T. Scheibel[2] and E. Sedlák[3]

[1]Department of Biophysics, Faculty of Science, P. J. Šafárik University, Jesenná 5, 040 01 Košice, Slovakia

[2]Department of Biomaterials, Faculty of Engineering Science, University of Bayreuth, Universitätsstraße 30, 95440 Bayreuth, Germany

[3]Center for Interdisciplinary Biosciences, P. J. Šafárik University, Jesenná 5, 040 01 Košice, Slovakia

SC15 **Interactions within the lipid membranes mimicking preclinical conformational diseases**

O. Ivankov,[1] T. Murugova,[1] T. Kondela,[1,2] S. Kurakin,[1,3] E. Ermakova,[1] E. Dushanov,[1,4] D. Badreeva,[1] D. Soloviov,[5] Kh. Kholmurodov,[1,4] A. Kuklin[1,6] and N. Kučerka[1,7]

[1]Joint Institute for Nuclear Research, Dubna, Russia
[2]Faculty of Mathematics, Physics and Informatics, Comenius University Bratislava, Slovakia
[3]Kazan Federal University, Kazan, Russia
[4]Dubna State University, Dubna, Russia
[5]Institute for Safety Problems of Nuclear Power Plants NAS of Ukraine, Kyiv, Ukraine
[6]Moscow Institute of Physics and Technology, Dolgoprudny, Russia
[7]Faculty of Pharmacy, Comenius University Bratislava, Slovakia

SC16 **SARS-CoV-2 antivirals inhibition effect on membrane fusion models**

M. Klacsová[1], B. Košáňová[1], J.C. Martínez[2] and D. Uhríková[1]

[1] Department of Physical Chemistry of Drugs, Faculty of Pharmacy, Comenius University in Bratislava, Odbojárov 10, 832 32 Bratislava, Slovakia.

[2] ALBA Synchrotron, Cerdanyola del Vallés, 082 90 Bracelona, Spain.

SC17 **Interaction kinetics reveal distinct properties of conformational ensembles of three-repeat and four-repeat tau proteins**

O. Cehlár[1], L. Horňáková[1,2,3], J. Šinský[1], S. Slušná[1,2], J. Galba[4,5], J. Piešťanský[6,7], A. Kováč[1], J. Hanes[1] and R. Škrabana[1]

[1] *Institute of Neuroimmunology of the Slovak Academy of Sciences, Dubravska cesta 9, 84510 Bratislava, Slovakia*

[2] *Department of Biochemistry, Faculty of Natural Sciences, Comenius University, Ilkovicova 6, 84215 Bratislava, Slovakia*

[3] *Present address: Institute of Medical Chemistry, Biochemistry and Clinical Biochemistry, Medical Faculty, Comenius University, Sasinkova 2, 81108 Bratislava, Slovak Republic*

[4] *Biomedical Research Center of the Slovak Academy of Sciences, Dubravska cesta 9, Bratislava, 84510, Slovakia*

[5] *Department of Pharmaceutical analysis and nuclear pharmacy, Faculty of Pharmacy*

[6] *Department of Pharmaceutical Chemistry, Faculty of Pharmacy*

[7] *Toxicological and Antidoping Center, Faculty of Pharmacy, Comenius University in Bratislava, Ulica odbojárov 10, 832 32 Bratislava, Slovakia*

SC18 **Structural clues to different aggregation propensities of tau protein isoforms**

R. Skrabana[1], K. Rafajova[1], I. Jahodova[1], N. Zemanova[1], O. Cehlar[1], O. Bagarova[1]

[1] *Institute of Neuroimmunology, Slovak Academy of Sciences*
Laboratory of Structural Biology of Neurodegeneration
Dubravska cesta 9, 84510 Bratislava, Slovakia

SC19 **Aggregation mechanism and morphologies of myelomatic human light chain**

V. Džupponová[1] and G. Žoldák[2]

[1] *Department of Biophysics, Faculty of Science, Pavol Jozef Šafárik University, Jesenná 5, 040 01 Košice, Slovakia..*

[2] *Center for Interdisciplinary Biosciences, Technology and Innovation Park, Pavol Jozef Šafárik University, Jesenná 5, 041 54 Košice, Slovakia.*

SC20 **Influence of herbal extracts' constituents on the amyloid aggregation of proteins**

M. Gancar[1], E. Kurin[2,*], Z. Bednarikova[1], J. Marek[1], P. Mucaji[2], M. Nagy[2] and Z. Gazova[1]

[1] *Department of Biophysics, Institute of Experimental Physics Slovak Academy of Sciences, Watsonova 47, 040 01, Kosice, Slovakia*

[2] *Department of Pharmacognosy and Botany, Faculty of Pharmacy, Comenius University in Bratislava, Odbojarov 10, 832 32, Bratislava, Slovakia*

LIST OF POSTERS

PO1 **Singlet Oxygen Detection in Live Cells**

A. Hovan[1], V. Pevná[1], V. Huntošová[2], P. Miškovský[2] and G. Bánó[1]

[1] Department of Biophysics, Faculty of Science, P. J. Šafárik University, Jesenná 5, 041 54 Košice, Slovak Republic.

[2] Center for Interdisciplinary Biosciences, TIP, P. J. Šafárik University, Jesenná 5, 041 54 Košice, Slovak Republic

PO2 **Design and isolation of new mutant LOV2 proteins**

K. Felčíková[1], V. Dzurillová[1], A. Hovan[1], G. Banó[1], T.Kožár[2], E. Sedlák[2]

[1] Department of Biophysics, Faculty of Science, P.J. Šafárik University, Jesenná 5, 040 54 Košice, Slovakia.

[2] Center for Interdisciplinary Biosciences, Technology and Innovation Park, P.J. Šafárik University, Jesenná 5, 041 54 Košice, Slovakia

PO3 **Structural in-depth analysis of iron complexes of tannic acid and other related polyphenols as revealed by spectroscopic techniques**

A. Espina[1], M. V. Cañamares[2], S. Sanchez-Cortes[2,3], Z. Jurašeková[1]

[1]Department of Biophysics, Faculty of Science, P. J. Šafárik University, Jesenná 5, 040 01 Košice, Slovakia

[2] Institute of the Structure of Matter, IEM-CSIC, Serrano 121, 28006 Madrid, Spain

[3] Center for Interdisciplinary Biosciences, Technology and Innovation Park, P. J. Šafárik University, Jesenná 5, 040 01 Košice, Slovakia

PO4 **Autophagic response of U87MG cells in 3D spheroids stimulated with photodynamic therapy**

V. Pevna[1], P. Miskovsky[2] and V. Huntosova[2]

[1] Department of Biophysics, Institute of Physics, Faculty of Science, P.J. Safarik University in Kosice, Jesenna 5, 041 54 Kosice, Slovakia.

[2] Center for Interdisciplinary Biosciences, Technology and innovation park, P.J. Safarik University in Kosice, Jesenna 5, 041 54 Kosice, Slovakia.

PO5 **Redox state of F-type ferryl intermediate of bovine cytochrome c oxidase**

T. Sztachová[1], A. Tomková[1] , D. Jancura[1] and M. Fabián[2]

[1] Department of Biophysics, Faculty of Science, P.J.Šafárik University, Jesenná 5, 041 54 Kosice, Slovakia.

[2] Center for Interdisciplinary Biosciences, Technology and Innovation Park P. J. Šafárik University,

Jesenná 5, 041 54 Košice, Slovakia

PO6 **Calorimetric characterization of ferryl intermediates of bovine cytochrome c oxidase**

A. Tomková[1] , T. Sztachová[1], M. Fabián[2] and D. Jancura[1]

[1] Department of Biophysics, Faculty of Science, P.J. Šafárik University, Jesenná 5, 041 54 Kosice, Slovakia.

[2] Center for Interdisciplinary Biosciences, Technology and Innovation Park, P. J. Šafárik University, Jesenná 5, 041 54 Košice, Slovakia

PO7 **Development of a new highly selective and sensitive detection method of the glyphosate pesticide by Surface-Enhanced Raman Scattering**

F. Fuenzalida Sandoval[1], S. Sanchez-Cortes [2,3], P. Miškovský [4,5], Z. Jurašeková[1]

[1]Department of Biophysics, Faculty of Science, P. J. Šafárik University, Jesenná 5, 040 01 Košice, Slovakia

[2] Institute of the Structure of Matter, IEM-CSIC, Serrano 121, 28006 Madrid, Spain

[3] Center for Interdisciplinary Biosciences, Technology and Innovation Park, P. J. Šafárik University, Jesenná 5, 040 01 Košice, Slovakia

[4] Technology and Innovation Park, P. J. Šafárik University, Trieda SNP 1, 040 11 Košice, Slovakia

[5] SAFTRA photonics, s.r.o., Moldavská cesta 51, 040 11 Košice, Slovakia

PO8 **Thermal Stability of Human Serum Albumin in the Presence of Hydroxyquinone Molecules: a Differential Scanning Calorimetry Study**

G. Fabriciová[1], V. Vaník[2] and D. Jancura[1]

[1] Department of Biophysics, Institute of Physics, P. J. Šafárik University in Košice, Jesenná 5, 041 54, Košice, Slovakia.

[2] Department of Biophysics, Institute of Experimental Physics, Slovak Academy of Sciences, Bulharská 1, 040 01 Košice, Slovakia.

PO9 **Effect of Random Copolymer Nanosystems on Model Membranes and Whole Human Blood Rheological Properties**

N. Naziris[1], S. Šutý[2], D. Selianitis[3], J. Jacko[2], Z. Garaiová[2], S. Pispas[3], M. Ionov[1], M. Bryszewska[1] and I. Waczulikova[2]

[1] Department of General Biophysics, Faculty of Biology and Environmental protection, University of Lodz, 141/143 Pomorska, 90-236 Lodz, Poland.

[2] Department of Nuclear Physics and Biophysics, Faculty of Mathematics, Physics and Informatics, Comenius University, Mlynska Dolina F1, 84248 Bratislava, Slovakia.

[3] Theoretical and Physical Chemistry Institute, National Hellenic Research Foundation, 48 Vassileos Constantinou Avenue, 11635 Athens, Greece.

PO10 **Deep learning in confocal microscopy of cardiomyocytes**

A. Zahradnikova jr.[1] and P. Skrabanek[2]

[1] Institute of Experimental Endocrinology, Biomedical Research Center of the Slovak Academy of Sciences, Bratislava, Slovakia.

[2] Institute of Automation and Computer Science, Brno University of Technology, Brno, Czech Republic.

PO11 **Robust estimation of parameters of calcium signals recorded from cardiac myocytes.**

I. Baglaeva[1], B. Iaparov[1], A. Zahradníková jr.[1] , I. Zahradník[1] and A. Zahradníková[1]

[1] Department of Cellular Cardiology, Institute of Experimental Endocrinology, Biomedical Research Center, Slovak Academy of Sciences, Bratislava, Slovakia.

PO12 **Calcium transient alterations in cardiac myocytes of voluntarily running rats detected by calcium indicator Fluo-3**

M. Cagalinec[1,2], I. Baglaeva[1], A. Zahradníková ml[1], B. Iaparov[1], I. Zahradník[1] and A. Zahradníková[1]

[1] *Dept. of Cellular Cardiology, Institute of Experimental Endocrinology, Biomedical Research Center, Slovak Academy of Sciences, Dúbravská cesta 9, 845 05 Bratislava.*

[2] *Centre of Excelence for Advanced Material Application, Slovak Academy of Sciences, Dúbravská cesta 9, 845 11 Bratislava.*

PO13 **Inertial self-propelled particles in narrow channels**

D. Horváth[1], C. Slabý[2], A. Hovan[2], Z. Tomori[3], P. Miškovský[1] and G. Bánó[2]

[1]*Center for Interdisciplinary Biosciences, TIP, P. J. Šafárik University, Jesenná 5, 041 54 Košice, Slovak Republic*

[2]*Department of Biophysics, Faculty of Science, P. J. Šafárik University, Jesenná 5, 041 54 Košice, Slovak Republic.*

[3]*Institute of Experimental Physics SAS, Department of Biophysics, Watsonova 47, 040 01 Košice, Slovak Republic*

PO14 **Characterization of Exosomes and their Interactions with Amphiphilic Dendrons Using Electron Microscopy**

K. Čechová[1] , M. Velísková[1], D. Kosnáč[2], M. Bábelová[2], M. Kopáni[2], Š. Polák[2], M. Zvarík[1], L. Šikurová[1] and I. Waczulíková[1]

[1] *Department of Nuclear Physics and Biophysics, Faculty of Mathematics, Physics and informatics, Comenius University in Bratislava, Mlynská Dolina, 842 48 Bratislava, Slovakia.*

[2] *Institute of Histology and Embryology, Faculty of Medicine of the Comenius University, Sasinkova 4, 811 04 Bratislava, Slovakia*

PO15 **Modification of casein micelles by aptamers for targeted drug delivery purposes**

Z. Garaiová[1], I. Kráľová[1], M. Garaiová[2], R. Holič[2], and T. Hianik[1]

[1] *Faculty of Mathematics, physics and informatics, Department of nuclear physics and Biophysics, Comenius University, Mlynska dolina F1, Bratislava, 842 48 Slovakia*

[2] *Institute of Animal Biochemistry and Genetics, Centre of Biosciences, Slovak Academy of Sciences, Dubravska cesta 9, Bratislava 840 05, Slovakia*

PO16 **Interactions of amphiphilic phosphorous dendrons with model membranes and whole human blood**

Š. Šutý[1], P.Mydla[1],K. Ládiová[1] , P.Vitovič[2], M. Kopáni[3], D. Shcharbin[4] and I.Waczulíková[1]

[1] Department of Nuclear Physics and Biophysics, Faculty of Mathematics, Physics and Informatics, Comenius University in Bratislava

[2] Department of simulation and virtual medical education, Faculty of Medicine, Comenius University in Bratislava

[3]Institute of Medical Physics, Biophysics, Informatics and Telemedicine

Faculty of Medicine, Comenius University in Bratislava

[4]Institute of Biophysics and Cell Engineering, National Academy of Sciences of Belarus

PO17 **The viscoelastic parameters of photopolymer nanowires**

C. Slabý[1], J. Kubacková[2], D. Horvath[3], A. Hovan[1], G. Žoldák[3], Tomori[2] and G. Bánó[1]

[1]Department of Biophysics, Faculty of Science, P. J. Šafárik University, Jesenná 5, 041 54 Košice, Slovak Republic

[2]Institute of Experimental Physics SAS, Department of Biophysics, Watsonova 47, 040 01 Košice, Slovak Republic

[3]Center for Interdisciplinary Biosciences, TIP, P. J. Šafárik University, Jesenná 5, 041 54 Košice, Slovak Republic

PO18 **Interaction of amphiphilic phosphorous dendrons with lipid membranes studied by size exclusion chromatography**

M. Velísková[1], M. Zvarík[1], K. Čechová[1] and I. Waczulíková[1]

[1]Department od Nuclear Physics and Biophysics, Faculty of Mathematics, Physics and Informatics, Mlynská dolina F1, 842 48 Bratislava.

PO19 **Interaction of potential SARS-CoV-2 antiviral GRL0617 with selected phospholipids**

A. Čelková[1], A. Búcsi[1], J. Gallová[1], J.C. Martínez[2] and D. Uhríková[1]

[1]Department of Physical Chemistry of Drugs, Faculty of Pharmacy, Comenius University in Bratislava, SK-832 32, Odbojárov 10, Bratislava, Slovakia.

[2] BL-11 NCD beamline, Alba Synchrotron, Carrer de la Llum 2-26, 08290 Cerdanyola del Vallès, Barcelona, Spain.

PO20 **Differences in membrane properties of sensitive and resistant yeast strains *Candida auris***

J. Jacko[1], M. Morvová Jr.[1], N. Toth-Hervay[2], L. Šikurová[1], Y. Gbelská[2]

[1] Faculty of Mathematics, Physics and Informatics, Comenius University, Mlynská dolina F1, 842 48 Bratislava, Slovakia

[2] Faculty of Natural sciences, Comenius University, Ilkovičova 6, 842 48 Bratislava, Slovakia

PO21 **The effect of Budesonide on the bilayer of exogenous pulmonary surfactant**

A. Keshavarzi[1], A. Asi Shirazi[1], A. Čelková[1], M. Klacsová[1], J.C. Martínez[2] and D. Uhríková[1]

[1]*Faculty of Pharmacy, Comenius University Bratislava, Bratislava, Slovakia.*

[2]*Alba synchrotron, 08290 Cerdanyola del Vallès, Barcelona, Spain.*

PO22 **The interaction of Cathelicidin LL-37 with exogenous pulmonary surfactant – Curosurf®**

A. Asi Shirazi[1], A. Keshavarzi[1], N. Královič[1], M. Klacsová[1], J.C. Martínez[2] and D. Uhríková[1]

[1]*Faculty of Pharmacy, Comenius University Bratislava, Bratislava, Slovakia*

[2]*Alba synchrotron, 08290 Cerdanyola del Vallès, Barcelona, Spain*

PO23 **α-lactalbumin amyloid fibrillization in the presence of chloride salts cations**

A. Antosova[1], M. Gancar[1], E. Bystrenova[2], Z. Bednarikova[1], J. Marek[1] and Z. Gazova[1]

[1]*Institute of Experimental Physics Slovak Academy of Sciences, Watsonova 47, 040 01 Kosice, Slovakia*

[2]*Consiglio Nazionale delle Ricerche - Istituto per lo Studio dei Materiali Nanostrutturati (CNR-ISMN) via P. Gobetti 101, 40129 Bologna, Italy*

PO24 **Protein amyloid self-assembly, polymorphism and biological significance**

Z. Bednarikova[1], E. Bystrenova[2], M. Barbalinardo[2] and Z. Gazova[1]

[1] *Institute of Experimental Physics Slovak Academy of Sciences, Watsonova 47, Košice, Slovakia.*

[2] *Institute of Nanostructured Materials I.S.M.N – C.N.R., via Gobetti 101, Bologna, Italy.*

PO25 **Dual activity of dipeptides on amyloid fibrils of insulin and $A\beta_{40}$**

B. Borovská[1*], Z. Bednáriková[1], M. Tvrdoňová[2] and Z. Gažová[1]

[1]*Institute of Experimental Physics Slovak Academy of Sciences, Kosice, Slovakia.*
[2]*Institute of Chemistry, Faculty of Sciences, Pavol Jozef Safarik University in Kosice, Slovakia.*

PO26 **Modulation of insulin amyloid aggregation by amino acid-based ionic liquids: anion role**

D. Fedunova[1], M. Guncheva [2], V. Vanik[1], Z. Bednarikova[1], M. Gancar[1] and Z. Gazova[1]

[1] *Institute of Experimental Physics, Slovak Academy of Sciences, Watsonova 47, 040 01 Kosice, Slovakia.*

[2] *Institute of Organic Chemistry with Centre of Phytochemistry, Bulgarian Academy of Sciences, Acad. G. Bonchev 9, Sofia 1113, Bulgaria.*

PO27 **Amino acid-coated magnetite nanoparticles as potential inhibitors of α-lactalbumin amyloid aggregation**

O. Parmar[1], A. Antosova[1], M. Gancar[1], Z. Bednarikova[1], E. Bystrenova[2], M. Kubovcikova[1], M. Koneracka[1], V. Zavisova[1] and Z. Gazova[1]

[1]*Institute of Experimental Physics, Slovak Academy of Sciences, Košice, Slovakia*

[2]*Institute of Nanostructured Materials, Bologna, Italy*

PLENARY LECTURES

Coupling between neuronal electrical activity and metabolism.

A. Dhoundiyal, V. Goeschl, S. Boehm, H. Kubista and M. Hotka

Center of Physiology and Pharmacology, Department of Neurophysiology and Neuropharmacology, Medical University of Vienna, Waehringerstrasse 13a, 1090, Vienna, Austria.

e-mail: matej.hotka@meduniwien.ac.at

Electrical activity in neurons is a highly energy-demanding process accompanied by rises in cytosolic Ca^{2+}. Among the many types of Ca^{2+}-permeable channels found in the plasmatic membrane of neurons, L-type Ca^{2+} channels (LTCC) are privileged to adapt mitochondrial ATP synthesis to the corresponding energetic need [1]. LTCC-mediated increases in cytosolic Ca^{2+}, secure energy supply by pushing mitochondrial metabolism either through augmented NADH transfer into mitochondria via the malate aspartate shuttle (MAS) or via direct activation of dehydrogenases of the TCA cycle after passing into the matrix through the mitochondrial Ca^{2+} uniporter (MCU). Another Ca^{2+}-sensitive booster of mitochondrial ATP synthesis is the glycerol-3-phosphate shuttle (G3PS) whose role in neuronal energy supply has remained elusive. While all essential components of G3PS are expressed in hippocampal neurons, its functionality and interaction with other neuronal metabolic components is unclear. To answer this question, we performed metabolic measurements on single neurons using genetically encoded fluorescent indicators in combination with electric field stimulation to stimulate neurons with the neuronal electrical activity of defined intensity.

Our results suggest that neuronal bioenergetics is modulated by the intensity of synaptic activity. ATP synthesis at lower workloads is met by stimulatory action of cytosolic Ca^{2+} on MAS, while direct stimulation of the TCA cycle occurs preferentially at higher workloads. Individual inhibition of either MAS, G3PS, or MCU alone has no detectable effect on ATP synthesis, implicating that they operate in substituting manner. However, when all three mechanisms are compromised, mitochondria fail to stimulate their ATP production. Furthermore, we found that G3PS efficiently secures ATP levels, and its activity increases under conditions of absent MAS and MCU. Under these conditions, G3PS is required for appropriate action potential firing.

Neurons gain their metabolic flexibility through the compensatory action of Ca^{2+}-sensitive metabolic machinery. Unexpectedly, much of this flexibility is achieved through the increased activity of G3PS, which acts as a bioenergetic backup mechanism.

Acknowledgment
This work was supported by FWF, Project P-33797.

References

[1] M. Hotka, M. Cagalinec, K. Hilber, L. Hool, S. Boehm and H. Kubista, Sci. Signal. 13 (2020) eaaw6923.

Structure-function relationships of the ryanodine receptor

A. Zahradníková[1], B. Iaparov[1] and I. Zahradník[1]

[1] *Department of Cellular Biophysics, Institute of Experimental Endocrinology, Biomedical Research Center, Slovak Academy of Sciences, Dúbravská cesta 9, 845 05 Bratislava, Slovakia.*

e-mail: alexandra.zahradnikova@savba.sk

Ryanodine receptor (RyR) is the calcium-conducting homotetrameric channel of the sarcoplasmic reticulum that controls calcium release in various tissues. In the cardiac myocytes, calcium flux through RyR channels clustered in calcium release sites of dyads generates calcium sparks, the observable calcium release events. The molecular structure of RyR channels is known from cryoelectron microscopy and molecular biology studies. RyR function is impaired in many cardiac diseases related to excessive calcium release that causes calcium leak from the sarcoplasmic reticulum and arrhythmias. Here we present the known structural correlates of RyR activation by Ca^{2+} and describe the construction of a Markov model of RyR gating that accounts for the structural findings.

RyRs are activated by caffeine, ATP, and Ca^{2+} ions that bind to their specific binding sites, situated near each other on each RyR monomer. The structure of the calcium-binding site [1] differs in the open and closed channels (**Fig. 1**) so calcium binding to the activation site allosterically promotes the opening of the RyR channel and the binding of Ca^{2+} ions to the open channel is much stronger [2]. Magnesium ions act as a competitive inhibitor of Ca^{2+} ions at the activation site [3]. The ionic diameter of Mg^{2+} is 34% less and its hydration energy is 52% more than that of Ca^{2+} [4]. It is therefore plausible that the binding of a partially dehydrated Mg^{2+} ion will be stronger to the closed channel and may thus allosterically suppress the opening transition. Additionally, magnesium ions inhibit the channel by binding at a specific RyR inhibition site [3], the molecular identity of which is not yet known. Of interest are indications that some cases of RyR dysfunction may be due to changes in the regulation of RyR activity by Mg^{2+} [5].

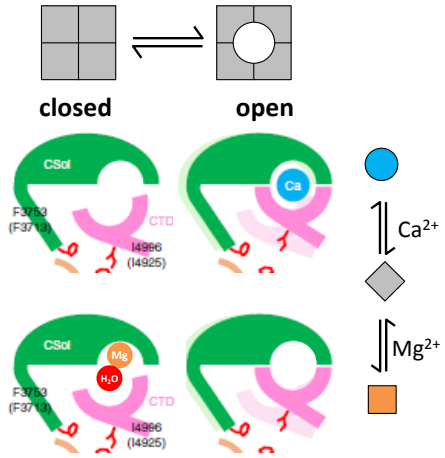

Fig. 1. Binding of ions at the RyR activation site. Top: Schematic diagram of the transition between the closed and the open state of the RyR channel tetramer. The open state is energetically more favourable when it contains bound Ca^{2+} ions in their binding sites, while the closed state is energetically more favourable when it does not contain bound Ca^{2+} ions. Middle: Binding of Ca^{2+} to the activation site. The diameter of the Ca^{2+} binding site in the closed state is too large to bind a calcium ion tightly but gets constricted in the open state [1]. Therefore the binding of calcium ions promotes the open state of the channel and channel opening promotes the binding of calcium ions. Bottom: binding of Mg^{2+} to the activation site. We hypothesize that the Ca^{2+} binding site in the open state is too large to bind a dehydrated Mg^{2+} ion but too small to bind a partially hydrated Mg^{2+} ion, while in the closed state it is large enough to bind a partially hydrated Mg^{2+} ion. Therefore the binding of magnesium ions promotes the closed state of the channel and channel closure promotes the binding of magnesium ions. Right: Schematic depiction of Ca^{2+} and Mg^{2+} binding to the activation site. The cartoon of the binding site is adapted from [1].

To elucidate the effect of Ca^{2+} and Mg^{2+} binding on the activity of the RyR, we have developed a mathematical model of RyR gating [6] that incorporated the allosteric interaction between the binding of Ca^{2+} or Mg^{2+} to the activation site and channel opening. The interaction of Mg^{2+} with the RyR inhibition site was treated as a second-order process [3]. The parameters of the model were determined by fitting the available experimental data on calcium- and magnesium-dependent RyR open probability, open time, and rate of activation. The rate of Ca^{2+} binding to the

activation site was diffusion-limited, while that of Mg^{2+} was 100 times slower. While Ca^{2+} was a strong allosteric activator (f_{Ca} = 0.0058), Mg^{2+} was a weak allosteric inhibitor (f_{Mg} = 3.25). The dissociation constants of Ca^{2+} and Mg^{2+} at the activation site were 4.18 and 92.3 μM, respectively, and the Mg^{2+} dissociation constant at the inhibition site was 546 μM. The simulated data show that changes in Mg^{2+} binding had a prominent effect on RyR open probability (P_O), mean open time (t_O), mean closed time (t_C), as well as on the rate of activation (**Fig. 2**). Mg^{2+} acted as a strong inhibitor of RyR opening, and a change of Mg^{2+} binding and unbinding rates corresponding to a doubling or halving of either of the two Mg^{2+} dissociation constants had a profound effect on RyR gating kinetics, open probability, and rate of activation.

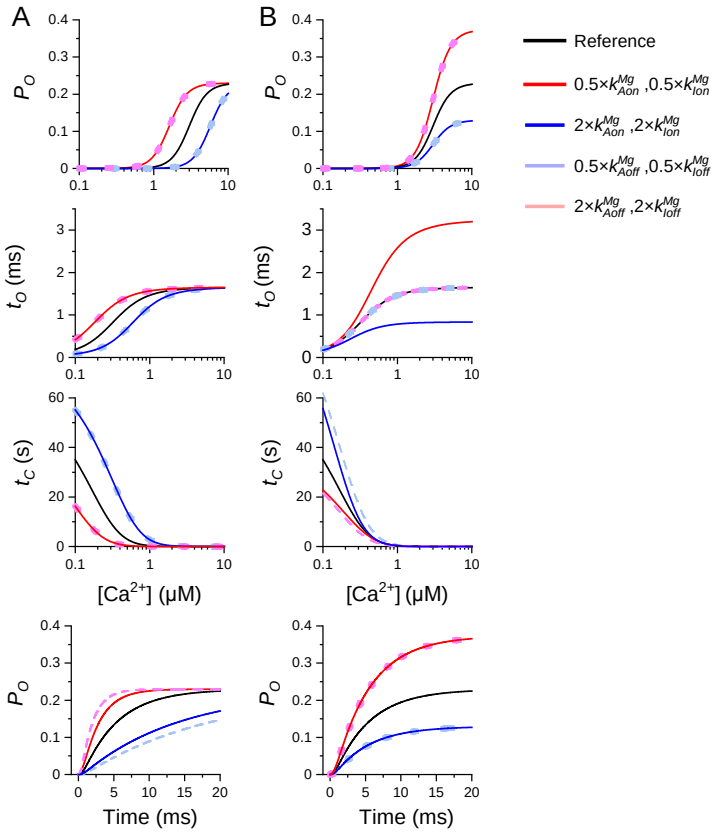

Fig. 2. Effect of Mg^{2+} on the calcium dependence of RyR activity. A – binding to the activation site; B – binding to the inhibition site. Red lines denote weaker Mg^{2+} binding (increased channel activity). Blue lines denote stronger Mg^{2+} binding (decreased channel activity). Pastel colours denote changes in the unbinding rates, saturated colours denote changes in the binding rates. Changes in Mg^{2+} binding to the activation site induce a shift in the calcium sensitivity of open probability, open time, and closed time, as well as a change in the rate constant of activation. The relative change of RyR activity in response to changes in Mg^{2+} binding to the inhibition site is independent of calcium concentration, and the rate constant of activation is not affected.

The presented model of RyR gating is in very good agreement with the experimental data, accounts for the known structural details of the activation site, and has the potential to explain the important role of Mg^{2+} regulation of RyR activity.

Acknowledgment

This work was supported by the SAV-TUBITAK project JRP/2019/836/RyRinHeart, by the project VEGA 2/0182/21, and by the Operational Programme Integrated Infrastructure for the project: Long-term strategic research of prevention, intervention, and mechanisms of obesity and its comorbidities, IMTS: 313011V344, co-financed by the European Regional Development Fund.

References

[1] A. des Georges, O.B. Clarke, R. Zalk, Q. Yuan, K.J. Condon, R.A. Grassucci, W.A. Hendrickson, A.R. Marks andJ. Frank, Cell, 167 (2016), 145–157.
[2] A. Dashti, G. Mashayekhi, M. Shekhar, D. Ben Hail, S. Salah, P. Schwander, A. des Georges, A. Singharoy, J. Frank and A. Ourmazd, Nat. Commun., 11 (2020), 4734.
[3] A. Zahradníková, M. Dura, I. Györke, A.L. Escobar, I. Zahradník and S. Györke, Am. J. Physiol. Cell. Physiol., 285 (2003), C1059–C1070.
[4] Z. Qian, H.M. Miedema, L.C.P.M. de Smet and E.J.R. Sudhölter, Desalination, 521 (2022), 115398.
[5] W. Guo, B. Sun, J.P. Estillore, R. Wang and S.R.W. Chen, J. Biol. Chem., 295 (2020), 15622–15635.
[6] B. Iaparov, I. Baglaeva, I. Zahradník and A. Zahradníková, Front. Physiol. 12 (2022), 805956.

METHODS LECTURES

Electrical detection of DNA synthesis

Miloslav Karhanek[1], Alexandra Zahradníková[2]

[1]*Specialized Bioinformatics Laboratory, Biomedical Research Center SAS, Dubravska 9, 84505 Bratislava*
[2]*Institute of Experimental Endocrinology, Biomedical Research Center SAS, Dubravska 9, 84505 Bratislava.*

e-mail: miloslav.karhanek@savba.sk

Introduction

DNA detection methods based on sequencing by synthesis rely mostly on optical readouts. We discovered that the incorporation of a complementary deoxynucleotide (dNTP) into a self-primed single-stranded DNA attached to the surface of a gold electrode evokes an electrode surface charge, which can be used for direct electrical detection of DNA synthesis [1].

Method

The patent's summary [2] describes the invention as "a method and device for direct electrochemical detection of enzymatically catalyzed DNA synthesis by induced surface charge perturbation." One of the claims specifically refers to a method for detecting a chemical reaction where the reactants "generate a charged particle that is a proton or an electron."

Results and Discussion

Based on a general understanding of polarizable interfaces, we proposed that the electrode detects proton removal from the 3'-OH group of the DNA molecule during phosphodiester bond formation. This event can be detected as a transient current by a voltage-clamp amplifier (see Figure 1). Ion Torrent used this patent and a high-density array chip of micro-machined wells for performing sequencing in a massively parallel way with the launch of the first Ion Personal Genome Machine (PGM) in 2010. This technology laid down a path for further improvements and enabling next-generation sequencing (NGS) on the Ion Torrent platform [3].

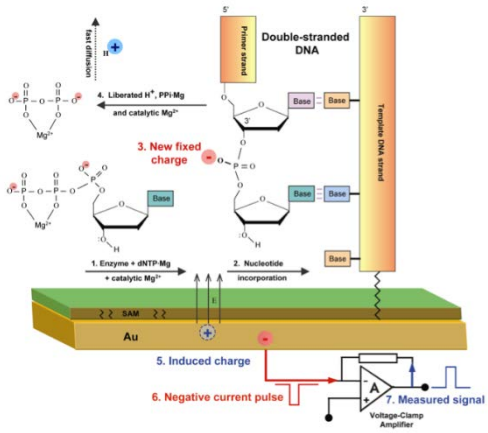

Fig. 1. Detection mechanism. Incorporation of nucleotide (step 2), increases a negative charge on the backbone phosphate group (step 3), produced by the removal of a proton from the 3'-OH group of the DNA primer during the catalytic step of the reaction (step 4) and by rapid diffusion of the proton into the surrounding solution (step 4). The induced charge (step 5) is detected as a negative current pulse by a voltage-clamp amplifier, called also a trans-impedance amplifier (step 6). Adapted from [1].

Acknowledgment
The original work was supported by National Institutes of Health Grants 1R21 A1059499-01 and HG 000205.
This presentation was supported by the Slovak Research and Development Agency project APVV-20-0236.

References

[1] N. Pourmand, M. Karhanek, H. H. J. Persson, C. D. Webb, T. H. Lee, A. Zahradníková and R. W. Davis, Proc. Natl. Acad. Sci. U. S. A., 103 (2006), 6466-6470.
[2] N. Pourmand, M. Karhanek and R. W. Davis, United States Patent 7785785, August 31, 2010 (original).
[3] J. M. Rothberg, W. Hinz, T. M. Rearick et al., Nature 475 (2011), 348-52.

Bioimaging opportunities using X-FEL MHz tomoscopy

P. Vagovič[1], J. Uličný[2*]

[1]*Center for Free-Electron Laser, Notkestraße 85, 22607 Hamburg, Germany*
[2]*Faculty of Science, Department of Biophysics, Institute of Physics, P. J. Šafárik University, Jesenná 5, 04154 Košice, Slovakia*

*e-mail: jozef.ulicny@upjs.sk

Experimental observation of nonrepetitive dynamics of especially opaque samples remains a challenging problem despite growing demand from many areas of science and technology. Using X-ray sources, 3D images can be obtained by conventional computed tomography (CT), for both macroscopic objects (patients) [1] and microscopic, or even submicroscopic objects (micro-CT). For micro-CT, the imaging setup is stationary, while the sample rotates to provide a full tomographic scan as a set of 2D projections. The mechanical rotation limits the micro-CT to no more than 1000 CT scans per second [2], thus making faster processes inaccessible. Also, stroboscopic imaging, which allows recollection of 3D images from randomly sampled, repetitive processes does not allow to follow processes of stochastic nature.

To overcome the above-mentioned limitations, both the imaging setup and the sample must remain static, so that the source intensity and the spatial, temporal, and dynamical resolution of the detector become the new bottlenecks. By avoiding sample rotation, and thus circumventing centrifugal forces, the native dynamics of the objects can be followed at the sampling rate determined by timing constraints of illumination source and detector.

In our approach, we have taken advantage of a unique high-brilliance pulsed X-ray laser at European XFEL to create a multi-projection setup based on a beam-splitter and a detector array [4]. With a maximum repetition rate of 4.5 MHz and pulse duration typically 30 fs (with less than 10 fs achievable now), we can sample processes with velocities of propagation up to hundreds of meters per second, while taking multiple differential phase-contrast images in hard X-ray regime (for now up to 25 keV). High photon flux and coherence properties of the XFEL pulse pushe the temporal and spatial resolution above what is achievable using synchrotron sources [3].

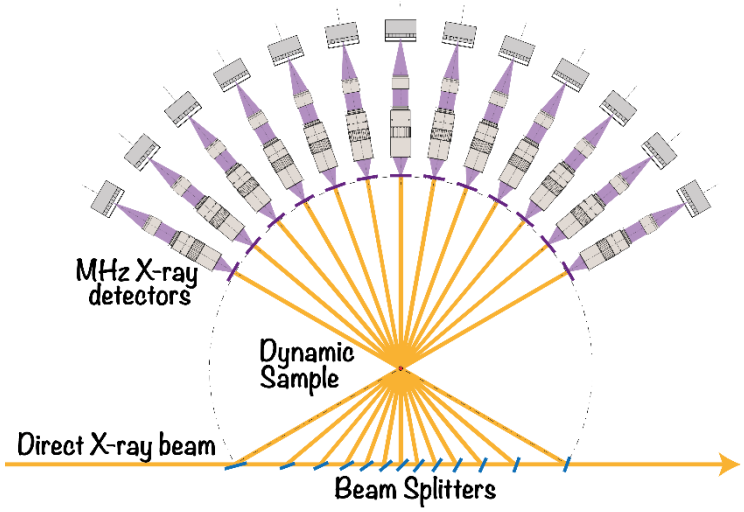

Fig. 1. Hard X-ray Multi-Projection Imaging system for SASE beams, P. Vagovic, V. Bellucci, P. Villanueva-Perez, W. Yashiro (patent pending, application number: EP21200564.9, 1. 10. 2021)

Recently, the international consortium of 8 partners from 5 countries, including UPJŠ Slovakia, was granted the Horizon Europe EIC project "MHz-TOMOSCOPY" [5] to develop further the experimental prototype of microscopy to 4D (3D plus time) for wider scientific and application community. While first applications are from aerospace and additive manufacturing material engineering, highly sensitive phase contrasting makes this modality also especially suitable for fast biological imaging, where we are looking for further applications.

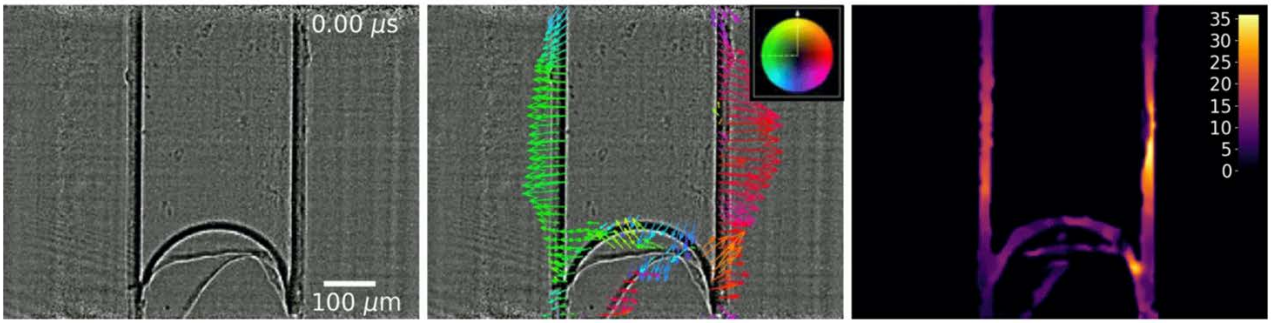

Fig. 2. Laser-induced capillary breakage, recorded using a 1.128 MHz sampling rate at EuXFEL. The middle figure shows displacement vectors of moving parts and the figure on the right shows velocities in m/s units. Performed at the SPB instrument (2019) [3].

Acknowledgment

This work was supported by Horizon EU Project 101046448 (MHz-TOMOSCOPY).

References

[1] T. M. Buzug (2008). Computed Tomography: From Photon Statistics to Modern Cone-Beam CT (Berlin Heidelberg: Springer-Verlag).
[2] F. García-Moreno,, P. H. Kamm, T. R. Neu, F. Bülk, M. A. Noack, M. Wegener, N. von der Eltz, C. M. Schlepütz, M. Stampanoni and J. Banhart, J. Adv. Mater. *33* (2021), 2104659.
[3] P. Vagovic, T. Sato, L. Mikes, G. Mills, R. Graceffa, F. Mattsson, P. Villanueva-Perez, A. Ershov, T. Farago, J. Ulicny et al. OPTICA 6 (2019), 1106–1109.
[4] patent pending, application number: EP21200564.9
[5] Project 101046448 (MHz-TOMOSCOPY) HORIZON-EIC-2021-PATHFINDEROPEN-01-01 - EIC Pathfinder Open 2021

COMPANY PRESENTATIONS

Be always in control of water quality
PickMol™ technology
SAFTRA Photonics Ltd

P. Miškovský[1,2] and G. Bánó[3]

[1] *SAFTRA photonics Ltd., Moldavská 51, 04011 Košice.*
[2] *Cassovia New Industry Cluster, Tr. SNP 1, 04001 Košice.*
[3] *KBF PF UPJŠ, Jesenná 5, 04154 Košice.*

e-mail: pavol.miskovsky@upjs.sk

SAFTRA photonics Ltd. brings to the market PickMol™ nanotechnology for screening purpose (Fig. 1). This technology detects if water or any food matrix is contaminated with persistent organic pollutants (POPs)/pesticides/drugs. We offer a rapid method (10 minutes) to detect presence of the most POPs/pesticides/drugs in water/milk/beverages, carrying out an in-situ analysis for less than 40€ per sample and with the same sensitivity (ppb level) as reached by certified methods (i.e. GC-MS). The patented PickMol™ technology was recently validated by certified laboratory and can be tailored for any organic molecule, which means its large potential for application also in other fields like pharmaceutical & chemical industry, security and sport (doping control).

PickMol™ technology is:

- Sensitive (ppb concentration level)
- Selective (target a molecule)
- Efficient (saving up to 90% of costs)
- Fast (10 minutes for analysis)
- Portable
- Instant (analysis on the spot)

With the PickMol™ technology the people will be safer and healthier in their daily lives as the precise quality control of water/milk/food can be performed continuously in more sites. Therefore, the PickMol™ technology can significantly affects human life.

Fig. 1. PickMol nanotechnology unit.

Acknowledgment
The work has been supported (biomedical part) by the BioPickmol (NFP 313010AUW6) project.

Introducing the Next Generation in Protein Structure Determination - Microfluidic Modulation Spectroscopy

J. Golda[1] and J. Tkáč[1]

[1] *Specion Ltd., Budějovická 55, 140 00 Praha 4, Czech Republic.*

e-mail: golda@specion.biz

Infra-Red (IR) analysis has been long accepted as a powerful tool in protein characterization, particularly in the Amide I band (~1600 – 1700 cm^{-1}), which gives detailed secondary-structural information that can be critical in determining protein structure-activity relationships, stability, batch-to-batch comparisons and in formulation studies as a few examples. Technologies traditionally used for secondary structure analysis, such as benchtop Fourier Transform IR (FTIR) or Circular Dichroism (CD), suffer from a number of issues that have prevented their routine use in this area, preventing this application from reaching its full potential. These include concentration and buffer restrictions, incompatibility with a range of excipients, a lack of automation, low spectral reproducibility and for FTIR, water subtraction problems.

Microfluidic Modulation Spectroscopy (MMS) is a new key technology that was brought to market in 2019 by RedShift Bioanalytics. It focuses on the IR Amide I region to produce exceptionally high data quality and reproducibility that aim to solve the aforementioned issues encountered with traditional technologies. It is fully automated, running samples from 24- and 96-well plates, compatible with a very broad concentration range (0.1 to >200 mg/ml), and is also compatible with a wide range of complex buffer systems and excipients, including those that absorb in the amide I region, surfactants and organic solvents. The platform includes a powerful software package that facilitates data analysis, and can be included in the automation procedure. This presentation highlights the technical benefits of MMS and its application in the protein structural workflow, giving relevant application examples.

SHORT COMMUNICATIONS

Alteration of hippocampal excitability by prenatally applied antidepressant.

L. Hoppanová[1], B. Jurkovičová-Tarabová[1], A. Idunková[1], M. Tomko[1], M. Dubovický[2], Ľ. Lacinová[1]

[1]Institute of Molecular Physiology and Genetics, Center of Bioscience
[2]Institute of Experimental Pharmacology and Toxicology, Center of Experimental Medicine
Dúbravská cesta 9, Bratislava, Slovakia

e-mail: lubica.lacinova@savba.sk

Introduction: Major depression is a common illness that severely limits psychosocial functioning and diminishes the quality of life. The prevalence of major depression for women is about twice that for men. An additional risk for women is represented by the period of pregnancy. Depression affects up to 20% of women in the perinatal period [1]. Newborns of mothers suffering from depression during pregnancy can be negatively affected in the early postnatal period and have an increased risk of cognitive, emotional, and behavioral disorders [2]. Therefore, the treatment of prenatal depression should be considered. However, it may affect the physical health of the pregnant mother, as well as the fetal and neonatal development of the individual. Effects of various antidepressants on a mother's health are frequently investigated, however, studies of offspring prenatally exposed to antidepressants are quite rare. Therefore, we have focused on the possible adverse effects of third-generation antidepressant mirtazapine on offspring. Mirtazapine belongs to a small group of most effective antidepressants according to recent metastudy [3]. It is a presynaptic α2 receptor antagonist that enhances noradrenergic and serotonergic neurotransmission in the central nervous system.

Aims: We have focused on the alteration of hippocampal excitability of newborn rats prenatally exposed to the antidepressant mirtazapine. Hippocampus was chosen because of its relevance for cognitive, emotional, and behavioral disorders observed in offspring of depressed mothers.

Methods: Adult female Sprague-Dawley rats were used. Animals were randomly assigned to four experimental groups: (1) - non-depressive untreated female rats and their offspring; (2) depressive non-treated female rats and their offspring; (3) non-depressive mirtazapine-treated female rats and their offspring; (4) depressive mirtazapine-treated female rats and their offspring.

To create a model of depression rats were subjected to randomly alternating stressors for three weeks. Depression-like status of this model was confirmed by an anhedonia test [4]. Then, rats were mated and onset of pregnancy was detected by the presence of sperms in vaginal smears. Antidepressant mirtazapine was administered to pregnant rats at the 10th - 20th days of pregnancy at the dose of 10 mg/kg/day. Animals from the non-treated groups were administered with a vehicle.

Hippocampal neurons were isolated from newborn pups (postnatal day 0) and a primary culture was established. Hippocampal excitability was measured in neuronal culture (day in vitro 8-10) using a whole-cell patch clamp in the current-clamp configuration. Pyramidal hippocampal neurons were visually identified by their morphology. Resting membrane potential (V_{rest}) was evaluated immediately after establishing the current-clamp configuration with zero holding curre4nt applied and was corrected for a liquid junction potential. For the rest of the experiment holding current was applied to maintain -70 mV resting membrane potential. Input resistance (R_{input}) was measured by the application of five hyperpolarizing current steps. Action potential (AP) generation was activated by a series of depolarizing current pulses.

Results and Discussion: V_{rest} in the neurons of the stress + mirtazapine group was significantly hyperpolarized compared to the other groups. We also observed a significant decrease in R_{inp} in both stressed groups compared to the non-stressed groups. Changes in both parameters suggest an altered expression of potassium channels which participate in setting resting membrane potential. Individual AP parameters (threshold, amplitude, rise time, width) were not significantly altered in any group. A higher depolarization was required to initiate an AP firing in the stressed group suggesting modulation of voltage-gated sodium channels. This activation shift was compensated by mirtazapine.

Conclusions: Pregestational stress altered hippocampal excitability of newborn pups to a minor extent. Administration of the antidepressant mirtazapine during gestation partly relieved this effect.

Acknowledgment
This work was supported by grants APVV-19-0435 and VEGA 2/081/22.

References

[1] T. Pearlstein, Best Pract Res Clin Obstet Gynaecol 29 (2015), 754-764.
[2] N. K. Grote, J.A. Bridge, A. R. Gavin, J. L. Melville, S. Iyengar, W. J. Katon, Arch Gen Psychiatry 67 (2010), 1012-1024.
[3] A. Cipriani, T. A. Furukawa, G. Salanti, A. Chaimani, L. Z. Atkinson, Y. Ogawa, S. Leucht, H. G. Ruhe, E. H. Turner, J. P. T. Higgins, M. Egger, N. Takeshima, Y. Hayasaka, H. Imai, K. Shinohara, A. Tajika, J. P. A. Ioannidis, J. R. Geddes, Lancet 391 (2018), 1357-1366.
[4] E. Bogi, K. Belovicova, L. Moravcikova, K. Csatlosova, E. Dremencov, L. Lacinova, M. Dubovicky, Behav Brain Res 375 (2019), 112131.

Cough modulation by changes in afferent inputs at low temperature

M. Šimera[1], M. Veterník[1], L. Martvoň[1], K. F. Morris[2], T. Pitts[3], D.C. Bolser[4], I. Poliaček[1]

[1] *Department of Medical Biophysics, Jessenius Faculty of Medicine in Martin, Comenius University in Bratislava, Slovakia*
[2] *Department of Molecular Pharmacology and Physiology, College of Medicine, University of South Florida, Tampa, FL, USA.*
[3] *Department of Neurological Surgery, Kentucky Spinal Cord Injury Research Center, University of Louisville, Louisville, KY, USA.*
[4] *Dept. of Physiological Sciences, College of Veterinary Medicine, University of Florida, Gainesville, FL, USA*

e-mail: michal.simera@uniba.sk

Vagal afferents play an important role in evoking respiratory reflexes such as cough in response to the mechanical and chemical stimulation of the airways [1]. The nerve's cooling technique is based on the fact that the neural conduction of myelinated fibers can be efficiently blocked by cooling the nerve trunk to 6–7 °C while the blocking temperature of non-myelinated fibers is 3 °C or lower.

Our aims were to investigate the relative contribution of myelinated and non-myelinated fibers in the modulation of spatio-temporal parameters of tracheobronchial (TB) and laryngopharyngeal (LPh) cough by cooling (< 5 °C) of the vagus and the superior laryngeal nerve (SLN), respectively. We also employed computational modeling of cough response based on our experimental results.

Cooling of vagus nerve protocol [2]*:* Unilateral cooling of the vagus nerve (Fig. 1) was employed to modulate TB in 20 anesthetized cats. Cough was induced by mechanical stimulation of the tracheobronchial airways. The number of coughs during vagal cooling was decreased by more than 70% ($p < 0.001$). Inspiratory cough efforts were reduced by approximately 30% ($p < 0.001$) and expiratory motor drive by more than 80% ($p < 0.001$). Temporal analysis showed prolonged inspiratory and expiratory phases, the cough cycle duration, and the interval between maxima of the diaphragm and the abdominal activity during coughing ($p < 0.001$). There was no significant difference in the average effects on the cough reflex between cooling of the left or the right vagus nerve, however, the dominance of one vagus nerve was confirmed.

Cooling of SLN protocol [3]*:* Unilateral and bilateral cooling of SLN were employed to modulate mechanically induced TB and LPh cough in 12 anesthetized cats. There was a little effect of SLN block on TB. Bilateral SLN cooling reduced the number of LPh (<50 %, $p < 0.05$), amplitudes of diaphragm EMG activity (<55 %, $p < 0.05$), and cough expiratory efforts (<40 %, $p < 0.01$) during LPh. Effects after unilateral SLN cooling were less pronounced. Temporal analysis of LPh showed only shortening of the diaphragm and abdominal muscles burst overlap in the inspiratory–expiratory transition after unilateral SLN cooling. Bilateral cooling shortened the expiratory phase and total cough cycle duration. There was no significant difference in the average effects of cooling left or right SLN on LPh.

Simulation protocol [4]: Unilateral vagal cooling was simulated by a reduction of simulated cough afferent input to the model computer respiration/cough neuronal network. Simple attempts (reduction of the number of afferent fibers, synaptic terminals, and synaptic strength) resulted in only a mild reduction of simulated coughing. Multifactorial alterations of model input characteristics were required to approximate cough motor patterns that were observed during unilateral vagal cooling *in vivo*. Our simulation data support the plausibility of several mechanisms that could contribute to *in vivo* results with a unilateral cold block of the vagus nerve. Our simulation results motivated parameter revision in the computer respiration/cough neuronal network

afferent processing circuit, consistent with a more profound impairment of central processing as a result of partial vagal deafferentation than we predicted.

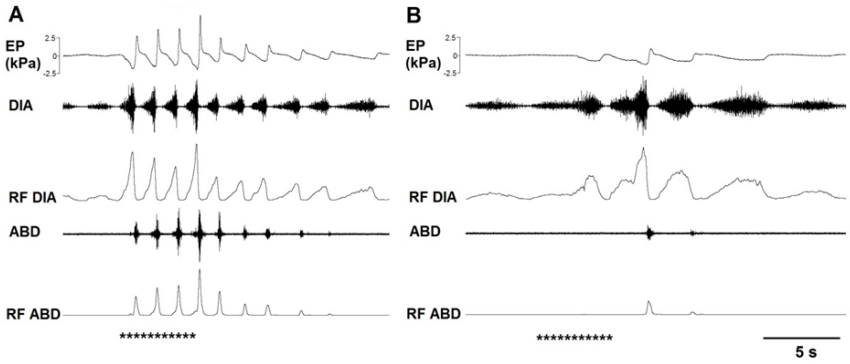

Fig. 1. Tracheobronchial cough reflex induced by mechanical stimulation (***) and effect of vagal cooling. **A:** intact vagus. **B:** partial unilateral vagal block (cooling <5 °C). EP - esophageal pressure; DIA EMG, ABD EMG—EMG activities of the diaphragm, abdominal muscles; RF—rectified (moving average) EMG activities.

Fig. 2.

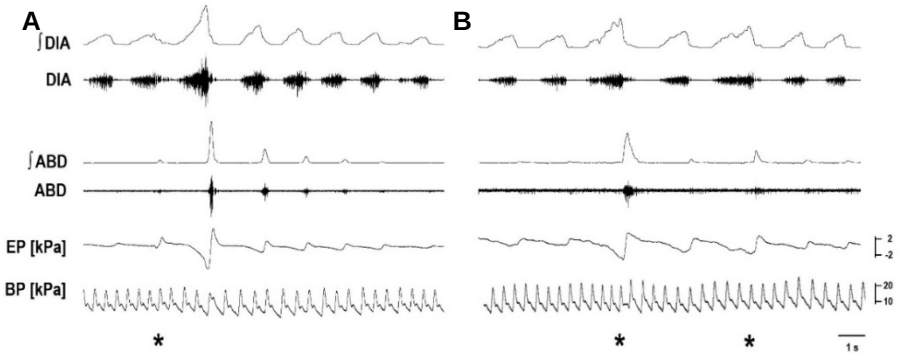

Laryngopharyngeal cough reflex induced by mechanical stimulation (* single touch) and effect of bilateral SLN cooling (representative trials). **A:** intact SLN; **B:** bilateral SLN cooling (temperature of both nerves < 5 °C, two coughs were induced by each touch). DIA: diaphragm EMG; ABD: abdominal EMG; EP: esophageal pressure; BP: arterial blood pressure; ∫: integrated (moving average).

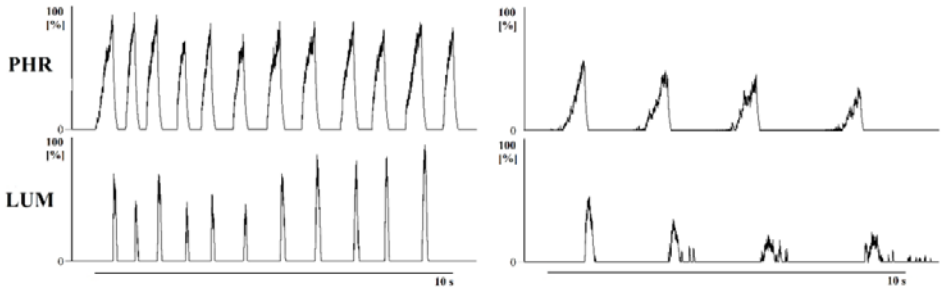

Fig. 3: Graphical representation of the simulations, **left:** control coughs, **right:** simulated vagal cooling with reduction of cough fibers, their synaptic strength and terminals from slowly adapting lung stretch receptors to pump cells. PHR – inspiratory motoneurons integrated activity, LUM – expiratory motoneurons integrated activity.

Acknowledgments

This work was supported by grants VEGA1/0275/19; VEGA1/0092/20.

References

[1] D.N. Franz, A. Iggo, Conduction failure in myelinated and non-myelinatedaxons at low temperatures. J. Physiol. 199 (1968), 319–345.

[2] M. Simera, I. Poliacek , M. Veternik, L. Babalova, Z. Kotmanova, J. Jakus, Changes in vagal afferent drive alter tracheobronchial coughing in anesthetized cats. Respir Physiol Neurobiol. 230 (2016), 36-43.

[3] M. Simera, M. Veternik, L. Martvon, Z. Kotmanova, S. Mostafavi, O. Bosko, O. Kralikova, I. Poliacek, Distinct modulation of tracheal and laryngopharyngeal cough via superior laryngeal nerve in cat. Respir Physiol Neurobiol. 293 (2021), 716-720.

[4] L. Martvon, M. Veternik, M. Simera, Z. Kotmanova, L. Babalova, K.F. Morris, T. Pitts, D.C. Bolser, I. Poliacek, Modeling and simulation of vagal afferent input of the cough reflex. Respir Physiol Neurobiol. 2022, 301:1 *In Press.*

Effects of photobiomodulation on rotenone challenged human glioma cells.

S. Tomkova[1], S. Kolesarova[1,2] and K. Stroffekova[1]

[1]Department of Biophysics, Faculty of Sciences, PJ Safarik University, Jesenna 5, Kosice, Slovakia.
[2]Department of Biochemistry, Faculty of Sciences, PJ Safarik University, Moyzesova 15, Kosice, Slovakia.

e-mail: katarina.stroffekova@upjs.sk

According to the World Health Organization (WHO), between 2015 and 2050, the proportion of the world's population over 60 years will nearly double from 12% to 23% [1]. While overall neurological disorders are projected to increase from 2005 to 2030 by approximately a 12%, Alzheimer's and other dementias are projected to show a 66% increase, which instigates a great socio-economic impact. The etiology of most neurodegenerations is not clear; however, interactions between genetic and environmental factors, lifestyles, and dietary factors were shown to play a role in Parkinson's and Alzheimer's diseases (PD, AD), and in ALS (amyotrophic lateral sclerosis). Long-term/low dose exposures to metals, pesticides, solvents, and petrochemicals were indicated as environmental risk factors in PD, AD, and ALS [2]. PD was positively associated with two groups of pesticides, including rotenone (ROT) and paraquat (PAR), defined by mechanisms that impair mitochondrial function and those that increase oxidative stress, further supporting the role for these mechanisms in PD pathophysiology [3]. The ROT and PQ are used extensively in *in vitro* and *in vivo* PD models. Photobiomodulation (PBM) by low-level near-infrared (NIR) radiation showed the beneficial effects in treatment of PD and AD and the treatment of traumatic brain injuries including stroke [4-6]. PBM was shown to prevent mitochondrial dysfunction and dopamine loss in Parkinson's disease patients [7].

The present study aims to investigate PBM effects in a 2D cellular PD model (rotenone challenged U87 MG cells). Specifically, the study is focused on PBM effects on cell viability, oxidative stress response, mitochondria dysfunction, and morphology.

Cell viability was assessed by tetrazolium MTT (3-(4, 5-dimethylthiazolyl-2)-2,5-diphenyltetrazolium bromide) viability assay. Detection of oxidative stress, mitochondria morphology, and mass was determined by confocal microscopy with the use of specific fluorescent markers (MitoSoxRed®, CellROX® Green, TMRM, NAO). Mitochondria function was assessed by metabolic flux measurement in intact cells (Agilent Seahorse XF MINI analyzer). Statistical analysis was carried out by either Student's t-test or ANOVA using SigmaPlot (Ver. 12.0; SystatSoftw. Inc.). A $p < 0.05$ was considered significant.

Chronic treatment (48hr) with rotenone (0.1-10μM) resulted in a concentration-dependent decrease in cell viability of up to 47%, increased mitochondria fragmentation, and increased ROS. Cell metabolic flux measurements revealed that even at treatment by very low rotenone concentrations (100 and 200nM), mitochondria function was deeply diminished, which was not revealed by viability assay (Fig.1).

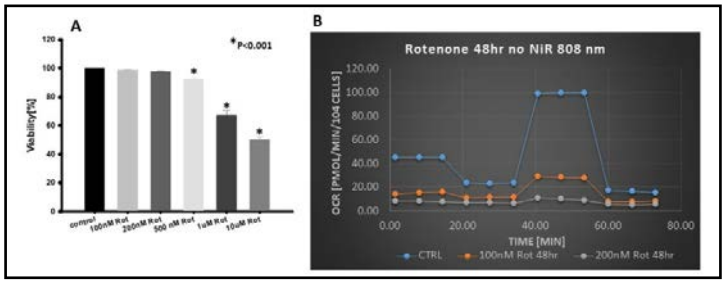

Fig. 1. Effect of rotenone and PBM treatment on cell viability and mitochondria function in U87 MG cells.

PBM treatment of 2.5 J/cm^2 with 808 nm laser improved cell survival by up to 20%, decreased the level of ROS as well as mitochondrial fragmentation (Fig.2). PBM treatment did improve mitochondrial function, mainly the levels of basal respiration and respiratory capacity, which are indicators of cell ability to cope with stress.

Conclusions: Our data indicate that exposure to low-dose rotenone resulted in mitochondrial fragmentation, increased ROS, and mitochondrial dysfunction. PBM treatment at 808 nm improved mitochondrial function and morphology. Thus PBM has the potential to improve overall mitochondria condition, which could be further implemented in the treatment of neurodegenerative diseases.

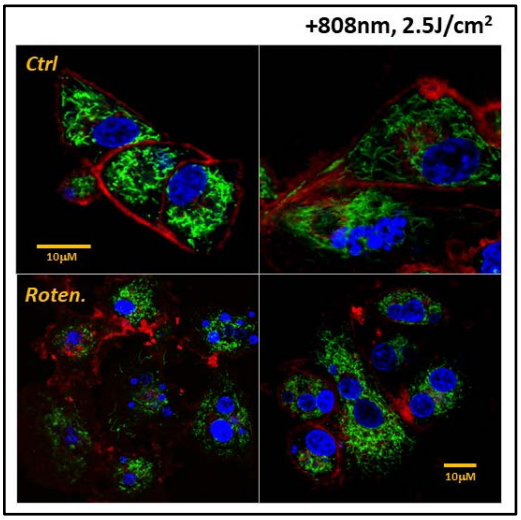

Fig. 2. Rotenone and PBM effect on mitochondria in U87 MG cells.

Acknowledgment
This work was supported by the EU ERDF grant OPENMED (ITMS2014+: 313011V455), by the Slovak grants VEGA 1-0421-18; VEGA 1-0557-20; APVV-15-0485 and APVV-16-0158.

References

1. WHO, Neurological disorders : World Health Organization . ISBN 92 4 156336 2.
2. M.R. Hamblin and Y. Huang., Handbook of Photomedicine, 2014, CRC press.
3. M. Vos, B. Lovisa, A. Geens, V.A. Morais, G. Wagnières and H. van den Bergh. PLoS One. 8 (2013), e78562.
4. X.Tang, Y. Luo, H. Z. Chen and D.P. Liu, Front. Physiol.. 5 (2014), 175.
5. M.L. McEwen,PG Sullivan, AG. Rabchevsky, and JE. Springer Neurotherapeutics, 8 (2011), 168-179.
6. Z.Q. Jia, G. Li, Z.Y. Zhang, H.T. Li, J.Q. Wang, Z.K. Fan, L.V. Gang, Neural Regen. Res. 11 (2016), 137-143.
7. M. Germain, J. Mathai, H. Mcbride and G.Shore, EMBO J, 24 (2005), 1546-56.

Singlet oxygen deactivation as a probe of heme availability in heme proteins

A. Hovan[1], D. Sedláková[2], M. Berta[1], G. Bánó[1] and E. Sedlák[3]

[1] *Department of Biophysics, Faculty of Science, P.J. Šafárik University in Košice, Jesenná 5, 041 54 Košice, Slovakia.*
[2] *Department of Biophysics, Institute of Experimental Physics, Slovak Academy of Sciences, Watsonova 47, 040 01 Košice, Slovakia.*
[3] *Center for Interdisciplinary Biosciences, Technology and Innovation Park, P.J. Šafárik University in Košice, Jesenná 5, 041 54 Košice, Slovakia.*

e-mail: andrej.hovan@upjs.sk

Singlet oxygen, the lowest electronic excited state of molecular oxygen, is mostly known for its crucial role in photodynamic therapy of cancer. The deactivation of singlet oxygen by proteins is usually described through the interaction of singlet oxygen with certain amino acids. Changes in accessibility of these amino acids influences the quenching rate and the singlet oxygen phosphorescence kinetics. Moreover, numerous proteins with covalently bound or encapsulated cofactors are present in cellular environment. These cofactors could also influence the deactivation of singlet oxygen, which has received little attention. To confront this issue, we used cytochrome *c* (cyt *c*) and apocytochrome *c* (apocyt *c*) to illustrate how the heme prosthetic group influences the rate constant of singlet oxygen deactivation upon acidic pH-induced conformational change of cyt *c* [1]. Based on these results we then studied molten globule state formation and heme availability to singlet oxygen with three different salts: sodium perchlorate, sodium chloride and sodium sulfate. Additionally, the effect of amino acids and heme accessibility on the FMN triplet state deactivation was also analyzed.

Photosensible flavin mononucleotide (FMN) was used to produce singlet oxygen. To verify and justify our results, we used circular dichroism and fluorescence measurements.

Our data show that the heme group has a significant and measurable effect on singlet oxygen quenching when the heme is exposed to the solvent and is therefore more accessible to singlet oxygen.

Acknowledgement

This work was supported by Slovak Research and Development Agency through the project APVV-20-0340 and by the grant agency of the Ministry of Education, Science, Research, and Sport of the Slovak Republic (grants no. VEGA 1/0557/20 and no. VEGA 1/0074/22). This publication is the result of the implementation of the project OPENMED (Open Scientific Community for Modern Interdisciplinary Research in Medicine) ITMS2014+: 313011V455 from the Operational Program Integrated Infrastructure funded by the ERDF.

References

[1] A. Hovan, M. Berta, D. Sedláková, P. Miskovsky, G. Bánó, E. Sedlák , Phys Chem Chem Phys., 23(2021), 15557-15563.

Flavoproteins as singlet oxygen producers

E.Sedlák

Center for Interdisciplinary Biosciences, Technology and Innovation Park, Jesenná 5, Slovakia
and Department of Biochemistry, Faculty of Science at P.J. Šafárik University, 041 54 Košice

e-mail: erik.sedlak@upjs.sk

Introduction. Photosensitizers are widely used in photodynamic therapy. Recently, significant efforts have been invested into the design of protein-based PSs containing flavin mononucleotide (FMN) – flavoproteins – due to a high value of the quantum yield of the $^1O_2$ production, Φ_Δ, of the proteins-based PS. FMN belongs to a group of efficient endogenous photosensitizers in cells with rather high $^1O_2$ quantum yield within the range 0.51-0.65 [1]. Depending on FMN concentrations and concentrations of available oxygen, the flavin(s) can be even more effective $^1O_2$ generators than exogenous porphyrins - of which several analogues are clinically approved photosensitizers for PDT in oncology. To minimize the potential deleterious effect of flavins on cells, typically the isoalloxazine moiety of flavin cofactors is deeply buried in the protein core of flavoproteins or storage proteins [2]. On the other hand, genetically encoded fluorescent proteins have inherently very low efficiency of $^1O_2$ production (Φ_Δ<0.09). As a consequence, we were interested in what factors determine the efficiency of $^1O_2$ production.

Aims. We present detailed analysis of the irradiation effects on two variants of the LOV2 domain from *Avena sativa* (AsLOV2); wild type, AsLOV2 wt, and the variant with a replaced critical cysteine residue, AsLOV2 C450A, which is responsible for the formation of cysteinyl-flavin adduct in the phototropin 1 photocycle.

Methods. For the analysis, we utilized set of experimental methods including: (i) sample irradiation (by laser) and singlet oxygen phosphorescence determination, (ii) measurements of FMN triplet state lifetime, (iii) spectral analysis by UV-VIS absorption, fluorescence, circular dichroism, (iv) molecular modeling, and (v) mass spectrometry approaches, namely top-down and bottom-up analyses.

Results and Discussion. The experimental time-courses of the $^1O_2$ phosphorescence signals are shown in Figure 1A and 1B for the AsLOV2 wt and the C450A variant, respectively. In the case of low irradiation (blue points), the phosphorescence signal is only present during the first 15-20 µs following the laser pulse for the AsLOV2 wt, while it persists well after 50 µs for AsLOV2 C450A. This observation is in qualitative agreement with the measured ^{3}FMN lifetime values (1.6 µs and 53 µs) and taking the lifetime of singlet oxygen in water (ca. 3.5 µs) into account.

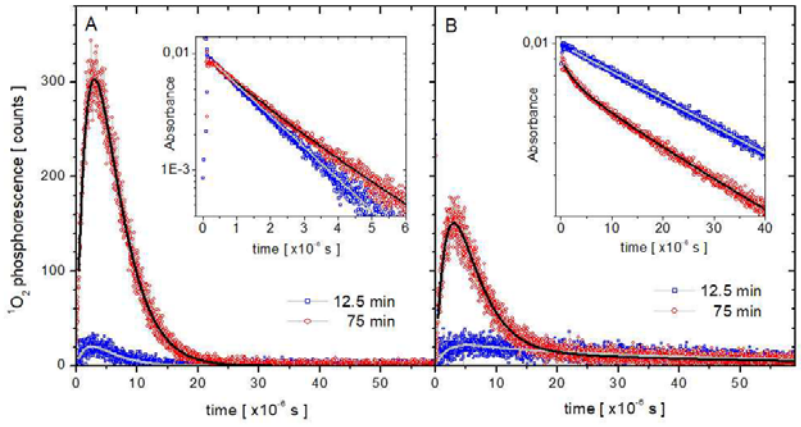

Fig. 1. The time course of the singlet oxygen phosphorescence signal for AsLOV2 wt (A) and AsLOV2 C450A (B). The solid blue and the open red points belong to samples after short and extensive irradiation (12.5 min and 75 min), respectively. The lines represent the results of the fitting procedures. Inserts: The decay of the FMN triplet state absorbance following the excitation laser pulse as measured for AsLOV2 wt and AsLOV2 C450A at 633 nm.

The phosphorescence kinetics changes dramatically upon prolonged irradiation of the samples. For both the wild type and the C450A variants of AsLOV2, the intensity of the phosphorescence signal increased significantly after 75 min of irradiation, indicating enhanced $^1O_2$ production. This production can be assigned to FMN dissociated from the protein and released to the water environment [3].

Based on the mass-spectrometry data it can be concluded that: (i) the modifications occurring in AsLOV2 upon irradiation consist of various products of amino acid side chain oxidations, (ii) the modifications are light-dependent as the overall extent of the oxidative modifications is much higher in irradiated samples of both AsLOV2 wt and the AsLOV2 C450A variant, (iii) generally the same amino acids are oxidized in AsLOV2 wt and its C450A variant, (iv) the extent of some oxidative modification is higher in AsLOV2 C450A variant compared to

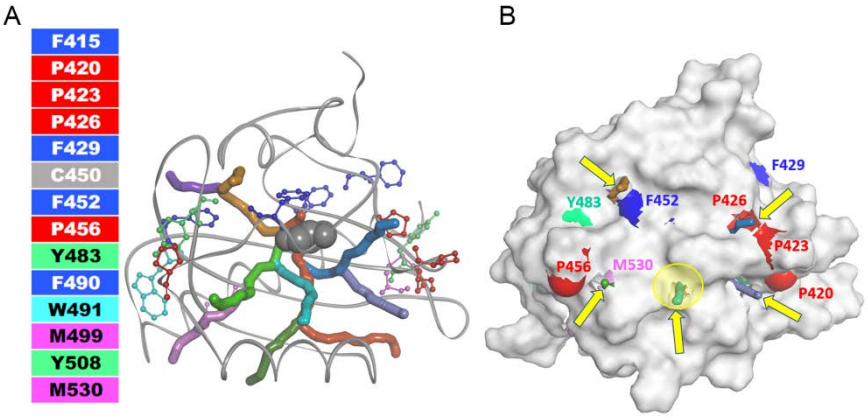

Fig. 2. Discovery Studio visualization of Caver-calculated tunnels of minimized PDB ID: 2v0u structure. **A)** Ribbon representation of the protein with color-coded amino acids modifies upon irradiation shown in ball and stick representation. C450 is shown in grey CPK representation. **B)** Surface representation of the protein with color coding of the amino acids of interest on the surface. The yellow arrows highlight the tunnels reaching the protein surface. The ribityl chain of FMN structure (not shown) overlaps with the circled tunnel 1 (yellow semitransparent circle).

AsLOV2 wt (Figure 2).

Conclusion. We show that an irradiation-induced increase of $^1O_2$ production in the AsLOV2 variants is due to a release of FMN to solvent as a result of oxidative modification of certain amino acids, predominantly the reactive cysteine 450, localized nearby the isoalloxazine ring in the AsLOV2 structure. Our findings may be utilized in design of more efficient genetically encoded photosensitizers based on LOV domains, as follows. In this case, the protein scaffold serves merely as a carrier and the flavin cofactor as a payload that is released at the site of action. The release of the flavin can be achieved by any perturbation of protein structure such as intensive blue light irradiation or combined approach including both irradiation and thermogenesis [4]. The irradiation can be more efficient in releasing FMN, if the binding site of isoalloxazine ring becomes repulsive upon irradiation, either through steric clashes or through charge repulsion.

Acknowledgement
This work was supported by Slovak Research and Development Agency through the project APVV-20-0340 and by the grant agency of the Ministry of Education, Science, Research, and Sport of the Slovak Republic (grant no. VEGA 1/0557/20). This publication is the result of the implementation of the project OPENMED (Open Scientific Community for Modern Interdisciplinary Research in Medicine) ITMS2014+: 313011V455 from the Operational Program Integrated Infrastructure funded by the ERDF.

References
[1] M. Westberg, M. Bregnhøj, M. Etzerodt, P.R.Ogilby, J. Phys. Chem. B, 121 (2017), 2561-2574.
[2] R. Baron, C. Riley, P. Chenprakhon, K. et al., Proc. Natl. Acad. Sci. U.S.A. 106 (2009), 10603-10608.
[3] M. Petrenčáková, F. Filandr, A. Hovan, et al., Sci. Rep. 10 (2020), 4119.
[4] M. Petrenčáková, R. Varhač, T. Kožár, et al., Biophys. Chem. 259 (2020),106337.

Mechanics and evolution of Hsp70

G. Žoldák[1]

[1] *Department of Biophysics, Faculty of Science, Pavol Jozef Šafárik University, Jesenná 5, 040 01 Košice, Slovakia..*

e-mail: gabriel.zoldak@upjs.sk

Protein allostery requires a communication channel for functional regulation between distal sites within a protein. In the molecular chaperone Hsp70, a two-domain enzyme, the ATP/ADP status of an N-terminal nucleotide-binding domain regulates the substrate affinity of a C-terminal substrate-binding domain. Recently available three-dimensional structures of Hsp70 in ATP/ADP states have provided deep insights into molecular pathways of allosteric signals. However, direct mechanical probing of long-range allosteric coupling between the ATP hydrolysis step and domain states is missing.

In my talk, I will focus on the single-molecule mechanics and evolution of bacterial Hsp70 [1-4]. Using laser optical tweezers, my group examined the mechanical properties of a truncated two-domain DnaK(1-552ye) in apo/ADP/ATP and peptide-bound states. We find that in the apo and ADP states, DnaK domains are mechanically stable and rigid. However, in the ATP-state, SBD*ye is mechanically destabilized as the result of interdomain docking followed by the unfolding of the α-helical lid. By observing the folding state of the SBD, we could observe the continuous ATP/ADP cycling of the enzyme in real time with a single molecule. The SBD lid closure is strictly coupled to the chemical steps of the ATP hydrolysis cycle even in the presence of peptide substrate.

In a recent paper[4], we examined how such an opening and formation of alternative subdomain interfaces of Hsp70 is affected during their evolution. In particular, insertion and deletion events (indels) can be highly disruptive for the mechanical events since such changes introduce a collective shift in the pairing interactions at communicating interfaces. Based on a multiple sequence alignment analysis of data collected from Swiss-Prot/UniProt database, we find several indel-free regions (IFR) in Hsp70. The two largest IFRs are located in interdomain regions that participate in allosteric structural changes. We speculate that the reason why the indels have a lower likelihood of occurrence in these regions is that indel events in these regions cause dysfunction in the protein due to perturbations of the mechanical balance.

Thus, the development of functional allosteric machines requires including a concept of the balance between mechanical structural elements.

Acknowledgement

This work was supported by research grants from the Slovak research and development agency (No. APVV-18-0285), the Slovak Grant Agency VEGA No 1/0024/22, EU H2020 TWINNING program GA. No. 952333 project CasProt, BioPickmol, ITMS2014+: 313011AUW6 supported by the Operational Programme Integrated Infrastructure, funded by the ERDF.

References

[1] Bauer D., et al., Proc Natl Acad Sci U S A., 2015, **112(33)**, 10389-10394.
[2] Mandal S.S. et al., Proc Natl Acad Sci U S A., 2017, **114(23)**, 6040-6045.
[3] Bauer D.. et al., Proc Natl Acad Sci U S A. 2018, **115(18)**, 4666-4671.
[4] Gala M., Pristaš P., Žoldák G., Int J Mol Sci., 2022, **23(5)**, 2788.

Directed evolution of a staphylokinase, a thrombolytic agent, by ribosome display technology

M. Tomková [1], V. Dzurillová[2], E. Sedlák[1]

[1]*Center for Interdisciplinary Biosciences, Technology and Innovation Park, P. J. Šafárik University, Jesenná 5, 041 51 Košice, Slovakia*
[2]*Department of Biophysics, Faculty of Science, P. J. Šafárik University, Jesenná 5, 041 51 Košice, Slovakia*

e-mail: maria.tomkova@upjs.sk

Ischemic stroke and myocardial infarct are leading causes of death and disability worldwide. Usage of currently available thrombolytics is limited due to their high immunogenicity and haemorrhagic complications. Staphylokinase (SAK) is a single chain extracellular protein secreted by *Staphylococcus aureus*. It initiates the fibrinolytic cascade to help invading bacterium move deeper into the tissues. SAK is highly fibrin specific, and its characteristics makes it a promising new thrombolytic target. However, not all SAK features are optimized for its practical applications, leaving a room for its improvement. Engineering the affinity and selectivity of SAK could increase its residence time on plasmin, thus reducing the severity of side effects [1].

Directed evolution is a powerful approach to tailor protein properties toward new or enhanced functions [2]. We employed ribosome display (Figure 1), *in vitro* selection and evolution method, to improve SAK affinity for plasmin. Although ribosome display has been used in our laboratory for evolving several different proteins, SAK evolution workflow needed some principal adjustments. Human plasmin was used as an antigen, against which SAK variants were selected.

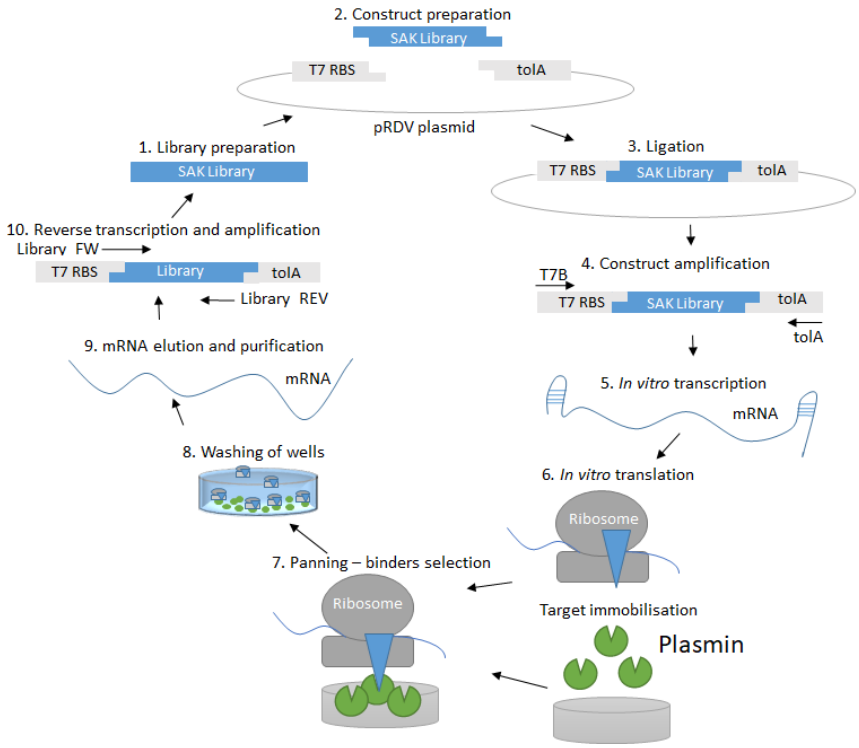

Fig. 1. Overview of the ribosome display selection.

We have successfully implemented selection of SAK variants by ribosome display and after first round of display we proved that it is feasible to evolve SAK by this technology. Evolution

techniques usually require several consecutive rounds, therefore we accomplished second and third round of the display. Sequencing of individual clones after 3rd round of ribosome display revealed some identical amino acid substitutions, that were found in several different mutants, indicating that such residues might be involved in SAK-plasmin interaction and its replacement might change SAK property towards higher plasmin affinity.

Inefficient binding to plasmin is the main factor limiting overall SAK effectivity. Enhancement of SAK's affinity for plasmin is a highly desirable objective. Preliminary data obtained from SAK engineered by ribosome display showed that the evolution approach has high potential to improve the properties of SAK. However, to prove this statement we need to perform further rounds of ribosome display followed by detailed biophysical characterisation of selected mutants.

Acknowledgement

This work was supported by Slovak Research and Development Agency through the project APVV-20-0340 and by the grant agency of the Ministry of Education, Science, Research, and Sport of the Slovak Republic (grant no. VEGA 1/0074/22). This publication is the result of the implementation of the project OPENMED (Open Scientific Community for Modern Interdisciplinary Research in Medicine) ITMS2014+: 313011V455 from the Operational Program Integrated Infrastructure funded by the ERDF.

References

[1] D. Nikitin, J. Mican, M. Toul, D. Bednar, M. Peskova, P. Kittova, S. Thalerova, J. Vitecek , J. Damborsky, R. Mikulik, S.J. Fleishman , Z. Prokop and M. Marek, Comput. Struct. Biotechnol. J., 20 (2022), 1366-1377.

[2] Ch. Zahnd, P. Amstutz and A. Plückthun. Nat. Methods, 4 (2007), 269-279.

Utilisation of HaloTag technology in directed evolution of haloalkane dehalogenase DhaA

V. Dzurillová[1], E. Sedlák[2]

[1] *Department of Biophysics, Faculty of Science, P.J. Šafárik University, Jesenná 5, 041 54 Košice, Slovakia*
[2] *Center for Interdisciplinary Biosciences, Technology and Innovation Park, P.J. Šafárik University, Jesenná 5, 041 54 Košice, Slovakia.*

e-mail: veronika.dzurillova@student.upjs.sk

Haloalkane dehalogenases (HLDs) represent a group of hydrolyses enabling cleavage of carbon-halogen bond by which facilitate the conversion of toxic halogenated hydrocarbons to non-hazardous alcohols. The dehalogenation catalysed by these enzymes is a reaction of great industrial importance. HLDs are used in a wide variety of applications in biocatalysis, decontamination, biosensing or cellular imaging [1]. Its considerable application potential is highlighted in the field of bioremediation of eminent environmental pollutants such as 1,2-dichloroethane or 1,2,3-trichloropropane [2]. However, the practical use of HLDs has several limitations, such as limited stability and insufficient catalytic efficiency of natural HLDs. Modification of these complex properties of enzymes can be achieved using efficient methods of directed protein evolution.

To address the issue of low catalytic efficiency of selected HLD, we applied powerful protein evolution method - the ribosome display, which enable us to perform robust selection from protein libraries containing up to 10^{12} members per selection round. In order to obtain enrichment of improved HLD, the HaloTag technology [3] was implemented for capturing of protein library against immobilized biotinylated chloroalkane. The stable covalent bond between displayed enzyme and substrate (HaloTag Ligand) was mediated through formation of alkyl-enzyme intermediate based on underlying principle of HaloTag technology [Fig. 1]. DhaA variants from randomised libraries were successfully selected upon several consecutive rounds of ribosome display. Based on following sequence analysis, we were able to identify several hot-spot mutations. Our results suggest the feasibility using ribosome display and HaloTag technology in evolution-directed engineering of HLDs.

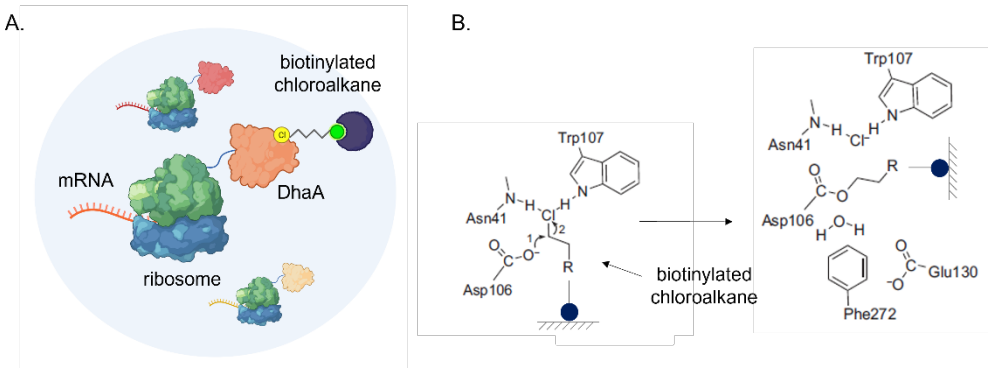

Fig. 1. A. Immobilization of mutant enzyme DhaA through biotinylated chloroalkane in ribosome display during selection step after *in vitro* translation. B. Formation of covalent bond between chloroalkane and Asp106 inside the catalytic site of DhaA [3].

Acknowledgement
We would like to express our thanks to prof. Jiří Damborský for providing us plasmids carrying haloalkane dehalogenase genes. This work was supported by Slovak Research and Development Agency through the project APVV-20-0340 and by the grant agency of the Ministry of Education, Science, Research, and Sport of the Slovak Republic (grant no. VEGA 1/0557/20). This publication is the result of the implementation of the project OPENMED (Open Scientific Community for Modern Interdisciplinary Research in Medicine) ITMS2014+: 313011V455 from the Operational Program Integrated Infrastructure funded by the ERDF.

References

[1] T. Koudelakova et al., Biotechnol. J., 8 (2013), 32-45.
[2] D. Janssen,, Curr Opin Chem Biol., 8 (2004), 150-159.
[3] G. Los, et al., ACS Chem. Biol., 3 (2008), 373-382.

Mg^{2+} binding to RyRs moderates spontaneous calcium sparks

B. Iaparov, I. Baglaeva, I. Zahradník and A. Zahradníková

Department of Cellular Cardiology, Institute of Experimental Endocrinology, Biomedical Research Center, Slovak Academy of Sciences, Dúbravská cesta 9, 845 05 Bratislava, Slovak Republic.

e-mail: bogdan.iaparov@savba.sk

In cardiac muscle cells, ryanodine receptors (RyRs) form thousands of calcium release sites (CRSs) aimed to release calcium ions (Ca^{2+}) from the sarcoplasmic reticulum to the cytoplasm and so to initiate the contraction of sarcomeres. *In situ* [1,2] and *in vitro* [3,4] experiments demonstrated the inhibitory effect of magnesium ions (Mg^{2+}) on ryanodine receptor activity due to Mg^{2+} binding to the RyR inhibition site as well as due to Mg^{2+}/Ca^{2+} competition at the RyR activation site.

Despite being important for the understanding of intracellular calcium dynamics, the impact of RyR modulation by Mg^{2+} on calcium release is not well understood. To shed light on the effects of Mg^{2+}, we developed an *in silico* model of the CRS based on a quantitative description of RyR geometric arrangement in the CRS, RyR gating and ion binding, and calcium diffusion to analyse the dependence of simulated calcium release events (CREs), i.e., calcium sparks, on the strength and kinetics of Mg^{2+} binding to RyRs.

The results of numerical simulations allowed us to classify CREs into three subtypes, differing by the number of RyRs recruited by a random opening of one RyR of a CRS, namely quarks (a single opening of a RyR), blips (openings of several RyRs), and sparks (openings of a larger RyR number). To quantitatively characterize the relationship between the characteristics of CREs (frequency of CREs and the maximum number of simultaneously open RyRs during the CRE) and the determinants of CRSs, such as RyR placement (RyR vicinity v_i [5]), calcium current (i_{Ca}), allosteric coupling ($1/f_{Mg}$) and Mg^{2+} binding to the RyR activation (k_{AoffMg}, k_{AonMg}) and inhibition (k_{IoffMg}, k_{IonMg}) sites [6], we introduced the effective coupling strength between RyRs as:

$$\varphi_i^{effF} = v_i \, i_{Ca}^{\alpha} \left(\frac{1}{f_{Mg}^{rel}}\right)^{\beta}, \tag{1a}$$

$$\varphi_i^{effA} = v_i \, i_{Ca}^{\alpha} \frac{\left(k_{AoffMg}^{rel}\right)^{\gamma_{off}}}{\left(k_{AonMg}^{rel}\right)^{\gamma_{on}}}, \tag{1b}$$

$$\varphi_i^{effI} = v_i \, i_{Ca}^{\alpha} \frac{\left(k_{IoffMg}^{rel}\right)^{\delta_{off}}}{\left(k_{IonMg}^{rel}\right)^{\delta_{on}}}, \tag{1c}$$

where the exponents α, β, γ_{off}, γ_{on}, δ_{off}, and δ_{on} are the weight factors that determine the contribution of the respective RyR parameters to CRS activity relative to the contribution of RyR vicinity [6]. The index *rel* means that the parameters are relative to the reference values. The exponents were determined by maximizing the mutual information [7] between the effective coupling strengths and the characteristics of CREs.

A closer inspection of Figure 1 (see pairs of symbols representing changes of individual Mg-binding parameters) revealed that the characteristics of CREs react sensitively and specifically to the respective changes of the effective coupling strength. Moreover, $\gamma_{off} \neq \gamma_{on}$ and $\delta_{off} \neq \delta_{on}$, i.e., the effect of binding and unbinding on the effective coupling strength is asymmetric. For the frequency of CREs, the unbinding rate from the activation site and the binding rate to the inhibition site contribute the most. An increased effective coupling strength leads to an increased frequency of spontaneous sparks.

The results of simulations revealed the role of Mg^{2+} ions as a protector of the CRS from the spontaneous activation in the absence of an external stimulus. This finding is of principal physiological importance since spontaneous calcium sparks may cause arrhythmias, glucose intolerance, and neuronal disorders [8].

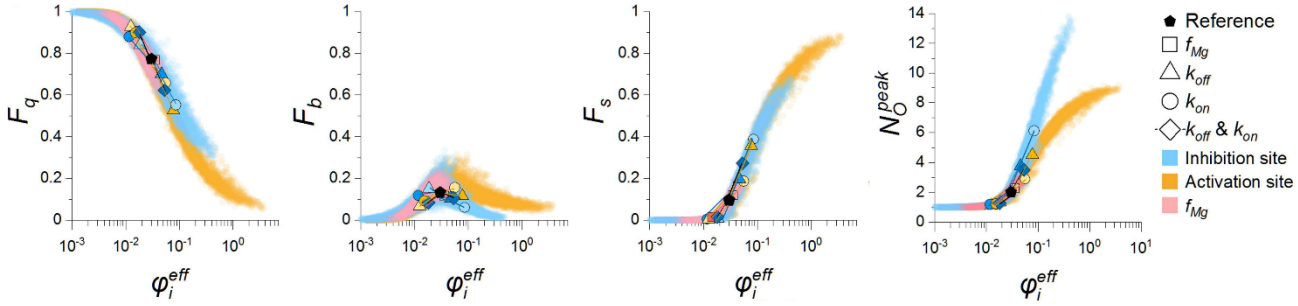

Fig. 1. The characteristics of simulated calcium release events at different effective coupling strengths. F_q, F_b, F_s are the frequencies of quarks, blips, and sparks, respectively, N_O^{peak} is the mean maximum number of open channels. The dots show the whole dataset on all panels for various Mg-binding parameters of the RyR activation site (orange), allosteric coupling (pink), and the RyR inhibition site (blue), which were obtained for all RyR vicinities and all single-channel calcium currents (not indicated). The circles, triangles, and diamonds mark results for decreased (×0.5; lighter color) or increased (×2; darker color) Mg-binding parameter values (see legend), relative to the reference parameter values (black pentagons). Adapted from [6].

Acknowledgment

The research was supported by the SAV-TUBITAK project JRP/2019/836/RyRinHeart, by the project VEGA 2/0182/21, and by the Operational Programme Integrated Infrastructure for the project: Long-term strategic research of prevention, intervention, and mechanisms of obesity and its comorbidities, IMTS: 313011V344, co-financed by the European Regional Development Fund.

References

[1] V. Lukyanenko, S. Viatchenko-Karpinski, A. Smirnov et al., Biophys. J. 81 (2001), 785–798.
[2] K. Gusev and E. Niggli, J. Gen. Physiol. 132 (2008), 721–730.
[3] D. Laver, M. Baynes and A. Dulhunty, J. Membr. Biol. 156 (1997), 213–229.
[4] A. Zahradnikova, M. Dura, S. Gyorke et al., Am. J. Physiol. 285 (2003), C1059–C1070.
[5] B. Iaparov, I. Zahradnik, A. Moskvin and A. Zahradnikova, J. Gen. Physiol. 153 (2021), e202012685.
[6] B. Iaparov, I. Baglaeva, I. Zahradnik and A. Zahradnikova, Front. Physiol. 12 (2022), 805956.
[7] C. Shannon, Bell Syst. Tech. J. (1948), 379–423.
[8] Y. Sleiman, A. Lacampagne and A. C. Meli, Cell Death Dis. 12 (2021), 1041.

The cardiac ryanodine receptor provides a suitable pathway for the rapid transport of zinc (Zn^{2+})

J. Gaburjakova[1] and M. Gaburjakova[1]

[1] *Institute of Molecular Physiology and Genetics, Centre of Biosciences, Slovak Academy of Sciences, Dubravska cesta 9, 840 05 Bratislava, Slovak Republic.*
e-mail: marta.gaburjakova@savba.sk

Zinc (Zn^{2+}) is one of the most abundant metal cations in mammalian cells, with diverse functions in numerous physiological processes. Both Zn^{2+} deficiency and its excess have been documented in a wide range of pathological conditions, including cancer, cardiovascular and neurodegenerative diseases. While catalytic and structural functions of Zn^{2+} are well-established in a great number of metalloproteins, Zn^{2+} signaling capacities have only recently received extensive attention. The sarcoplasmic reticulum (SR) in cardiac muscle is suggested to act as dynamic storage for Zn^{2+} release and reuptake, albeit it is primarily implicated in the Ca^{2+} signaling required for the cardiac cycle [1,2]. A large Ca^{2+} release from the SR is mediated by the cardiac ryanodine receptor (RYR2), and while this has a prominent conductance for Ca^{2+} *in vivo* [3], it also conducts other divalent cations (Mg^{2+}, Sr^{2+}, or Ba^{2+}) *in vitro* [4,5].

Since both Mg^{2+} and Zn^{2+} possess similar physical properties relevant to permeation through ion channels [6], we examined whether the RYR2 channel provides a suitable permeation pathway for Zn^{2+}.

RYR2 channels isolated from rat ventricular muscle [5] were incorporated into planar lipid membranes (BLMs) and examined under voltage-clamp conditions as described in [7]. Representative RYR2 recordings when 8 mM $[Zn^{2+}]_L$ was present in the luminal compartment and the membrane voltage was applied are shown in Fig. 1. At 0 mV, the Zn^{2+} current was 0.927 ± 0.093 pA. It is comparable to but significantly smaller than those obtained for luminal Ca^{2+} (2.835 ± 0.094 pA) or even Mg^{2+} (1.822 ± 0.079 pA) under similar conditions. Accordingly, the values of ion conductance (G) fall in the sequence Ca^{2+} (127.5 ± 1.8 pS) > Mg^{2+} (95.3 ± 1.4 pS) > Zn^{2+} (81.1 ± 2.4 pS).

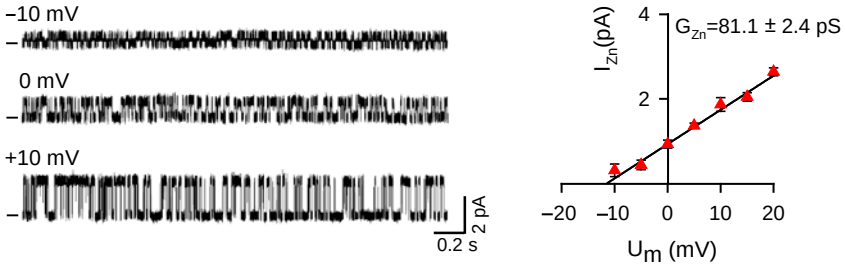

Fig. 1. Representative RYR2 currents, shown as upward deflections from the marked zero-current level, in the presence of 8 mM $[Zn^{2+}]_L$ and at the membrane voltage of −10, 0, and +10 mV. The RYR2 channel was activated by 6–7 mM caffeine in the presence of 90 nM free $[Ca^{2+}]_C$. The current-voltage relationship was well-fitted by a straight line with the G_{Zn} value of 81.1 ± 2.4 pS. Data shown are average ± SEM of 5–7 experiments.

Furthermore, we evaluated the Zn^{2+} permeability coefficient relative to Ca^{2+}. We performed mole-fraction experiments with a mixture of Zn^{2+} and Ca^{2+} on the luminal side (8 mM total concentration) and monitored the changes in RYR2 permeation properties. The permeability coefficient for Zn^{2+} (P_{Ca}/P_{Zn} = 2.65 ± 0.19), estimated by fitting dependence of reversal potential on the composition of Zn^{2+}/Ca^{2+} mixture by the well-known Goldman-Hodgkin-Katz equation, was found to be ~2.3-fold lower than that of Mg^{2+} (P_{Ca}/P_{Mg} = 1.146 ± 0.071) determined in a luminal Mg^{2+}/Ca^{2+} mixture. Our results clearly indicate that the RYR2 channel can differentiate, albeit only moderately, between Zn^{2+} and Mg^{2+} or Ca^{2+}, providing a slower path to Zn^{2+}. The existence of a

Zn^{2+} gradient across the SR membrane, albeit ~166-fold smaller than for Ca^{2+}, together with a considerable RYR2 permeability for Zn^{2+}, is compatible with the biological significance of the RYR2 Zn^{2+} current. Tuncay et al. [8] support this idea by visualizing ryanodine-sensitive Zn^{2+} transients in cardiomyocytes having similar kinetics to those of Ca^{2+}. In an attempt to identify a potential target of the RYR2 Zn^{2+} current, we calculated the free [Zn^{2+}] profile around an open RYR2 pore. [Zn^{2+}] in the picomolar-nanomolar range has been shown to shape Ca^{2+} release by amplifying the Ca^{2+}-induced RYR2 activity [9]. According to our simple calculations, the Zn^{2+} current of more than or equal to 4.1×10^{-6} pA (~ 0.0008% of the RYR2 current in cardiomyocytes) should be sufficient for the building up of activating [Zn^{2+}] near neighboring RYR2 channels (Fig. 2). In addition, we assessed whether the channel itself could be a direct target of the Zn^{2+} current, having the Zn^{2+} finger extended into the cytosolic vestibular portion of the permeation pathway [10]. Considering the extremely high binding affinities of Zn^{2+} fingers in the femtomolar range, we estimated that even an extremely small Zn^{2+} current (from 1.5×10^{-12} pA to 1.5×10^{-9} pA) would be sufficient to saturate the Zn^{2+} finger (Fig. 2). We also attempted to displace Zn^{2+} from the RYR2 Zn^{2+} finger to induce its structural defects, which are associated with RYR2 dysfunction [10]. Zn^{2+} chelators were added to the cytosolic side of the channel or the strongly competing Cd^{2+} ions were allowed to permeate the RYR2 channel. Only the Cd^{2+} current was able to cause the decay of channel activity, presumably as a result of Zn^{2+} to Cd^{2+} replacement.

We identified the RYR2 channel as a novel Zn^{2+} transporting protein in the SR membrane that might play a role in local and/or global Zn^{2+} signaling in cardiomyocytes, considering the much faster ion movement through ion channels in comparison with the passive transport mediated by carrier-type transporters.

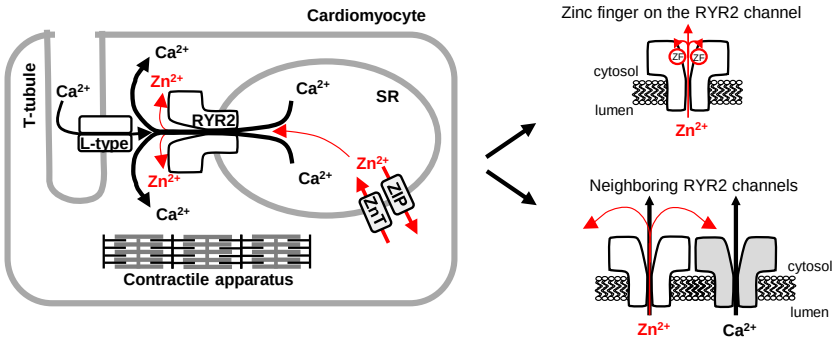

Fig. 2. Schematic illustrating three pathways (one novel) for Zn^{2+} transport across the cardiac SR membrane. Two Zn^{2+} transporter protein families, ZIP and ZnT, mediate a slow-rate transport. The RYR2 channel could also contribute to global and/or local Zn^{2+} signaling which requires a fast-rate transport. At the local scale, the Zn^{2+} current through the RYR2 channel might target its intrinsic Zn^{2+} finger (ZF). In addition, the RYR2 channel (colored gray) might be stimulated by Zn^{2+} cations emanating from the neighboring RYR2 channel (colored white).

Acknowledgment
This work was supported by VEGA 2/0018/21, VEGA 2/0008/20, ITMS 26230120009.

References

[1] M. Endo, M. Tanaka and Y. Ogawa, Nature, 228 (1970), 34–36.
[2] A. Fabiato, Am. J. Physiol., 245 (1983), C1–C14.
[3] A. Tinker, A. and A.J. Williams, J. Gen. Physiol., 100 (1992), 479–493.
[4] P.L. Diaz-Sylvester, M. Porta and J.A. Copello, PLoS One, 6 (2011), e26693.
[5] J. Gaburjakova and M. Gaburjakova, Bioelectrochemistry,109 (2016), 49–56.
[6] D. Gillespie, Biophys. J., 94 (2008), 1169–1184.
[7] J. Gaburjakova and M. Gaburjakova, Cells, 11 2022), 868.
[8] E. Tuncay, A. Bilginoglu, N.N. Sozmen, E.N. Zeydanli, M. Ugur, G. Vassort and B. Turan, Cardiovasc. Res., 89 (2011), 634–642.
[9] J. Woodier, R.D. Rainbow, A.J. Stewart and S.J. Pitt, J. Biol. Chem., 290 (2015), 17599–17610.
[10] W. Peng, H. Shen, J. Wu, W. Guo, X. Pan, R. Wang, S.R.W. Chen and N. Yan, Science, 354 (2016), aah5324.

Interaction of ligands and calcium pump

M. Májeková[1], V. Heger[1], L. Kissová[1] and Y. Rodríguez[2,3]

[1] *Centre of Experimental Medicine SAS, Institute of Experimental Pharmacology and Toxicology,Dubravska 9, 841 04, Bratislava, Slovakia.*
[2] *Department of Natural Sciences, CUNY's Hostos Community College, 475 Grand Concourse, Bronx, 10451, New York, United States of America.*
[3] *Department of Pharmacological Sciences, Icahn School of Medicine at Mount Sinai, 1425 Madison Avenue, New York, NY 10029, USA.*

e-mail: magdalena.majekova@savba.sk

The calcium pump (Ca^{2+}-ATPase, SERCA) (Fig. 1) plays a key role in maintaining the calcium homeostasis in cells. Thus, targeting SERCA represents an efficient way of treating various chronic diseases. During the catalytic process, SERCA undergoes several structural changes connected with phosphorylation, cation binding, and protonation. We demonstrate the basic conformation changes of SERCA connected with the transition of E1 to E2 state and reversely as well as the possible influencing of individual states by external/internal ligands.

We performed molecular docking and full optimization of SERCA bound with rutin derivatives (inhibitors) [1] and compound CDN1163 (activator) [2]. Moreover, for SERCA bound with rutin-arachidonate also molecular dynamics simulation of complex positioned in a dipalmitoyl-phosphatidylcholine bilayer membrane was completed.

According to our results, rutin-arachidonate was bound in the transmembrane region of SERCA, thus affecting the transport of calcium ions and protons. The compound CDN1163 was bound in the cytoplasmic region, which may be the source of its allosteric activation of SERCA.

Both results may be used in further studies of inhibition and activation mechanisms as well as in the design of novel compounds with therapeutic potential.

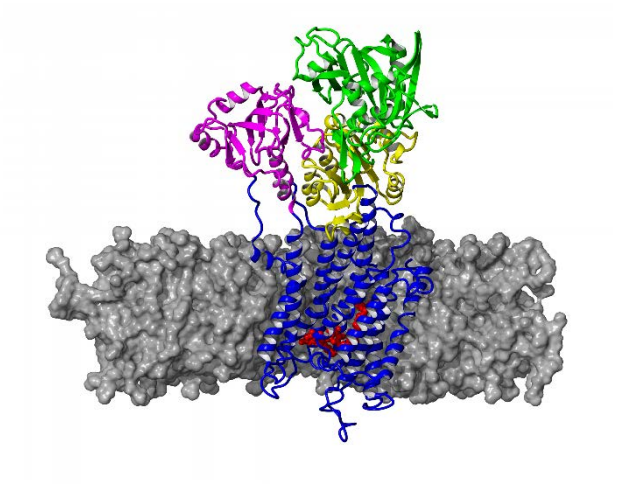

Fig. 1. The calcium pump SERCA, immersed in the membrane.

Acknowledgment
This work was supported by the VEGA 2/0103/22 and by the Slovak Research and Development Agency under contract No. APVV-20-0543.

References

[1] Y. Rodríguez and M. Májeková, Biomolecules, 10 (2020), 214.
[2] S. Kang, R. Dahl R, et al., J Biol Chem., 291 (2016), 5185–5198.

Application of nanoparticles modified by DNA aptamers in biosensing and targeted drug delivery

V. Subjakova, M. Tatarko , S. Mikulicova , S. Melikishvili and T. Hianik

Faculty of Mathematics, Physics and Informatics, Comenius University, Mlynska Dolina F1, 842 48 Bratislava, Slovakia

e-mail: veronika.subjakova@fmph.uniba.sk

Early diagnosis of disease, mainly cancer, or foodborne pathogens may prevent increasing mortality. In addition to early diagnosis, another important step is to select the appropriate and effective therapy for targeted drug delivery to avoid side effect for healthy tissue. Aptamers and nanoparticles offer potential tools for diagnosis and therapy for various disease. Nanoparticles possess unique chemical and physical properties depending on size, shape, structure, and material, for example gold, carbon, graphene, polymers, etc. Nanoparticles are promising candidates for immobilization platform or enhancement of signal due to high surface area in biosensors and can serve as carries for drugs. Aptamers are short single stranded DNA/RNA oligonucleotides that can bind different targets with high specificity and selectivity. They can fold in three-dimensional structure that allows application in design biosensing and targeted delivery in treatment [1].

One of the most often used sensing strategy is, for example, OFF-ON fluorescence switching. The strategy is based on the dye fluorescence quenching with a quencher due to fluorescence resonance energy transfer (FRET) [2]. Graphene oxide (GO) is often used as a quencher and can easily adsorb DNA through π–π interaction. Fluorescent labeled aptamer is adsorbed on the GO surface. In the presence of the target molecule, the aptamer changes its conformation and is released from the surface leading to an increase in fluorescence intensity and a change in fluorescence anisotropy. The aim of the presented work is an overview of the potential of nanoparticles and DNA aptamers for biosensing and targeted drug delivery, together with a FRET sensing strategy using graphene oxide.

Acknowledgement

This work was supported by Higher Education, Science Grant Agency, grant No. VEGA 1/0419/20 and by Agency for Promotion Research and Development under the contract SK-BY-RD-19-0019 and by NAWA International Academic Partnership Programme EUROPARTNER.

References

[1] V. Subjakova, V. Oravczova, T.Hianik, Polymers, 13 (2021), 1-4 .
[2] M. Beltrán-Gastélum, B. Esteban-Fernández de Ávila, H. Gong, P. Lekshmy Venugopalan, T. Hianik, J. Wang, V. Subjakova, ChemPhysChem. 20 (2019), 3177-3180.

Application of QCM-D for analysis of molecular interactions at surfaces

M. Tatarko[1], V. Šubjaková[1], M. Csiba[1], V. Oravczová[1], S. Spagnolo[1], J. Süle[2] and T. Hianik[1]

[1] *Department of Nuclear Physics and Biophysics, Faculty of Mathematics, Physics and Informatics, Comenius University, Mlynská dolina F1, 842 48 Bratislava, Slovakia*
[2] *Hungarian Dairy Research Institute Ltd., -HDRI Ltd., Lucsony u. 24, 9200 Mosonmagyaróvár, Hungary.*

e-mail: tatarko4@uniba.sk

Acoustic methods are promising tool for monitoring interactions between nucleic acid aptamers and their target. They are often employed in various aptamer-based biosensors with remarkable sensitivity and specificity. However, certain limitations, such as sensitivity to the buffer composition and possible matrix effect in a complex liquid prevent their wide applications.

Here we describe application of the multiharmonic quartz crystal microbalance with dissipation (QCM-D) to study the interactions between aptamers and their targets such as bacteria and cytochrome c (cyt c).

QCM-D monitors the changes in resonant frequency and dissipation of piezocrystal at various modification of its surface, for example by aptamers. It was used for detection of *Listeria innocua*, *Listeria monocytogenes* as well as *E. coli* as a nonspecific target [1]. Using Kelvin-Voigt viscoelastic model [2] we also analyzed viscoelastic properties of the layers. At higher concentration of bacteria, we observed anomalous increase of the resonant frequency, which may be explained by spring-like effect (Fig. 1). Determination of penetration depth, viscosity and elasticity parameters allowed us to receive information about the changes of these values for the surface layers.

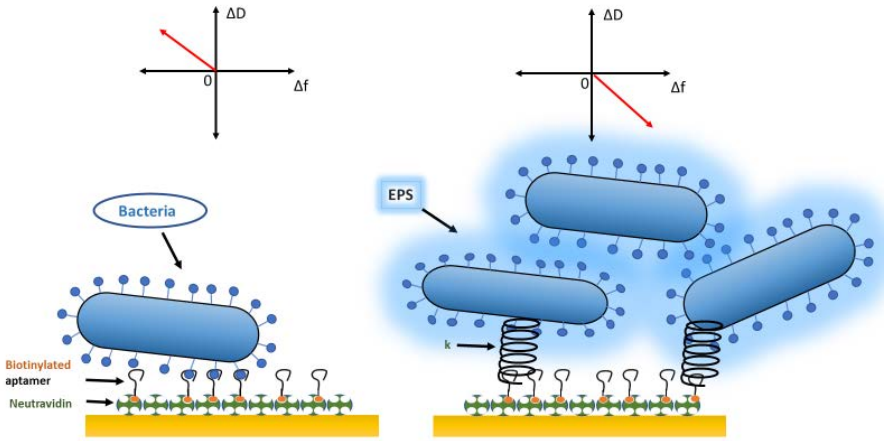

Fig. 1. Scheme of the interaction between aptamer layer and bacteria. Bacteria interacts with biotin-modified aptamers immobilized on the surface using NeutrAvidin layer (left). Higher concentration of bacteria forms extracellular polymeric substance (EPS) and causes “spring-like” effect of coupled resonators on the crystal surface (right).

We also studied the formation of lipid monolayers at the surface of piezocrystal modified by dodecanethiol and those following adsorption of cyt c. The lipid monolayers have been formed by fusion of small unilamellar liposomes composed of the mixed phospholipids: Dimyristoyl-sn-

glycero-3-phosphocholine (DMPC) and Dimyristoyl phosphatidylglycerol (DMPG) [3] that provide negatively surface charge onto which the cyt c has been adsorbed by electrostatic interactions. Cyt c acts as the main initiator for cell apoptosis. Thus, it can serve as useful biomarker for evaluation of chemotherapy efficacy. Lipid layer containing cyt c molecules was investigated for its interaction with specific aptamer [4]. In addition, nanowires modified with aptamer on the surface were used for possible enhancement of the signal. Analysis of viscoelastic properties provided valuable information about surface dynamics.

Application of multiharmonic QCM-D and Kelvin-Voigt model offers more detailed information about viscoelastic properties of adsorbed layers and molecular interactions which was impossible by traditional QCM that measure only fundamental resonant frequency.

Acknowledgment
This work has received funding from the European Union's Horizon 2020 research and in-novation programme under the Marie Skłodowska-Curie grant agreement No 101007299 and by the Science Grant Agency VEGA, project number: 1/0419/20.

References

[1] M.Tatarko, S. Spagnolo, V. Oravczová et al., Sensors (Basel). 21 (2021), 5585
[2] M. Voinova, Urban Clim.. 24 (2018), 264-275.
[3] T. Enoki, V. Henriques and M. Lamy, Chem. Phys. Lipids. 165 (2012), 826-837.
[4] A. Poturnayova, G. Castillo, V. Subjakova et al., Sens. Actuators B Chem. 238 (2017), 817–827.

Evaluation of the interaction of nano/microplastics with living organisms by microscopy methods

A. Marček Chorvátová[1,2] , M. Uherek[1] , A. Mateašík[1] and D. Chorvát[1]

[1] *Department of Biophotonics, International Laser Center, Slovak Centre of Scientific and Technical Information, Ilkovičova 3, 814 04 Bratislava, Slovakia.*
[2] *Department of Biophysics, FNS, Univ. Ss Cyril and Methodius, J Herdu 1, 917 02 Trnava, Slovakia.*

e-mail: Alzbeta.Marcek.Chorvatova@ucm.sk

Pollution by plastics and microplastics, disintegrating with time into nanoplastics, represents a serious environmental burden of the 21st century. Our aim is to evaluate interactions of nano/microplastics with photosynthetic organisms, based on the study of their endogenous fluorescence derived from chlorophylls. Our previous work demonstrated advantages to employ the fluorescence spectroscopy and microscopy methods to monitor the effect of various environmental stressors on endogenous fluorescence in algae and moss [1-3].

In this work, our aim is to examine the responsiveness of the endogenous chlorophyll fluorescence of sweet water algae *Chlorella sp.* under influence of nano/microplastics. Latex beads with different coatings, including amine-sulfate and sufate-modified polystyrene of 30 nm mean particle size, labelled with yellow-orange fluorescence ex/em 470nm/505nm (Sigma-Aldrich) were tested. Laser scanning confocal microscopy imaging with Axiovert 200 LSM 510 Meta (Carl Zeiss, Germany) equipped with objective C-Apochromat 40x, 1.2 NA was employed. Fluorescence of individual *Chlorella sp* algae was excited with the 458 nm laser-line (Kvant, Slovakia) and detected using a 16 channel META detector. Channel 1, recorded with BP 500-550 filter, served for monitoring the fluorescently-labelled latex beads (Fig. 1, green fluorescence), peaking at 510nm and channel 2, using BP 650-710 filter, was used to record the endogenous chlorophyll fluorescence of algae (Fig. 1, red fluorescence), peaking at 680 nm.

Performed experiments demonstrated maintained endogenous fluorescence of chlorophylls but, at the same time, pointed to the clustering of the nano/microplastic particles around the individual algae cell (Fig. 1 middle and left). Further work is necessary to fully understand the effect of the coating on the algae-plastic interaction and clustering capabilities. Performed research will lead to novel comprehension of the interaction of living organisms with nano/microplastics and will thus help monitoring and removal of this environmental pollution in water sources.

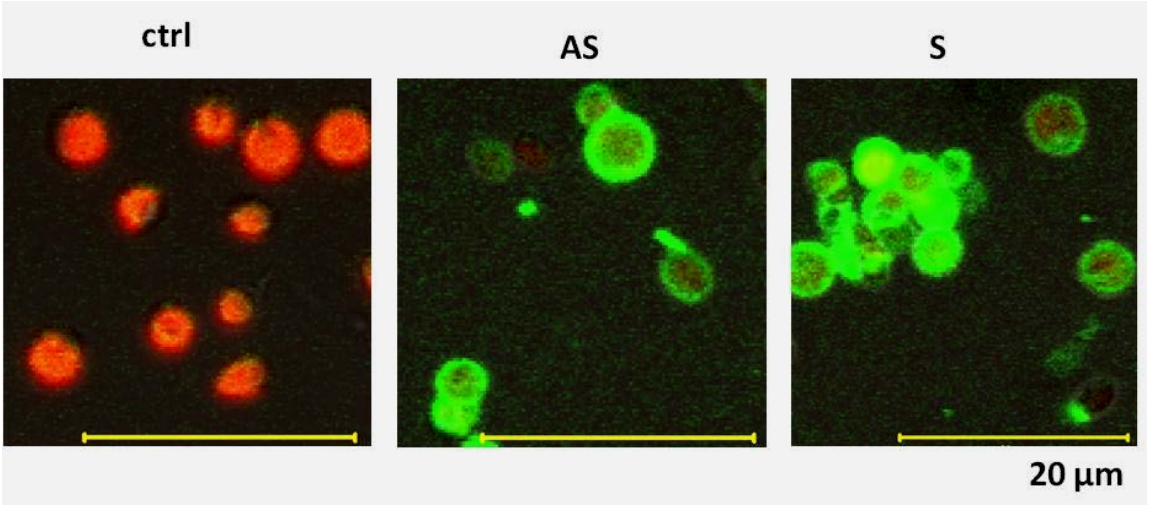

Fig. 1. Laser scanning confocal microscopy imaging of *Chlorella sp* algae, exc. 458nm, composite image of the green spectral region 500-550nm, red spectral region 650-710nm and the transmission image in control conditions (left) and in the presence of fluorescent amine-sulfate- (AS, middle) and sulfate-modified (S, right) polystyrene beads of 0.03 µm, scale 20 µm.

Acknowledgement
This work is supported by VEGA No. 2/0070/21, as well as the Integrated Initiative of European Laser Infrastructures LASERLAB-EUROPE V (grant agreement no. 871124, European Union's Horizon 2020 research and innovation programme).

References

[1] A. Marcek Chorvatova, M. Uherek,A. Mateasik and D. Chorvat Jr. , Front in Phys. 9 (2021), 634324: 1-9.
[2] A. Marcek Chorvatova , M. Uherek, A. Mateasik and D. Chorvat Jr., Methods Appl. Fluoresc. 8 (2020) 024007.
[3] Z. Pavlinska, D. Chorvat Jr., A. Mateasik M. Jerigova., D. Velic, N. Ivosevic DeNardis, A. Marcek Chorvatova, J. Biotechnol. 324S (2020), 100018.

On the pH effect on self-assembly of the recombinant spider silk protein eADF4(C16) into nanofibrils

V. Talafová[1], M. Humenik[2], G. Žoldák[3], T. Scheibel[2] and E. Sedlák[3]

[1] *Department of Biophysics, Faculty of Science, P. J. Šafárik University, Jesenná 5, 040 01 Košice, Slovakia*
[2] *Department of Biomaterials, Faculty of Engineering Science, University of Bayreuth, Universitätsstraße 30, 95440 Bayreuth, Germany*
[3] *Center for Interdisciplinary Biosciences, P. J. Šafárik University, Jesenná 5, 040 01 Košice, Slovakia*

email: veronika.talafova@student.upjs.sk

Protein nanofibrils represent a new class of scaffolds for various nanostructure materials and composites [1]. The recombinant spider silk protein eADF4(C16), which design is based on dragline protein *Araneus diandematus* fibroin 4 (ADF4), forms amyloid-like nanofibrils upon the addition of potassium phosphate [2].

Herein, we investigated the formation of nanofibrils in different pH environments (pH 3-10) in the presence or absence of potassium phosphate. The resulting protein aggregates were treated with fluorescence-specific dyes, 8-anilino-1-naphthalenesulfonic acid (ANS) and Thioflavin T (ThT) to detect hydrophobic sides and cross-beta structures in the assembles, respectively. The structural changes of the protein were investigated by circular dichroism and FT-IR spectroscopies, and the resulted morphologies were visualized by an electron microscopy. The identical conditions for nanofibrils formation were also used for another two variants of the protein where either all glutamic acid residues are substituted with lysine in positively charged eADF4(κ16) or glutamine in neutral eADF4(Ω16).

Experimental results showed that an acidic environment (pH 3-5) triggered in the absence of potassium phosphate the self-assembly of protein eADF4(C16) into the ordered nanofibrils as well as competitive amorphous aggregates (Fig.1). No fibril formation was observed from eADF4(κ16) and eADF4(Ω16) at the tested pH range 3-10. Based on the obtained results, we assume that the presence of glutamic acid in the sequences of the natural fibroins could be essential for preventing amorphous aggregation at neutral pH and directing protein eADF4(C16) into nanofibril formation triggered by the addition of kosmotropic salt at pH drop during the natural spinning process.

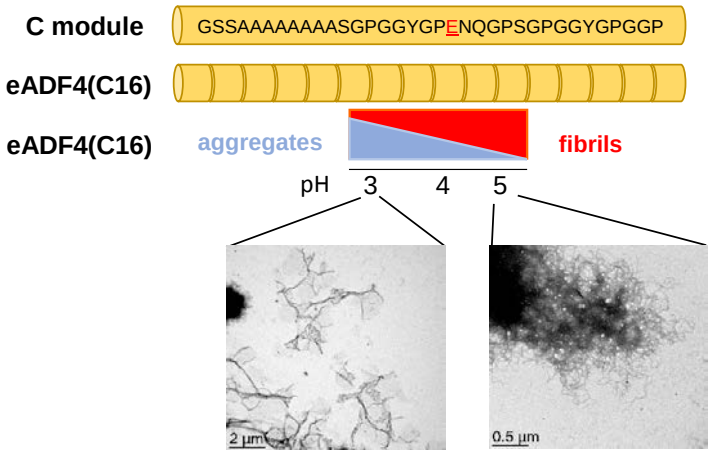

Fig.1 Aggregate states of recombinant spider silk protein eADF4(C16) depend on pH.

Acknowledgment
This work was supported by Slovak Research and Development Agency through the project APVV-20-0340 and by the grant agency of the Ministry of Education, Science, Research, and Sport of the Slovak Republic (grant no. VEGA 2/0034/22). This publication is the result of the implementation of the project OPENMED (Open Scientific Community for Modern Interdisciplinary Research in Medicine) ITMS2014+: 313011V455 from the Operational Program Integrated Infrastructure funded by the ERDF.

References:

[1] Industrial Applications of Nanomaterials, X.Ye, C. Lendel, M. Langton, et al. (ed.), Elsevier, p. 29-63, (2019).
[2] D. Huemmerich, C. W. Helsen, S. Quedzuweit, J. Oschmann, R. Rudolph, T. Scheibel, Biochem., 43 (2004), 13604-13612.

Interactions within the lipid membranes mimicking preclinical conformational diseases

O. Ivankov,[1] T. Murugova,[1] T. Kondela,[1,2] S. Kurakin,[1,3] E. Ermakova,[1] E. Dushanov,[1,4] D. Badreeva,[1] D. Soloviov,[5] Kh. Kholmurodov,[1,4] A. Kuklin[1,6] and N. Kučerka[1,7]

[1]Joint Institute for Nuclear Research, Dubna, Russia
[2]Faculty of Mathematics, Physics and Informatics, Comenius University Bratislava, Slovakia
[3]Kazan Federal University, Kazan, Russia
[4]Dubna State University, Dubna, Russia
[5]Institute for Safety Problems of Nuclear Power Plants NAS of Ukraine, Kyiv, Ukraine
[6]Moscow Institute of Physics and Technology, Dolgoprudny, Russia
[7]Faculty of Pharmacy, Comenius University Bratislava, Slovakia

e-mail: norbert.kucerka@fpharm.uniba.sk

Alzheimer's disease (AD) is a conformational disease caused by the formation of senile plaques, consisting primarily of amyloid-beta (Aβ) peptides. The crucial role in this process at its pre-clinical stage is likely imparted by peptide-membrane interactions. The experimental data suggest several intriguing structural properties of biomimetic membranes that modulate such interactions [1]. First, it is their sensitivity to the charge present in the surrounding environment. The structure of membranes changes for example with increasing concentration of ions, which appears to be an effect born by peculiar properties of ions and lipids themselves. Interestingly, the differences in lipid interactions with ions have been linked to the hydration properties of the ions. A plausible mechanism of action in the case of many membrane additives seems to be in shifting the water encroachment so that bilayers absorb more or fewer water molecules. The hydration interactions appear to determine also the location of membrane constituents, such as cholesterol, melatonin, and Aβ peptide. Moreover, cholesterol increases the order of lipid hydrocarbon chains while increasing the stiffness of the membrane, contrary to the fluidizing effect of melatonin.

The observations based on the neutron scattering experiments and MD simulations keep proving to be important for studies on amyloid toxicity and the molecular mechanism of AD. For example, we have observed recently the changes in the membrane structural properties that were driven by the incorporation of the Aβ peptide into the system [2]. During the temperature changes, the system experienced transitions between the vesicular and bicelle-like objects. The membrane shape changes were also accompanied by dramatic changes in the membrane thickness. We interpret the dramatic changes in the membrane's overall shape with parallel changes in its thickness as the $A\beta_{25-35}$ triggered membrane damage and a consequent reorganization of its structure. The suggested process is consistent with an action of separate peptides or a small number of peptide oligomers rather than the result of a large Aβ fibril.

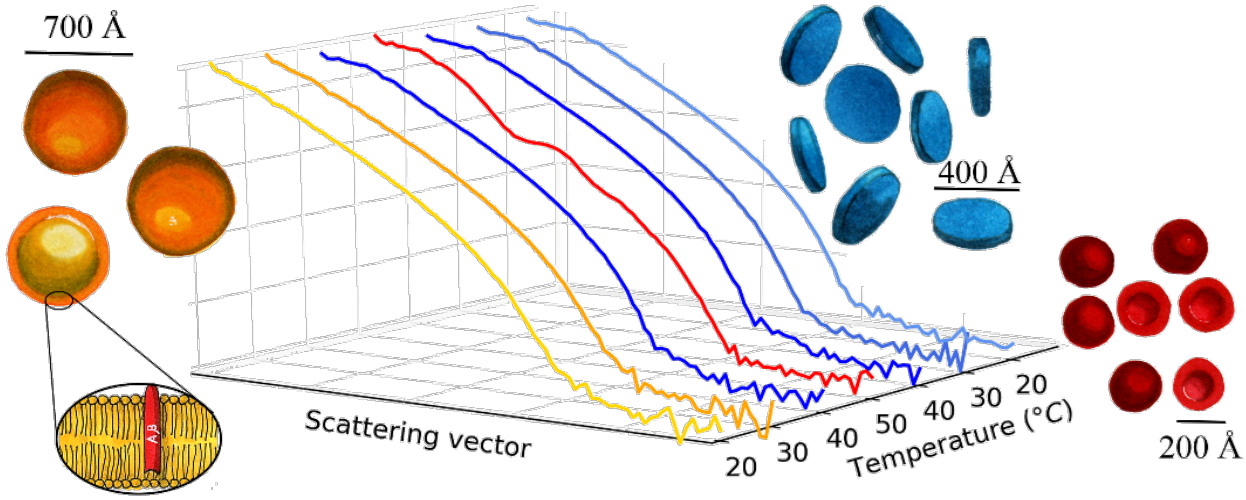

Fig. 1. The proposed scheme of the small-angle neutron scattering (SANS) suggested evolution of the DPPC/Aβ_{25-35} and DMPC/Aβ_{25-35} membrane organizations during the temperature changes. The SANS curves are colored corresponding to their best fit models depicted around. The transition from the initial extruded unilamellar vesicles (EULVs) to bicelle-like structures (BLSs) is irreversible, while the BLSs transition to small unilamellar vesicles (SULVs) reversibly.

Acknowledgment
This work was supported by the Russian Science Foundation under grant 19-72-20186, the JINR theme 04-4-1142-2021/2025. We acknowledge the utilization of IBR-2 facility through its user program and access to the computational heterogeneous cluster HybriLIT.

References

[1] O. Ivankov, E. Ermakova, T. Murugova, D. Badreeva, E. Dushanov, T. Kondela, Kh. Kholmurodov, A. Kuklin, N. Kučerka. In: Advances in Biomembranes and Lipid Self-Assembly. (Eds. A. Iglic, A. García Sáez, M. Rappolt), Elsevier (2020), pp. 185 – 214.
[2] O. Ivankov, T. N. Murugova, E. V. Ermakova, T. Kondela, D. R. Badreeva, P. Hrubovčák, D. Soloviov, A. Tsarenko, A. Rogachev, A. I. Kuklin and N. Kučerka, Sci Rep 11 (2021) 21990.

SARS-CoV-2 antivirals inhibition effect on membrane fusion models

M. Klacsová[1], B. Košáňová[1], J.C. Martínez[2] and D. Uhríková[1]

[1] *Department of Physical Chemistry of Drugs, Faculty of Pharmacy, Comenius University in Bratislava, Odbojárov 10, 832 32 Bratislava, Slovakia.*

[2] *ALBA Synchrotron, Cerdanyola del Vallés, 082 90 Bracelona, Spain.*

e-mail: klacsova@fpharm.uniba.sk

SARS-CoV-2 is a positive-sensed single-stranded enveloped RNA virus that belongs to the β-lineage of the coronaviruses. The life cycle of coronaviruses (CoVs) includes the viral attachment, membrane fusion, genomic replication, assembly, and budding of virions. Viral entry into the host cell is an essential factor for cross-species transmission, particularly for the β-CoVs. Therefore, viral entry is considered to be a promising therapeutic intervention point where the inhibition of virus-host cell membrane fusion efficiently enhances the process of evading viral genome delivery [1]. Moreover, enveloped CoVs can mediate cell-cell fusion between infected cells and neighbouring non-infected cells. This virus-mediated cell-cell fusion leads to the merging of membrane and cytoplasm contents and the formation of multinucleated cells that can express high amounts of viral antigens in tissues and organs of infected hosts [2].

Membrane fusion is a ubiquitous process in biological systems and involves the union of two opposing bilayers. Formation of non-bilayer structures (predominantly inverse hexagonal H_{II} phase) must take place in order to allow two lipid membranes to merge into one. Non-bilayer forming lipids are assumed to be of crucial importance for the transient and/or local formation of non-bilayer structures in the process of cell fusion. Stabilization of the membrane bilayer by antiviral drugs can thus play an important role in inhibiting membrane fusion and antiviral activity [3]. GC376 is a dipeptide-based bisulfite adduct prodrug, which was shown to have potency against SARS-Cov-2 [4]. GC376 strongly inhibits the main protease M^{pro}, a key viral enzyme essential for the viral life cycle of CoVs, involved in the process of transcription and replication.

We examined the effect of GC376 on the stabilization of the bilayer of a fluid lamellar L_α phase at the expense of non-lamellar structures using physical methods of small and wide-angle X-ray diffraction (SAXD/WAXD), excimer fluorescence (EF) and turbidimetry (TM). Model membrane systems were prepared using natural egg yolk phosphatidylethanolamine (EYPE). Stock solutions of EYPE and GC376 were prepared in a methanol:chloroform mixture. Desired amounts of stock solutions were mixed in glass vials. For EF measurements dipyrenylphosphatidylcholine probes (Pyr4PC and Pyr10PC) were added as methanol solutions at a probe:lipid ratio of 1:1500 molar ratio. All samples were dried under a stream of nitrogen gas and evacuated at 5 Pa. Before the measurement, samples were hydrated by 150 $mmol.l^{-1}$ NaCl solution to obtain sample concentrations of 1×10^{-4}, 4×10^{-4}, and 22×10^{-3} $mol.l^{-1}$ for EF, TM, and SAXD measurements, respectively. Homogenization was reached by repeated freezing-thawing cycles and vigorous vortexing. For TM measurements, unilamellar vesicles were prepared by extrusion through 100 nm filter. Experimental data were collected within the range of 30–80°C, at a heating rate of $1°Cmin^{-1}$. EF measurements were performed in quartz cuvettes using Fluoromax-4 (Horiba Jobin Yvon) fluorimeter at λ_{exc} = 345 nm. Emission intensity was collected for 120 s at 376 and 481 nm. The intensity ratio $\eta_{PyrnPC} = I_{481}/I_{376}$ was used as a measure of lateral pressure change within the bilayer. TM measurements were performed in quartz cuvettes using spectrophotometer HP 8452A. SAXD/WAXD measurements were performed at beamline NCD-sweet of the ALBA synchrotron, Barcelona. Samples were measured in quartz capillaries with a diameter of 1.5 mm for 10 s at each temperature. Diffraction peaks were fitted with Lorentzian functions. From the position of the first lamellar (L1) and hexagonal (H10) reflections, the corresponding lattice parameters were calculated as $d = 2\pi/q$ and $a = 4\pi/\sqrt{3}q$, where q is the scattering vector.

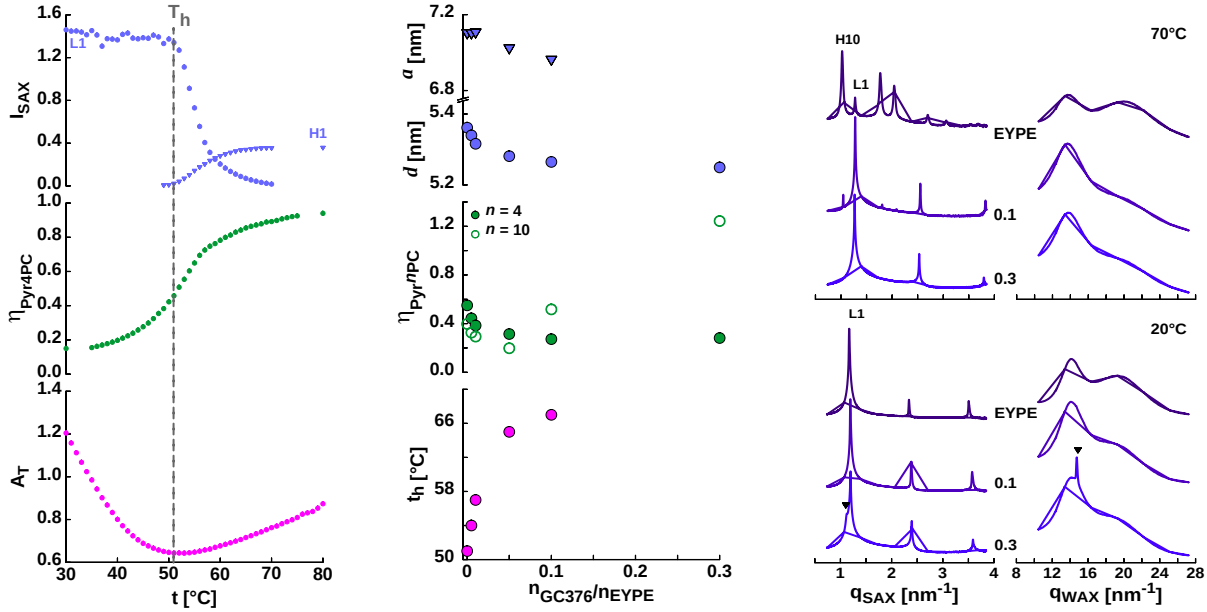

Fig. 1. Left: Temperature dependences of turbidity A_T at 400 nm, lateral pressure change η_{Pyr4PC}, and SAXD reflection intensities I_{SAX} obtained for neat EYPE. Middle: GC376 concentration dependence of the L_α-H_{II} phase transition temperature t_h, lattice parameters *d* and *a* of the L_α and H_{II} phase at 20 and 70°C, respectively, and lateral pressure η_{PyrnPC} at 50°C in the C4 and C10 position of the acyl chain. Right: SAXD/WAXD patterns obtained for EYPE+GC376 at designated molar ratios and temperatures.

The temperature dependences of turbidity, lateral pressure change, and SAXD reflection intensities were used to determine the fluid lamellar L_α to inverse hexagonal H_{II} phase transition temperature (t_h) from the minimum, inflection point, and sudden change of the respective dependences (Fig.1). For neat EYPE t_h~51°C was obtained. Upon addition of GC376 a dramatic increase in t_h is present, with Δt_h = 16°C at 0.1 mol/mol. Above 0.1 mol/mol bulk crystallization of GC376 within the bilayer, determined from the sharp reflections in the SAXD and WAXD spectra at 20°C (designated by an arrow on Fig.1), was observed. This is supposed to depress the formation of H_{II} phase. Lattice parameter *d* of the L_α phase decreases at 20°C until 0.05 mol/mol. At higher molar ratios the *d*-value does not change significantly. At the same time, the lattice parameter *a* of the H_{II} phase at 70°C remains unchanged at low GC376 concentrations, while from 0.05 mol/mol the *a*-value suddenly decreases. No more sign of crystallization was observed at 70°C. The lateral pressure η of the EYPE bilayer is decreasing upon addition of GC376 near the hydrophilic-hydrophobic interface (position C4 of the acyl chain) as well as in the hydrophobic core (position C10 of the acyl chain), up to 0.05 mol/mol. With further increase of GC376 concentration, η changes near the interface only slightly, while in the hydrophobic core η starts to increase suddenly.

We conclude that antivirals GC376 significantly affect the fluid lamellar L_α to inverse hexagonal H_{II} phase transition of model EYPE membranes in the favor of the L_α phase. It suggests a possible dual mechanism of action of GC376: aside from virus transcription and replication, also the virus entry into a host cell may be inhibited. Hereby, we observed signs of bilayer saturation above 0.05 mol/mol with a concomitant bulk crystallization of GC376 at higher concentrations.

Acknowledgment

This work was supported by VEGA 1/0223/20; JINR project 04-4-1142-2021/2025; APVV 17-0250 and PP-COVID-20-0010. SAXD/WAXD experiments were performed at BL11-NCD beamline (proposal 2021025016) at Alba Synchrotron with the collaboration of Alba staff.

References

[1] S. Muralidar, G. Gopal and S.V. Ambi, J. Med. Virol. 93 (2021), 5260.
[2] H. Leroy, M. Han, M. Woottum, L. Bracq, J. Bouchet, M. Xie and S. Benichou, Int. J. Mol. Sci. 21 (2020), 9644.
[3] C. D'Souza, M. Kanyalkar, M. Joshi, E. Coutinho and S. Srivastava, Biochim. Biophys. Acta, 1788 (2009), 484.
[4] W. Vuong, M.B. Khan, C. Fischer, E. Arutyunova, T. Lamer, J. Shields, H.A. Saffran, R.T. McKay, M.J. van Belkum, M.A. Joyce, H.S. Young, D.L. Tyrrell, J.C. Vederas and M.J. Lemieux, Nat. Commun., 11 (2020), 4282.

Interaction kinetics reveal distinct properties of conformational ensembles of three-repeat and four-repeat tau proteins

O. Cehlár[1], L. Horňáková[1,2,3], J. Šinský[1], S. Slušná[1,2], J. Galba[4,5], J. Piešťanský [6,7], A. Kováč[1], J. Hanes[1] and R. Škrabana[1]

[1] *Institute of Neuroimmunology of the Slovak Academy of Sciences, Dubravska cesta 9, 84510 Bratislava, Slovakia*
[2] *Department of Biochemistry, Faculty of Natural Sciences, Comenius University, Ilkovicova 6, 84215 Bratislava, Slovakia*
[3] *Present address: Institute of Medical Chemistry, Biochemistry and Clinical Biochemistry, Medical Faculty, Comenius University, Sasinkova 2, 81108 Bratislava, Slovak Republic*
[4] *Biomedical Research Center of the Slovak Academy of Sciences, Dubravska cesta 9, Bratislava, 84510, Slovakia*
[5] *Department of Pharmaceutical analysis and nuclear pharmacy, Faculty of Pharmacy*
[6] *Department of Pharmaceutical Chemistry, Faculty of Pharmacy*
[7] *Toxicological and Antidoping Center, Faculty of Pharmacy, Comenius University in Bratislava, Ulica odbojárov 10, 832 32 Bratislava, Slovakia*

e-mail: ondrej.cehlar@savba.sk

Alzheimer's disease (AD) is the most common cause of dementia and thus a disease that radically reduces the quality of life not only for patient but also for the patient's families. An important role in the development and progression of this disease is played by the accumulation of two intrinsically disordered proteins in the form of insoluble filaments, namely tau and β-amyloid, caused by changes in their structures.

The structural insights into the pathological and physiological tau protein conformations may help to answer the key questions of the pathogenesis of AD and other tauopathies. All six isoforms of tau protein expressed in CNS consist of four main domains and differ according to number of N-terminal inserts (0N, 1N, 2N tau isoforms) and repetitive domains (3R, 4R tau isoforms) (Fig. 1A). An important regulatory role is played by the C-terminal domain which is believed to be responsible for inhibition of tau protein aggregation [1].

We have been studying the kinetics of the interaction of an antibody DC39C, which epitope lies inside the last 12 C-terminal amino acids of tau, with various tau proteins by surface plasmon resonance and microscale thermophoresis [2]. According to recent insights into the structure of tau protein obtained by cross-linking guided discrete molecular dynamics, where tau molecule was modelled as a rather globular and compact [3], epitope of DC39C antibody should be hidden in between the beta strand of first N-terminal insert and N-terminus of tau protein (Fig. 1B). Global conformation that was observed by FRET method supports the positioning of the C-terminal domain between MTBR and N-terminal domain [4] (Fig. 1C). Our results had shown that isoforms without N-terminal inserts bind to DC39C antibody with the highest association rate. To support our kinetic data and their link to the conformational ensembles of tau proteins, we have performed chemical crosslinking mass spectrometry analysis, where we have observed substantial reduction in the number of identified intramolecular crosslinks in truncated tau forms in comparison to tau2N4R.

Subsequently, we have measured the kinetics of filament formation of 3R tau proteins to observe the effect of the C-terminal domain removal. The double truncated tau construct (tau151-391/3R) which causes Alzheimer´s like pathology in the rat model of tauopathy [5] has shown a very rapid filament formation; slightly slower rate of filament formation was observed with tau

protein that lacks C-terminal domain (tau1-391/3R), and the full length 3R tau isoform (2N3R) has shown the slowest rate of filament formation. Our results suggest a novel mechanism of splicing-driven regulation of the tau C-terminal domain with consequences on the specific roles of tau isoforms in microtubule assembly and pathological aggregation.

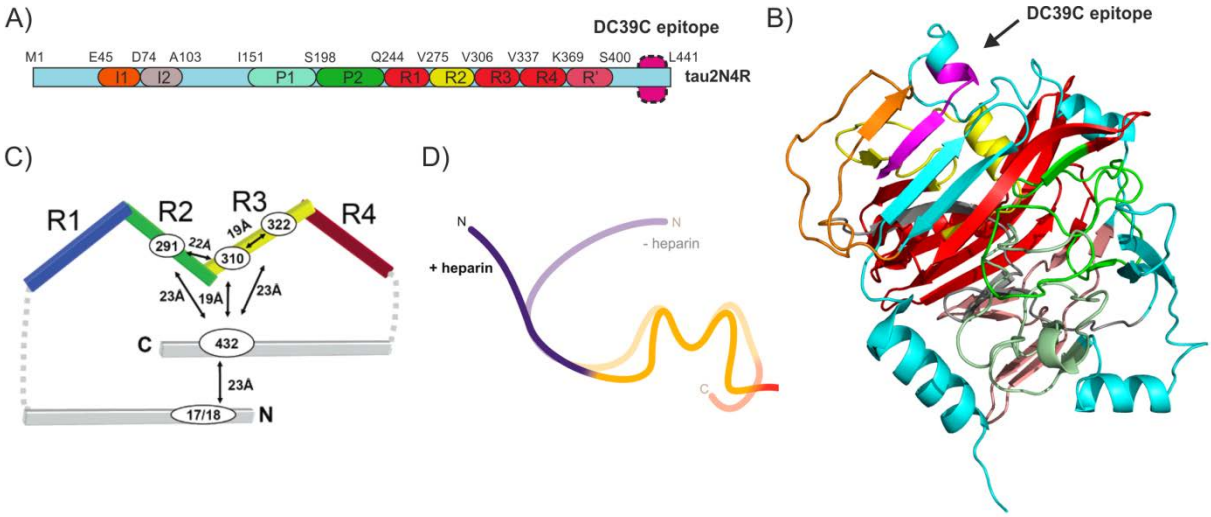

Fig. 1. Schematic domain structure and models of tau2N4R conformation. Tau 2N4R contains N terminal inserts I1 and I2, proline rich domains P1 and P2, microtubule binding repeats R1-R4 and the region following repeats R' (**A**). Models obtained using short distance cross-linking guided discrete molecular dynamics simulations (**B**), ensemble FRET (**C**) and single molecule FRET (**D**). Figure adapted from ref [2].

Acknowledgement

This work was supported by the Scientific Grant Agency of the Ministry of Education of the Slovak Republic (Grant Nos. 2/0145/19, 2/0163/19, 2/0150/19, 2/0123/21). CIISB research infrastructure project LM2018127 funded by MEYS CR is gratefully acknowledged for the financial support of the measurements at the CF BIC for MST measurements.

References

[1] Abraha, A., Ghoshal, N., Gamblin, T. C., Cryns, V., Berry, R. W., Kuret, J. & Binder, L. I., J Cell Sci 113, (2000), 3737-3745.

[2] Hornakova L, Sinsky J, Janubova M, Mederlyova A, Paulenka Ivanovova N, Piestansky J, Kovac A, Galba J, Skrabana R & Cehlar O, FEBS Lett (2022), doi: 10.1002/1873-3468.14339

[3] Popov, K. I., Makepeace, K. A. T., Petrotchenko, E. V., Dokholyan, N. V. & Borchers, C. H., Structure 27, (2019), 1710-1715 e1714.

[4] Jeganathan, S., von Bergen, M., Brutlach, H., Steinhoff, H. J. & Mandelkow, E., Biochemistry-Us 45, (2006), 2283-2293.

[5] Filipcik, P., Zilka, N., Bugos, O., Kucerak, J., Koson, P., Novak, P. & Novak, M., Neurobiol Aging 33, (2012) 1448-1456.

Structural clues to different aggregation propensities of tau protein isoforms

R. Skrabana[1], K. Rafajova[1], I. Jahodova[1], N. Zemanova[1], O. Cehlar[1], O. Bagarova[1]

[1] *Institute of Neuroimmunology, Slovak Academy of Sciences*
Laboratory of Structural Biology of Neurodegeneration
Dubravska cesta 9, 84510 Bratislava, Slovakia

e-mail: rostislav.skrabana@savba.sk

Six neuronal tau protein isoforms are unequally represented in pathological tau filaments of various human tauopathies. This is rather puzzling given the common beta-structure prone aggregation core (amino acids VQIVYK) [1]. Individual tau protein isoforms differ in the number of relatively short alternatively spliced N-terminal inserts and C-terminal repeats (Figure 1). All tau isoforms are intrinsically disordered in the native state, therefore, their pathological as well as physiological function is determined by the sub-state composition of their conformational ensembles (CEs).

In this work we aimed at an overall characterization of tau isoforms' CEs by biophysical means. Obtained results are discussed with data from tau interaction and aggregation studies.

Dimension of the tau isoform CE was measured by dynamic light scattering of tau in solution, using homogeneous recombinant tau samples, and compared with calculated random-coil values. We found that overall compactness of tau molecule inversely correlates with the molecular size and the number of alternatively spliced sequences. To make an insight into the structural base of observed changes in CEs we quantified the secondary structure of tau isoforms using the amide I band of their infrared absorption spectra.

Differences of tau isoforms' CEs may result in pronounced variability of interaction capacities, observed in kinetic and aggregation experiments [2].

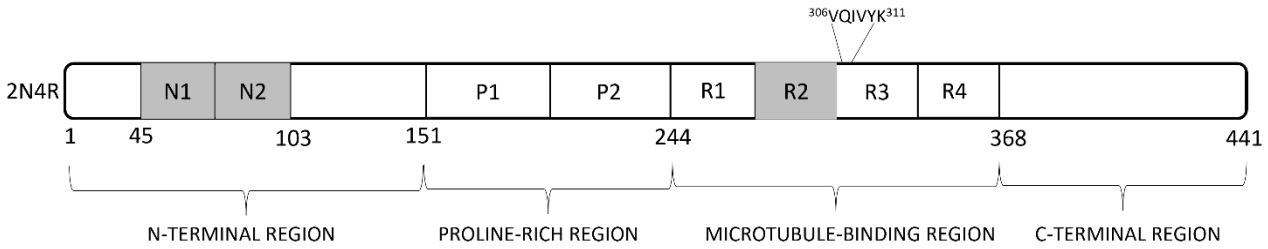

Fig. 1. Longest CNS tau isoform 2N4R. Specific alternative splicing of grey-shaded regions gives in total six isoforms (0N3R, 1N3R, 2N3R, 0N4R, 1N4R, 2N4R).

Acknowledgement
This work was supported by VEGA grants 2/0145/19 and 2/0163/19.

References

[1] M. von Bergen, P. Friedhoff, J. Biernat, J. Heberle, E. M. Mandelkow, E. Mandelkow, Proc Natl Acad Sci U S A, 97 (2000), 5129-34.
[2] L. Hornakova, J. Sinsky, M. Janubova, A. Mederlyova, N. Paulenka Ivanovova, J. Piestansky, A. Kovac, J. Galba, R. Skrabana, O. Cehlar, FEBS Lett., (2022) Mar 24. doi: 10.1002/1873-3468.14339. Epub ahead of print.

Aggregation mechanism and morphologies of myelomatic human light chain

V. Džupponová[1] and G. Žoldák[2]

[1] *Department of Biophysics, Faculty of Science, Pavol Jozef Šafárik University, Jesenná 5, 040 01 Košice, Slovakia..*
[2] *Center for Interdisciplinary Biosciences, Technology and Innovation Park, Pavol Jozef Šafárik University, Jesenná 5, 041 54 Košice, Slovakia.*

e-mail: veronika.dzupponova@upjs.sk

Protein stability is a crucial property for the proper biological function of proteins. Low protein stability leads to unfolding, followed by the formation of aggregates that are pathological to the body and, in many cases, cause serious diseases. Such diseases include amyloidosis and multiple myeloma of the immunoglobulin light chain. Multiple myeloma (MM) is a haematological malignancy manifested by uncontrolled proliferation and accumulation of damaged plasma cells in the bone marrow. As a result of genetic dysregulation of the heavy chain of immunoglobulin G (IgG) production, myeloma plasma cells produce elevated Ig light chain (LC) levels, which are subsequently secreted into the bloodstream. From the blood circulation, LC creates extracellular sediments in organs important for life, such as e. g. heart, kidney and liver, where due to the low colloidal stability of the LC aggregates are formed and the microscopic fibrils of amyloid deposits at final stages. Understanding the molecular nature of protein aggregation and the effect of the physicochemical environment that accelerates the conversion of functional forms of proteins into pathogenic aggregates is a key to discovering effective strategies to decline the high morbidity of these leukemic diseases. At the same time, discovering limiting steps in the aggregation would enable the rational development of drugs inhibiting the formation of toxic aggregates [1-3].

In our laboratory, we established a method for rapid and effective purification of recombinantly produced human light chain - JTO, derived from myelomatic LC that formed large sediments in the patient´s kidney. We investigated how the physicochemical environment *in vitro* affects the kinetic and colloidal stability of JTO hLC; based on obtained data, we created a model of JTO aggregation (Fig. 1a), and we developed a mathematical model for the prediction of time-dependence of colloidal stability of hLC in the soluble form (Fig. 1b) [4].

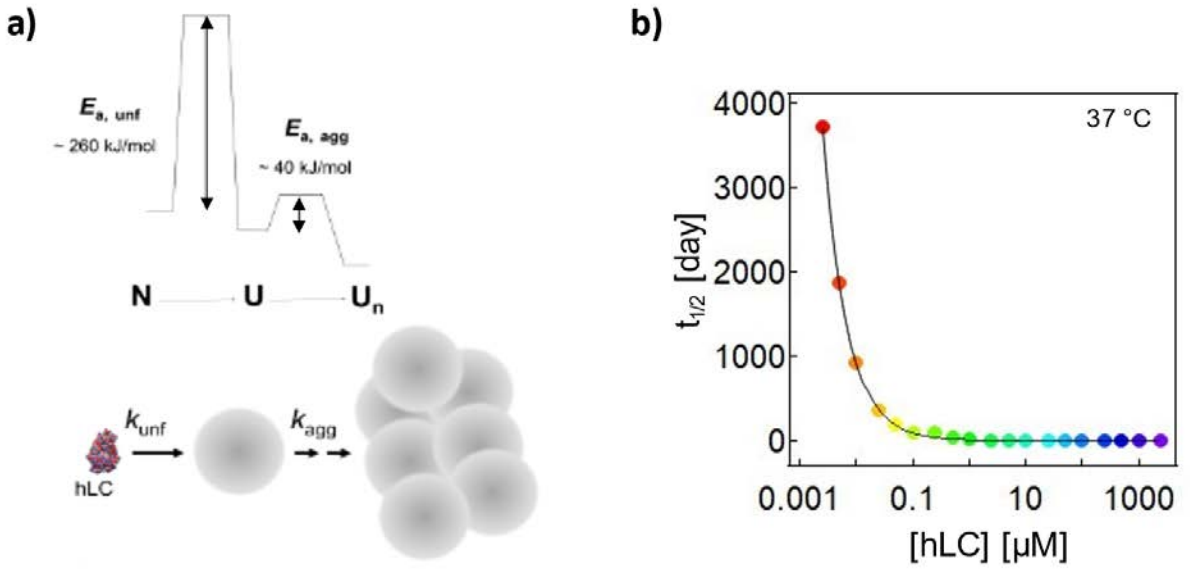

Figure 1: a) Kinetic model of hLC aggregation including different heights of energy barriers for unfolding and aggregation; b) Dependence of half-time of protein solubility as a function of protein concentration based on the simulations of the kinetic model comprising hLC unfolding and aggregation.

Next, we looked at how the reduction of disulfide bonds contributes to the formation of aggregates. Aggregation kinetics in different types of reducing agents (TCEP, DTT and GSH) were analyzed by extended Finke-Watzky model, which also includes pre-step of monomer-dimer equilibrium. The analysis reveals the critical steps that lead to the formation of LC aggregates with vastly different morphology and fractal properties (Fig. 2).

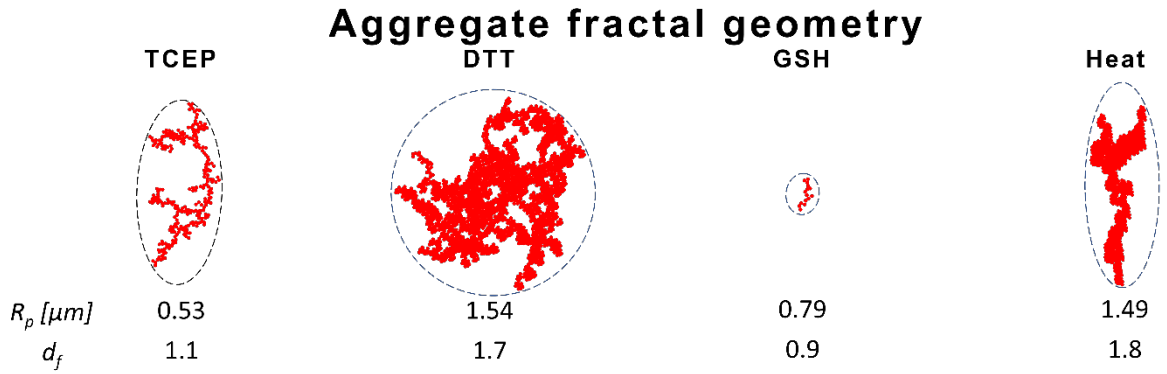

Figure 2: 3D morphologies of light chain aggregates formed after reducing disulfide bonds using different chemical reducing agents: TCEP, DTT, GSH or temperature. 3D morphologies were obtained by the fluorescent labeling of LC with Abberior STAR RED dye and visualized by the STEDYCON microscope.

Acknowledgement
This work was supported by research grants from the Slovak research and development agency (No. APVV-18-0285), the Slovak Grant Agency VEGA No 1/0024/22, Internal Scientific Grants System (VVGS) of Faculty of Science UPJŠ No vvgs-pf-2021-2072, EU H2020 TWINNING program GA. No. 952333 project CasProt, BioPickmol, ITMS2014+: 313011AUW6 supported by the Operational Programme Integrated Infrastructure, funded by the ERDF, and Open scientific community for modern interdisciplinary research in medicine (OPENMED), ITMS2014+: 313011V455 supported by the Operational Programme Integrated Infrastructure, funded by the ERDF.

References

[1] K. Andrich., et al., *Journal of Biological Chemistry*, 292 (2016), 2328–2344.
[2] F. Chiti, C.M. Dobson, *Annual Review of Biochemistry*, 86 (2017), 27–68.
[3] L. M. Blancas-Mejia, et al., *Chemical Communications*, 54 (2018), 10664-10674.
[4] V. Džupponová, V. Huntošová, G. Žoldák, *Protein Science*, 29 (2020), 2408 – 2421.

Influence of herbal extracts' constituents on the amyloid aggregation of proteins

M. Gancar[1], E. Kurin[2,*], Z. Bednarikova[1], J. Marek[1], P. Mucaji[2], M. Nagy[2] and Z. Gazova[1]

[1] *Department of Biophysics, Institute of Experimental Physics Slovak Academy of Sciences, Watsonova 47, 040 01, Kosice, Slovakia*

[2] *Department of Pharmacognosy and Botany, Faculty of Pharmacy, Comenius University in Bratislava, Odbojarov 10, 832 32, Bratislava, Slovakia*

e-mail: gancar@saske.sk

The phenomenon of protein amyloid aggregation poses a major health risk. Exogenous insulin, used as a therapeutic agent for diabetes, forms undesirable insoluble deposits containing fibrillar structures in the vicinity of the administration site leading to a pathological iatrogenic condition known as injection amyloidosis. Systemic lysozyme amyloidosis represents a hereditary condition characterized by the amyloid deposits of lysozyme within the various tissues leading to progressive organ dysfunction and failure. Natural herbal extracts, providing numerous lead molecules, may serve as a foundation in a search for effective drugs to relieve patients from symptoms and ultimately treat amyloidoses.

In our research, the *in vitro* effect of four green tea constituents: (-)-epigallocatechin gallate (EGCG), (-)-epicatechin (EC), gallic acid (GA) and caffeine (CF), and their equimolar mixtures against an aggregation of human insulin and lysozyme from hen egg-white has been evaluated and compared. An amyloid aggregation has been induced by acidic pH, high temperature and constant stirring. The anti-amyloid activity of compounds and their mixtures was subsequently analyzed by the Thioflavin T (ThT) fluorescence assay (IC_{50} – a half-effective concentration and kinetics), attenuated total reflectance – Fourier transform infrared spectroscopy (ATR-FTIR – protein secondary structure), atomic force microscopy (AFM - visualization) and supported by *in silico* calculations.

Concerning individually tested compounds, only EGCG reduced amyloid fibrils' number in the case of both proteins, while GA, EC, and CF did not exhibit activity. However, solo constituents EGCG and GA both slowed down the aggregation process of insulin, further joined by EC in the case of lysozyme. The presence of EGCG in equimolar combinations with GA, EC, and CF has been proven essential for the inhibitory activity of the respective mixtures. In the case of insulin, three mixtures (GA:EGCG, EGCG:EC:CF and GA:EGCG:EC:CF) showed better activity than the solo EGCG. On the other hand, none of the mixtures were deemed more effective compared to EGCG in the case of lysozyme. We observed diverse morphology and the amount of both insulin and lysozyme amyloid aggregates formed in the presence of studied compounds and mixtures. Using molecular docking, we have shown that EGCG interacts with an essential amyloidogenic region of insulin chain B and described the potentiating effect of individually inactive GA on the activity of EGCG when mixed together.

In summary, we have observed: 1) EGCG as the sole individually effective compound (both proteins); 2) the ineffectiveness of individual EC, GA, and CF molecules (both proteins); 3) in regards to insulin: the overall potentiating effect of GA and the negative effect of EC and CF on the activity of EGCG; 4) concerning lysozyme: the positive impact of EGCG-containing binary mixtures in terms of aggregation kinetics, however, deteriorating general anti-amyloid activity for tertiary and ternary mixtures. Importantly, obtained results indicate the need for analogous assays while confirming the biological activity of individual molecules since they are not directly applicable for predicting the effects of pooled samples.

Acknowledgment

This work was supported by the Slovak Research and Development Agency under the Contract no. APVV-18-0284; Slovak Grant Agency VEGA grants: 1/0226/22, 2/0164/22, 2/0176/21, and by the Operational Programme Integrated Infrastructure funded by the ERDF, the project implementation BIOVID-19 (ITMS2014+ 313011AVG3) and NANOVIR (ITMS2014+ 313011AUW7) and ITMS: 26240120023.

POSTER PRESENTATIONS

Singlet Oxygen Detection in Live Cells

A. Hovan[1], V. Pevná[1], V. Huntošová[2], P. Miškovský[2] and G. Bánó[1]

[1] *Department of Biophysics, Faculty of Science, P. J. Šafárik University, Jesenná 5, 041 54 Košice, Slovak Republic.*
[2] *Center for Interdisciplinary Biosciences, TIP, P. J. Šafárik University, Jesenná 5, 041 54 Košice, Slovak Republic*

e-mail: gregor.bano@upjs.sk

Photodynamic therapy of cancer is based on the cytotoxic effect of singlet oxygen. Singlet oxygen is generated by energy transfer between photo-activated drug molecules (photosensitizers) and molecular oxygen. The range of cytotoxic activity of singlet oxygen is determined by its diffusion rate and lifetime. Previous research in this area has not clarified the value of singlet oxygen lifetime in cells. There is currently no consensus in the scientific community on the proper method of measuring and evaluating the lifetime of singlet oxygen in cells. The results of various scientific groups range from several tens or hundreds of nanoseconds [1] up to a few microseconds [2]. The main objective of our work was to determine the lifetime of singlet oxygen in cell suspensions and to contribute to this key issue of photodynamic therapy.

The decay of singlet oxygen phosphorescence intensity was measured following nanosecond pulsed excitation of Hypericin, the natural photosensitizer, embedded into live cells of the SKBR3 (breast adenocarcinoma) cell line. The excitation wavelength was set to the Hypericin absorption maximum near 600 nm. After absorption of the light, the photosensitizer is excited to the singlet state S1, which populates the triplet state T1 through inter-system crossing. The triplet state photosensitizer reacts with an oxygen molecule, which is transferred to the highly reactive singlet oxygen state. It follows that the lifetime of the Hypericin triplet state plays an important role in understanding the kinetics of singlet oxygen phosphorescence. Due to this fact, the Hypericin triplet state was monitored by transient absorption measurements using a 532 nm laser.

The singlet oxygen lifetime was determined by analyzing the kinetics of the singlet oxygen phosphorescence signal. Our preliminary results indicate that the effective lifetime of singlet oxygen in the studied cells is approximately 1.2 ± 0.4 μs, which is in between the minimal and maximal values presented by other authors [1,2]. Further experiments are needed to clarify the reasons behind the observed differences.

Acknowledgment
This work was supported by Slovak Research and Development Agency through the project APVV-20-0340 and by the grant agency of the Ministry of Education, Science, Research, and Sport of the Slovak Republic (grants no. VEGA 1/0557/20 and no. VEGA 1/0074/22). This publication is the result of the implementation of the project OPENMED (Open Scientific Community for Modern Interdisciplinary Research in Medicine) ITMS2014+: 313011V455 from the Operational Program Integrated Infrastructure funded by the ERDF.

References

[1] M. Niedre, M. S. Patterson and B. C. Wilson, Photochemistry and Photobiology, 75 (2002), 382-391.
[2] M. K. Kuimova, G. Yahioglu and P. R. Ogilby, Journal of the American Chemical Society, 131 (2009), 332-340.

Design and isolation of new mutant LOV2 proteins

K. Felčíková[1], V. Dzurillová[1], A. Hovan[1], G. Banó[1], T.Kožár[2], E. Sedlák[2]

[1] *Department of Biophysics, Faculty of Science, P.J. Šafárik University, Jesenná 5, 040 54 Košice, Slovakia.*

[2] *Center for Interdisciplinary Biosciences, Technology and Innovation Park, P.J. Šafárik University, Jesenná 5, 041 54 Košice, Slovakia*

e-mail: kristina.didicova@student.upjs.sk

Photodynamic therapy is currently used as non-invasive treatment of cancer during which is infected tissue destroyed by light, molecular oxygen and special drug called photosensitizer [1]. In recent years significant effort is focused on using protein-based photosensitizer containing flavin mononucleotide (FMN) [2].

One of such proteins is the Light-Oxygen-Voltage (LOV) domain, particularly LOV domain 2 from *Avena sativa* (AsLOV2). In general, LOV domains form parts of the N-terminal photosensory domain in plant phototropins. They belong to the group of flavoproteins because of the non-covalently bound FMN in their structures [3]. Due to a high value of quantum yield of the singlet oxygen ($^1O_2$) production, FMN belongs to effective photosensitizers [2]. However, the efficiency of $^1O_2$ production of FMN encapsulated in the protein is significantly reduced due to the cofactor interactions with the protein matrix surroundings through hydrogen bonds, van der Waals interactions or π-π interactions [4]. Our approach relies on the FMN dissociation caused by irradiation-induced oxidation of sulfur-containing amino acids at the binding site (Figure 1). Since the binding site of FMN in the AsLOV2 domain contains only one such amino acid, cysteine 450, we performed analysis of the binding site and the determination of the suitable amino acids for an additional mutagenesis. The main idea was to suggest such mutation that would not cause destabilization of the structure but upon protein irradiation and subsequent oxidation of the mutated amino acid would increase its volume in such way that the cofactor would dissociate from the protein.

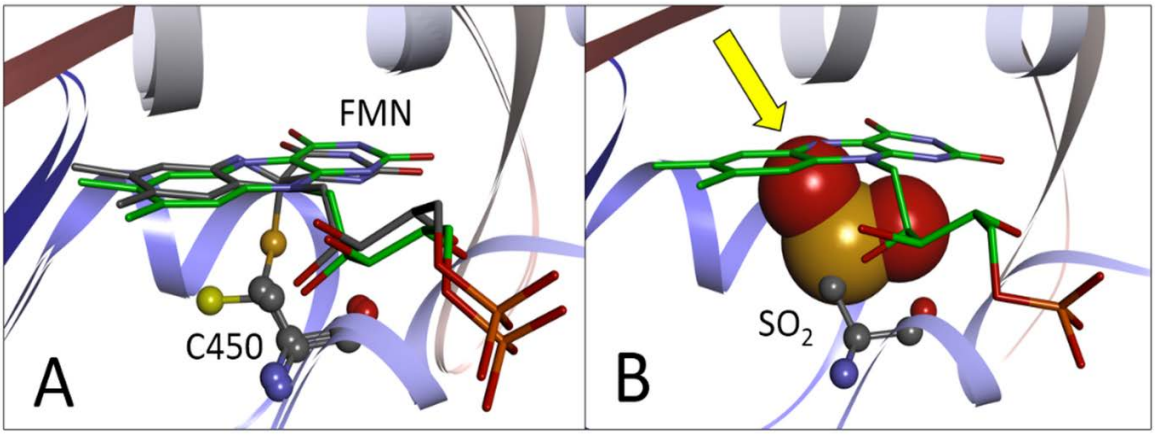

Figure 1. A) Superposition of AsLOV2 structures represented by PDB ID: 2w0u (FMN with carbons in green) and PDB ID: 2v0w (FMN bound to Cys450 with carbons in grey). **B)** -SH to $-SO_2^-$ substitution in C450 with marked atomic clash of the generated structure [5].

Performed molecular dynamics simulations of suggested mutants enabled us to determine their stability and selected suitable candidates for further biophysical analysis. In the molecular dynamics simulation, we particularly looked at the changes in the structure and interactions of FMN with amino acids at the binding site. These theoretical analyses were subsequently verified experimentally. Here, we present obtained results regarding the $^1O_2$ production by the selected mutants of AsLOV2.

Acknowledgement

This work was supported by Slovak Research and Development Agency through the project APVV-20-0340 and by the grant agency of the Ministry of Education, Science, Research, and Sport of the Slovak Republic (grant no. VEGA 1/0557/20). This publication is the result of the implementation of the project OPENMED (Open Scientific Community for Modern Interdisciplinary Research in Medicine) ITMS2014+: 313011V455 from the Operational Program Integrated Infrastructure funded by the ERDF.

References

[1] D.K. Chatterjee, L.S. Fong, Y. Zhang, Adv drug deliv rev., 60 (2008), 1627-1637.
[2] M. Westberg, M. Bregnhoj, M. Etzerodt, P.R. Ogilby, J Phys Chem B., 121 (2017), 2561-2574.
[3] J.M. Christie, Annu Rev Plant Biol., 58 (2007), 21-45.
[4] R. Baron, C. Riley, P. Chenprakhon, K. Thotsaporn, R.T. Winter, A. Alfieri, F. Forneris, W.J.H. van Berkel, P. Chaiyen, M.W. Fraaije, A. Mattevi, J.A. McCammon, Proc Natl Acad of Sci USA, 109 (2009), 10603-10608.
[5] M. Petrenčáková, F. Filandr, A. Hovan, G. Yassaghi, P. Man, T. Kožár, M.-S. Schwer, D. Jancura, A. Plückthun, P. Novák, P. Miškovský, G. Banó, E. Sedlák, Sci Rep., 10 (2020), 4119.

Structural in-depth analysis of iron complexes of tannic acid and other related polyphenols as revealed by spectroscopic techniques

A. Espina[1], M. V. Cañamares[2], S. Sanchez-Cortes[2,3], Z. Jurašeková[1]

[1]*Department of Biophysics, Faculty of Science, P. J. Šafárik University, Jesenná 5, 040 01 Košice, Slovakia*
[2] *Institute of the Structure of Matter, IEM-CSIC, Serrano 121, 28006 Madrid, Spain*
[3] *Center for Interdisciplinary Biosciences, Technology and Innovation Park, P. J. Šafárik University, Jesenná 5, 040 01 Košice, Slovakia*

e-mail: zuzana.jurasekova@upjs.sk

Phenolic compounds are the most abundant secondary metabolites in plants demonstrating many beneficiary properties and activities. The phenolic compounds existing in plant galls deserve special attention. In particular, oak galls contain a large amount of tannic acid and lower amounts of gallic and ellagic acids [1]. Generally, one of the main chemical properties of polyphenols is the high affinity to bind metals, leading to the formation of metal complexes. Therefore, the galls have been a principal ingredient used in the preparation of iron gall inks (IGIs) [2].

The investigation of IGIs is of great importance in the study of historical manuscripts with many implications for the Cultural Heritage. Admittedly, before the appearance of synthetic colorants in the second half of the 19th century, the most frequently used were IGIs. Raman spectroscopy (RS) has been demonstrated to be very useful in the identification of both the colorants employed in the fabrication of inks [3] as well as the IGIs themselves in historical manuscripts [4-6]. Moreover, Raman spectroscopy was employed in the analysis of the chemical structure of many phenols [7,8]. Nevertheless, less attention was devoted to an eventual structural characterization of IGIs by using the information provided by the Raman technique and the structure of the actual colorant in IGIs is still a matter of controversy [9]. The main reasons are the intrinsic complexity of the studied materials and the lack of appropriate and valid assignments of the vibrational bands. In any case, RS can afford crucial information regarding the analysis of iron interactions with phenolic compounds [10-17], and, therefore, its use in the study of IGIs represents a good opportunity to find and establish a proper correlation between the Raman bands and the IGI colorant structure.

In this work, a structural analysis of the polyphenol complexes with iron at several conditions is reported. The investigated polyphenols were tannic acid (TA), gallic acid (GA), pyrogallol (PY), and syringic acid (SA) (Figure 1), being components of the gallnuts usually employed in the past in the fabrication of IGIs [1,18]. PY and SA were employed as models to study the interaction of iron with similar structures to the GA one, and, more precisely, to evaluate the importance of the presence of both the carboxylic and the hydroxyl groups in the benzene ring. Although TA is only present in a limited range of plant species, it can serve to mimic all the different tannic structures present in oak gallnuts. This investigation was conducted by measuring the Raman, FTIR, UV-Vis absorption, and fluorescence spectra of the polyphenols and their iron complexes under different conditions: in solution and deposited on paper, and evaluating the effect of the pH, aging, and stoichiometric proportions between iron and polyphenols [19,20]. Moreover, to elucidate the structure of the IGIs as well as to aid in the normal mode assignment of their vibrations, an optimization of the geometry of GA and two different iron complexes, GA-Fe and GA-Fe_2, was also performed and the corresponding Raman spectra were calculated. Specifically, DFT calculations were performed for the first time on the gallic acid complex with iron.

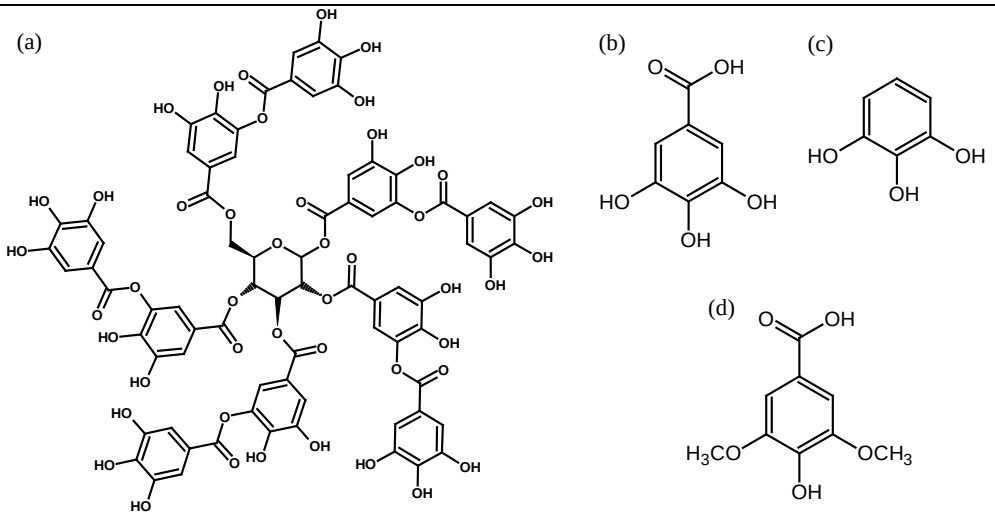

Figure 1. Chemical structure of tannic acid (a), gallic acid (b), pyrogallol (c) and syringic acid (d).

The complexation of iron with these molecules leads to a strong change in color, due to the deep restructuring of the polyphenol that can be clearly seen in their UV-Vis absorption, Raman, and FTIR spectra. Especially, three main characteristic Raman bands were recognized, at 1450-1490 cm^{-1} (ν_1), 1320-1345 cm^{-1} (ν_2) and 400-650 cm^{-1} (ν_3). The effect of pH and complex stoichiometry on these bands was also monitored and related to the structural changes undergone by polyphenols. The interaction with iron produces different optical effects such as a deep change in color, lowering of pH, and fluorescence quenching. Whereas the pH decrease is a negative effect when using IGIs because of the progressive degradation of the paper, the quenching of the polyphenol fluorescence facilitates the Raman inspection of manuscripts since polyphenols show a strong fluorescence emission that overlaps the Raman spectrum.

Acknowledgment

This work was supported by the research grant from the Slovak Grant Agency VEGA (No. 1/0557/20), and by the project implementation: Open scientific community for modern interdisciplinary research in medicine (Acronym: OPENMED), ITMS2014+:313011V455 supported by the Operational Programme Integrated Infrastructure, funded by the ERDF. This work has also been financially supported by the AEI Project, number PID2020-113900RB-I00.

References

[1] A. Daneshfar, P. Hashemi, B. Delfan, M. Tavakkoli and P.M. Rashno, Herbal Med. J. 2 (2017), 71–80.
[2] J.A. Jaén, L. González, A. Vargas and G. Olave, Hyperfine Interact. 148–149 (2003), 227–235.
[3] M. Ezcurra, J.M.G. Góngora, I. Maguregui and R. Alonso, Forensic Sci. Int. 197 (2010), 1–20.
[4] D.M. Goltz, Anal. Lett. 45 (2012), 314–329.
[5] B. Frühmann, F. Cappa, W. Vetter, M. Schreiner, and Father Petrus, Heritage Sci. 6 (2018), 10, 1-12.
[6] S. Valadas, R. Freire, A. Cardoso, J. Mirão, P. Vandenabeele, J.O. Caetano and A. Candeias, Micron 85 (2016), 15–25.
[7] S. Sánchez-Cortés and J.V. García-Ramos, J. V., J. Colloid Interface Sci. 231 (2000), 98–106.
[8] D.R. Pompeu, Y. Larondelle, H. Rogez,O. Abbas, J.A.F. Pierna and V. Baeten, Biotechnol. Agron. Soc. Environ. 22 (2018), 13–28.
[9] A. Ponce, L.B. Brostoff, S.K. Gibbons, P. Zavalij, C. Viragh, J. Hooper, S. Alnemrat, K.J. Gaskell and B. Eichhorn, Anal. Chem. 88 (2016), 5152–5158.
[10] D. Creagh, A. Lee, V. Otieno-Alego and M. Kubik, Radiation Phys. Chem. 78 (2009), 367–374.
[11] S. Bioletti, R. Leahy, J. Fields, B. Meehan, and W. Blau, J. Raman Spectrosc. 40 (2009), 1043–1049.
[12] E.A. Carter, F.R. Perez, J.M. Garcia and H.G.M. Edwards, Phil. Trans. A 374 (2016), 2082, 1-13.
[13] S. Liu, J. Feng, J. Lv and W. Zhang, Pigment Resin Technol. 43 (2014), 45–51.
[14] A.S. Lee, V. Otieno-Alego and D.C. Creagh, J. Raman Spectrosc. 39 (2008), 1079–1084.
[15] A. El Bakkali, T. Lamhasni, M. Haddad, S. Ait Lyazidi, S. Sanchez-Cortes, and E. del Puerto Nevado, J. Raman Spectrosc. 44 (2013), 114–120.
[16] S.A. Centeno, J. Raman Spectrosc. 47 (2016), 9–15.
[17] S. Bruni, S. Caglio, V. Guglielmi, G. Poldi, Appl. Phys. A 92 (2008), 103–108.
[18] J. Gao, X. Yang, W. Yin and M. Li, Evid. Based Complementary Altern. Med. 2018 (2018), 4930371, 1-9.
[19] A. Espina, S. Sanchez-Cortes and Z. Jurašeková, Molecules 27 (2022), 279, 1-17.
[20] A. Espina, M. V. Cañamares, Z. Jurašeková and S. Sanchez-Cortes, ACS Omega (2022) submitted.

Autophagic response of U87MG cells in 3D spheroids stimulated with photodynamic therapy

V. Pevna[1], P. Miskovsky[2] and V. Huntosova[2]

[1] *Department of Biophysics, Institute of Physics, Faculty of Science, P.J. Safarik University in Kosice, Jesenna 5, 041 54 Kosice, Slovakia.*
[2] *Center for Interdisciplinary Biosciences, Technology and innovation park, P.J. Safarik University in Kosice, Jesenna 5, 041 54 Kosice, Slovakia.*

e-mail: viktoria.pevnal@student.upjs.sk

Photodynamic therapy (PDT) belongs to the adjuvant modality of superficial cancer treatment. The light that stimulates the photosensitizer does not usually penetrate deep tissue. Most measurements in cell cultures are performed on monolayers under laboratory conditions. However, tissue is a 3D structure, and results obtained in monolayers may differ significantly in 3D. For this reason, we focused on the construction of 3D spheroids on the model cell line U87MG. These cell types form slightly spherical structures that differ in size. Uniformity of the 3D spheroid model can be achieved if it is grown using the hanging drop method. We used this approach in our study to create a model of a small glioblastoma with a diameter of 1 mm. Hypericin was used as a model of a hydrophobic molecule that induces PDT in cancer cells. Application of light doses of 2-10 J/cm^2 (at 590 nm) resulted in an increase in lactate dehydrogenase produced by spheroids exposed to 500 nM hypericin (see Table 1), which is proportional to the phototoxicity induced in the cells. The phototoxic effect of PDT induced by hypericin resulted in a decrease in spheroid size and regular shape. Figure 1 shows 10 µm sections of spheroids treated with hypericin before and after PDT. After PDT, fragmentation of the peripheral area can be seen. Using confocal fluorescence microscopy of the spheroid after PDT, an accumulation of LC3B vesicles was observed in this area. Western blot analysis of cell lysates extracted from the spheroids confirmed an increase in LC3B in the cells after PDT, similar to that previously observed in U87 MG cells in monolayers [1]. These results suggest stimulation of autophagy by PDT. However, the increased caspase-3 concentration in the same area observed with live imaging of NucView488, a caspase-3 substrate, suggests that apoptosis was also induced. More in-depth studies are needed to understand the effects of the switch between autophagy and apoptosis in 3D spheroids of cancer cells. The signalling between these PDT-induced processes will be the subject of our future study.

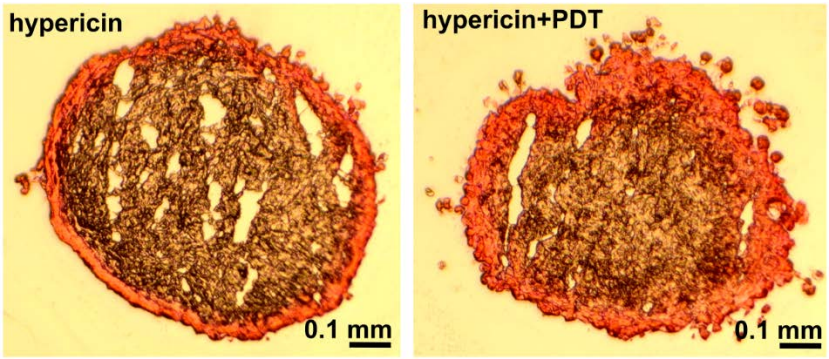

Fig. 1. Section through U87 MG 3D spheroids treated with hypericin and PDT. Fragmentation of the spheroid periphery is observed after PDT. The spheroids were quickly stained with eosin to highlight the peripheral cells.

Table 1. Lactate dehydrogenase levels in 3D spheroids of U87 MG cells measured by the LDH assay with absorbance reader at 450 nm. Spheroid size values measured 24 hours after PDT are summarized in the last column.

	absorption [a.u.]	sd [a.u.]	p (Student T-test)	size [mm]
control	0.456	0.005	-	0,861
hypericin	0.486	0.005	0.07626	0,787
hypericin + 2 J/cm^2	0.801	0.008	0.00016	0,738
hypericin + 4 J/cm^2	1.25	0.011	0.00005	0,671
hypericin + 6 J/cm^2	1.355	0.019	0.00072	0,596
hypericin + 10 J/cm^2	1.325	0.017	0.00044	0,538

Acknowledgment
This work was supported by projects of Slovak research agency APVV-20-0340, PF UPJŠ in Košice vvgs-pf-2021-1788, and the Ministry of education, science, research, and sport of the Slovak Republic, grant number VEGA 1/0156/18. This publication is the result of the project implementation: Open scientific community for modern interdisciplinary research in medicine (Acronym: OPENMED), ITMS2014+: 313011V455 supported by the Operational Program Integrated Infrastructure, funded by the ERDF.

References

[1] V. Pevna, G. Wagnieres and V. Huntosova, Biomedicines, 9 (2021), 1703.

Redox state of F-type ferryl intermediate of bovine cytochrome c oxidase

T. Sztachová[1], A. Tomková[1] , D. Jancura[1] and M. Fabián[2]

[1] *Department of Biophysics, Faculty of Science, P.J.Šafárik University, Jesenná 5, 041 54 Kosice, Slovakia.*
[2] *Center for Interdisciplinary Biosciences, Technology and Innovation Park P. J. Šafárik University, Jesenná 5, 041 54 Košice, Slovakia*

e-mail: tereza.sztachova@student.upjs.sk

In aerobic organisms, molecular respiration is performed by several membrane-bound protein complexes localized in the mitochondria of eukaryotes or in the cell membrane of prokaryotes. The last complexes of these respiratory chains are oxidases. Into this class belongs also cytochrome *c* oxidases (CcO) for which ferrocytochrome *c* (c^{2+}) is a substrate or electron donor. [1] The reduction of O_2 is associated with the transfer of four electrons from cytochrome *c* to CcO by four redox-active centers: Cu_A, the iron of heme *a* (Fe_a), the iron of heme a_3 (Fe_{a3}), and Cu_B. The flow of electrons occurs in sequence: $c^{2+} \rightarrow Cu_A \rightarrow Fe_a \rightarrow Fe_{a3}\text{-}Cu_B$. Where the binuclear $Fe_{a3}\text{-}Cu_B$ center (BNC) is the place of reduction of O_2.

The conversion of O_2 to H_2O at BNC occurs through a sequence of distinct intermediates determined by the number of electrons and protons delivered to this site. From these intermediates, two types of ferryl forms of heme a_3, named the **P** (**P_M**, **P_R**) and **F**-type, have been spectrally discriminated. The **P_M** form is observed when the two-electron reduced CcO reacts with O_2. In this state Tyr radical (Tyr244) should be created together with the ferryl iron (Fe_{a3}^{4+}=O) at the BNC (Fe_{a3}^{4+}=O OH-Cu_B^{2+} $YO^{\bullet}$). It means that this form is two oxidizing equivalents above the oxidized CcO. The following catalytic reduction of the Tyr radical, associated with the proton uptake to BNC, leads to the production of the ferryl **F** form (Fe_{a3}^{4+}=O H_2O-Cu_B^{2+} YOH). [2,3]

The spectrally equivalent **P_M** state can be also produced by the reaction of oxidized CcO with a single molecule of H_2O_2 in the alkaline solutions (Fe_{a3}^{3+} Cu_B^{2+} YOH +H_2O_2 $\rightarrow$ Fe_{a3}^{4+}=O OH-Cu_B^{2+} $YO^{\bullet}$). Surprisingly, the same reaction in the acidic buffers results in the ferryl intermediate with the spectral characteristics of the **F**-type ferryl form (**$F^{\bullet}$**). [4] Despite the spectral similarity of this acidic form with the catalytically produced **F** intermediates, it is assumed that the Tyr radical should be also present in the **$F^{\bullet}$** state (Fe_{a3}^{4+}=O H_2O-Cu_B^{2+} $YO^{\bullet}$). Consequently, the BNC in both the **P_M** and the **$F^{\bullet}$** are in the same redox state.

In this work, we have investigated the redox state of the **$F^{\bullet}$** state by optical spectroscopy, isothermal titration calorimetry together with the reduction of this form by the defined number of electrons. The data confirmed that the formation of the **$F^{\bullet}$** state is certainly linked with the radical formation at the BNC. However, the lifetime of the radical is much shorter comparing to that of the ferryl Fe_{a3}^{4+}=O state. At the time when the peroxide-produced **$F^{\bullet}$** state is spectrally fully developed the radical at the catalytic center is almost completely annihilated. It is very likely that under conditions of our measurements when the external electron donors are missing, the quenching of the radical is due to the autooxidation of the enzyme.

Acknowledgement

This work was supported by the project "Open scientific community for modern interdisciplinary research in medicine (OPENMED)-ITMS2014+: 313011V455" from the Operational Program Integrated Infrastructure funded by the ERDF, the Slovak Grant Agency (VEGA 1/0028/22), and the grant from P. J. Safarik University (VVGS-PF-2021-1790).

References

[1] F.L. Sousa, R. J. Alves, M. A. Ribeiro, J. B. Pereira-Leal, M. Teixeira and M. M. Pereira, Biochim. Biophys. Acta 1817 (2012) 629-637.
[2] M. Wikström, K. Krab and V. Sharma, Chem Rev 118(5) (2018) 2469-2490.
[3] A.A. Konstantinov, FEBS Lett 586(5) (2012) 630-9.
[4] M. Fabian and G. Palmer, Biochemistry 34(42) (1995) 13802-10.

Calorimetric characterization of ferryl intermediates of bovine cytochrome c oxidase

A. Tomková[1] , T. Sztachová[1], M. Fabián[2] and D. Jancura[1]

[1] *Department of Biophysics, Faculty of Science, P.J. Šafárik University, Jesenná 5, 041 54 Kosice, Slovakia.*
[2] *Center for Interdisciplinary Biosciences, Technology and Innovation Park, P. J. Šafárik University, Jesenná 5, 041 54 Košice, Slovakia*
e-mail: adriana.tomkova1@student.upjs.sk

Membrane bound respiratory cytochrome c oxidases catalyze the reduction of O_2 to H_2O by electrons donated by ferrocytochrome c (c^{2+}). The electron transfer (ET) in CcO is facilitated by four redox active centers: Cu_A, iron of heme *a* (Fe_a), iron heme a_3 (Fe_{a3}) and Cu_B. Cu_A is the first electron acceptor from c^{2+}. ET then continues rapidly to Fe_a and finally to the binuclear catalytic Fe_{a3}-Cu_B center. At the binuclear Fe_{a3}-Cu_B center (BNC), the reduction of O_2 takes place and also this is the site where the external ligands are bound. The process of O_2 reduction by CcO is associated with the generation of the transmembrane proton gradient. This gradient is produced by two different mechanisms. One is oxidation of c^{2+} on one side of membrane linked with the proton uptake for water formation from the other side of membrane. Second mechanism is the proton pumping. This process represents an additional proton translocation across the membrane. On average, one proton is pumped for one electron transferred by CcO from c^{2+} to O_2. However, in spite of large progress in the understanding of enzymology of the respiratory oxidases, the mechanism of the proton pumping has not been precisely determined yet [1, 2].

Clearly, the proton pumping is driven by energy released from redox reactions occurring in CcO. By application of different spectroscopic techniques it was possible to establish a sequence of the intermediates during the conversion of O_2 to H_2O. From these intermediates, two ferryl states of BNC are very likely involved in the proton translocation. The first one is the ferryl $\mathbf{P_R}$ form (Fe_{a3}^{4+}=O OH-Cu_B^{2+}), transiently observed in the reaction of fully reduced CcO with O_2. The $\mathbf{P_R}$ state after absorption of one H^+ into BNC is converted to the second ferryl form, **F** form (Fe_{a3}^{4+}=O H_2O-Cu_B^{2+}). The delivery of one electron and H^+ into the **F** state regenerates the fully oxidized CcO (**O**) (Fe_{a3}^{3+} Cu_B^{2+}) [2, 3, 4]. Each step in the sequence ($\mathbf{P_R \rightarrow F \rightarrow O}$) is also coupled with the pumping of one proton. Consequently, each conversion should liberate the sufficient energy to uptake of two H^+ from one side of membrane and to release one H^+ on the other side. Even though the transitions between these ferryl forms play a key role in the proton pumping, their detailed thermodynamic description is missing.

In this study we employed the isothermal titration calorimetry (ITC) and optical spectroscopy to determine the enthalpy (ΔH) and the entropy (ΔS) changes during $\mathbf{P_R \rightarrow O}$ and $\mathbf{F \rightarrow O}$ conversions. The preliminary measurements of heat released during one electron reduction of both $\mathbf{P_R}$ and **F** forms by ITC revealed only small values of ΔH. For $\mathbf{F \rightarrow O}$ transition the ΔH = -3.7 kcal/mol was found. (ΔH for $\mathbf{P_R \rightarrow O}$ conversion is ΔH = - 4.7 kcal/mol). Taking into account the estimated redox potentials of $\mathbf{P_R}$ and **F** [2], it was possible to calculate ΔS = +19.1 cal/mol.K for $\mathbf{F \rightarrow O}$ transformation and +18.3 cal/mol.K for the conversion of $\mathbf{P_R \rightarrow O}$. These results indicate that there is almost equal contribution of the enthalpic and entropic term to the Gibbs energy associated with these two transitions.

Acknowledgement
This work was supported by the project "Open scientific community for modern interdisciplinary research in medicine (OPENMED)-ITMS2014+: 313011V455" from the Operational Program Integrated Infrastructure funded by the ERDF, and the project of the Slovak Grant Agency (VEGA 1/0028/22).

References

[1] S. Yoshikawa, A. Shimada, Chem Rev, 115(4) (2015), 1936-1989.
[2] M. Wikstrom, K. Krab and V. Sharma, Chem Rev, 118(5) (2018), 2469-2490.
[3] K. Faxen, G. Gilderson, P. Adelroth and P. Brzezinski, Nature, 437(7056) (2005), 286-289.
[4] I.V. Belevich, M. Wikstrom, Nature, 440 (2006), 829-832.

Development of a new highly selective and sensitive detection method of the glyphosate pesticide by Surface-Enhanced Raman Scattering

F. Fuenzalida Sandoval[1], S. Sanchez-Cortes [2,3], P. Miškovský [4,5], Z. Jurašeková[1]

[1]*Department of Biophysics, Faculty of Science, P. J. Šafárik University, Jesenná 5, 040 01 Košice, Slovakia*

[2] *Institute of the Structure of Matter, IEM-CSIC, Serrano 121, 28006 Madrid, Spain*

[3] *Center for Interdisciplinary Biosciences, Technology and Innovation Park, P. J. Šafárik University, Jesenná 5, 040 01 Košice, Slovakia*

[4] *Technology and Innovation Park, P. J. Šafárik University, Trieda SNP 1, 040 11 Košice, Slovakia*

[5] *SAFTRA photonics, s.r.o., Moldavská cesta 51, 040 11 Košice, Slovakia*

e-mail: franciscabeleen.f@gmail.com

Glyphosate is an organophosphate compound with herbicidal properties. In 1974, Monsanto began marketing it as a broad-spectrum herbicide whereas several formulations of glyphosate-based herbicides have been sold in mixtures with various adjuvants used to increase its penetration in plants and thus, improve its activity [1]. Once in the plant, glyphosate binds to manganese, an essential element for the enzyme 5-enolpyruvyl-shikimate-3-phosphate synthase, which in turn is necessary for the biosynthetic pathway for the tyrosine, phenylalanine, and tryptophan formation [2]. Even a small amount of glyphosate accumulated in the crop, as a result of the spray drift with glyphosate or its direct application, can damage or even cause plant death after a few days [3, 4]. Besides, many studies pointed to the toxicity of the glyphosate-based herbicides negatively affecting also other living organisms such as amphibians, fish, reptiles, birds, etc. Moreover, the use of this herbicide, depending on the dose and exposure time, can also cause different undesirable effects in humans; for example, carcinogenic, hepatorenal, teratogenic, and tumorigenic effects, as well as endocrine disruption, metabolic alterations, or oxidative stress, even at concentrations below regulatory limits [5].

In the 1990s, commercial genetically modified crops resistant to glyphosate emerged, which resulted in both more hectares planted with resistant crops to be sprayed with glyphosate as well as more intensive application of the glyphosate [6]. Nowadays, glyphosate's use is evidenced in the vast majority of the EU countries, since its use is not banned currently. Nevertheless, its harmfulness and probable carcinogenicity [7] are continuously discussed and the issue of its monitoring is becoming increasingly important from the point of view of the EU and its environmental policy. Current European legislation allows glyphosate use until December 2022 [8]. Besides, it is interesting to point out the fact that the authorization of the European Commission for the use of glyphosate for further 5 years, renewed in 2017, was granted on the basis of scientific arguments/evidence provided exclusively by the manufacturers and their reports which are, moreover, confidential to general consultation [1, 7]. In this context, it is essential to have a reliable tool for on-site identification and quantification of glyphosate to assess the national security risks caused by this herbicide.

Surface-enhanced Raman spectroscopy (SERS), unlike techniques currently used for sensitive detection of glyphosate, such as GC, HPLC, UV absorption, and fluorescence spectroscopy, possesses several advantages: no need for sample pre-treatment, time- and cost-effective measurements, portable equipment [9, 10]. However, the SERS detection of glyphosate shows also a disadvantage: direct detection methods fail to achieve low detection limits [10]. The reason for this low sensitivity is attributed to the high polarity of the molecule, which seriously

hinders the approach of the pesticide to the surface of metallic nanostructures and the poor affinity for the metals of these nanostructures.

In the present work, the SERS detection method of glyphosate, based on the reaction proposed by Jan *et al.* [11], was tested and optimized. We have observed that an appropriate modification of the chemical structure of the molecule can result in a compound that demonstrates a higher affinity for the metal surface and, in consequence, increased sensitivity of the SERS analysis of this important pesticide leading to a limit of detection of 1 ppb.

Acknowledgment

This work has been supported by the Scientific Grants Agency of the Ministry of Education of the Slovak Republic (APVV-19-0580), by the grant of the Faculty of Sciences of the P.J. Šafárik University in Košice (VVGS-PF -2021-1770) and by the project OPENMED (ITMS2014+:313011V455) from the EU Structural funds. This work has also been financially supported by the AEI Project, number PID2020-113900RB-I00.

References

[1] C. Peillex and M. Pelletier, J. Immunotoxicol. 17 (2020), 163–174.
[2] M. E. Richmond, J. Environ. Stud. Sci. 8 (2018), 416–434.
[3] S. O. Duke, Pest Manag. Sci. 74 (2018), 1027–1034.
[4] A. H. C. Van Bruggen, M.M. He, K. Shin et al., Sci. Total Environ. 616–617 (2018), 255–268.
[5] I. M. Meftaul et al., K. Venkateswarlu, R. Dharmarajan et al., Environ. Pollut. 263 (2020), 114372.
[6] C. M. Benbrook, Environ. Sci. Eur. 28 (2016), 1–15.
[7] C. Martins-Gomes, T. L. Silva, T. Andreani, and A. M. Silva, J. Xenobiotics12 (2022), 21–40.
[8] https://ec.europa.eu/food/plant/pesticides/glyphosate_en
[9] S. Kodama, Y. Ito, A. Taga, et al., J. Health Sci. 54 (2008), 602–606.
[10] A. Feis, C. Gellini, M. Ricci, L. Tognaccini, M. Becucci, and G. Smulevich, Vib. Spectrosc. 108 (2020), 103061.
[11] M. R. Jan, J. Shah, M. Muhammad, and B. Ara, J. Hazard. Mater. 169 (2009) , 742–745.

Thermal Stability of Human Serum Albumin in the Presence of Hydroxyquinone Molecules: a Differential Scanning Calorimetry Study

G. Fabriciová[1], V. Vaník[2] and D. Jancura[1]

[1] *Department of Biophysics, Institute of Physics, P. J. Šafárik University in Košice, Jesenná 5, 041 54, Košice, Slovakia.*
[2] *Department of Biophysics, Institute of Experimental Physics, Slovak Academy of Sciences, Bulharská 1, 040 01 Košice, Slovakia.*

e-mail: daniel.jancura@upjs.sk

Human serum albumin (HSA) is the most abundant protein component of the circulatory system with several physiological functions. HSA is primarily involved in the binding and transport of fatty acids, hormones, metabolites, endogenous ligands, and drugs.

Understanding the relationship between the structure of proteins and the energetics of their stability and binding with other biomolecules is very important in biotechnology and is essential for the engineering of stable proteins and for the structure-based design of pharmaceutical ligands [1]. From this point of view, the study of the thermal stability of HSA as well as the investigation of the influence of the formation of the HSA-drug complex on the stability is of utmost importance for clinical and pharmaceutical practice. In the previous years, the thermal stability of HSA has been widely investigated mainly by differential scanning calorimetry (DSC) [2]. This technique enables direct determination of the thermodynamic parameters (calorimetric and van't Hoff enthalpies (ΔH_{cal} and ΔH_{vH}) and temperature (T_m)) of denaturation as well as evaluation of entropy and Gibbs energy of the transitions between the folded and unfolded states of the studied biopolymer.

Derivatives of anthraquinones (Fig. 1) constitute an important class of natural and synthetic compounds with a wide range of applications. Some of them have been used for centuries for medical applications, for example, as laxatives, antimicrobial and anti-inflammatory agents. Current therapeutic indications include constipation, arthritis, multiple sclerosis, and cancer.

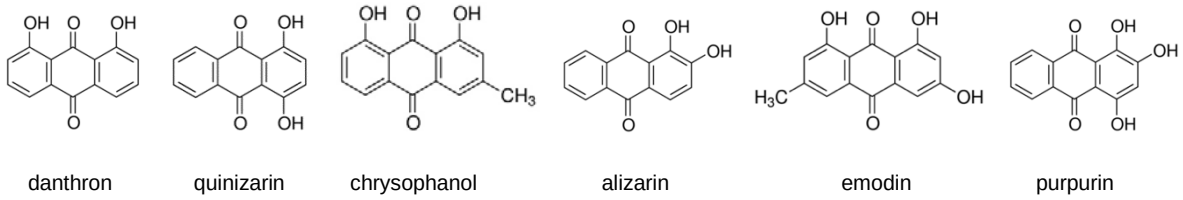

Fig. 1. Different types of hydroxyderivatives of anthraquinone.

Our results show that the presence of dihydroxyanthraquinones and trihydroxyanthraquinones in a solution of HSA can significantly stabilize this protein, and the stabilization effect depends on the position of hydroxyl groups in di- and trihydroxyanthraquinone structure. In the case of alizarin (1,2-dihydroxyanthraquinone) (Fig. 2D), emodin (6-methyl-1,3,8-trihydroxyanthraquinone) (Fig. 2E) and purpurin (1,2,4-trihydroxyanthraquinone) (Fig. 2F), a significant increase of the temperature and enthalpy of HSA denaturation is observed. On the other hand, the changes in the temperature and enthalpy of HSA denaturation in the presence of danthron (1,8-dihydroxyanthraquinone) (Fig.2A), quinizarin (1,4-dihydroxyanthraquinone) (Fig. 2B) and chrysophanol (1,8-dihydroxy-3-methyl-anthraquinone) (Fig. 2C) are almost negligible.

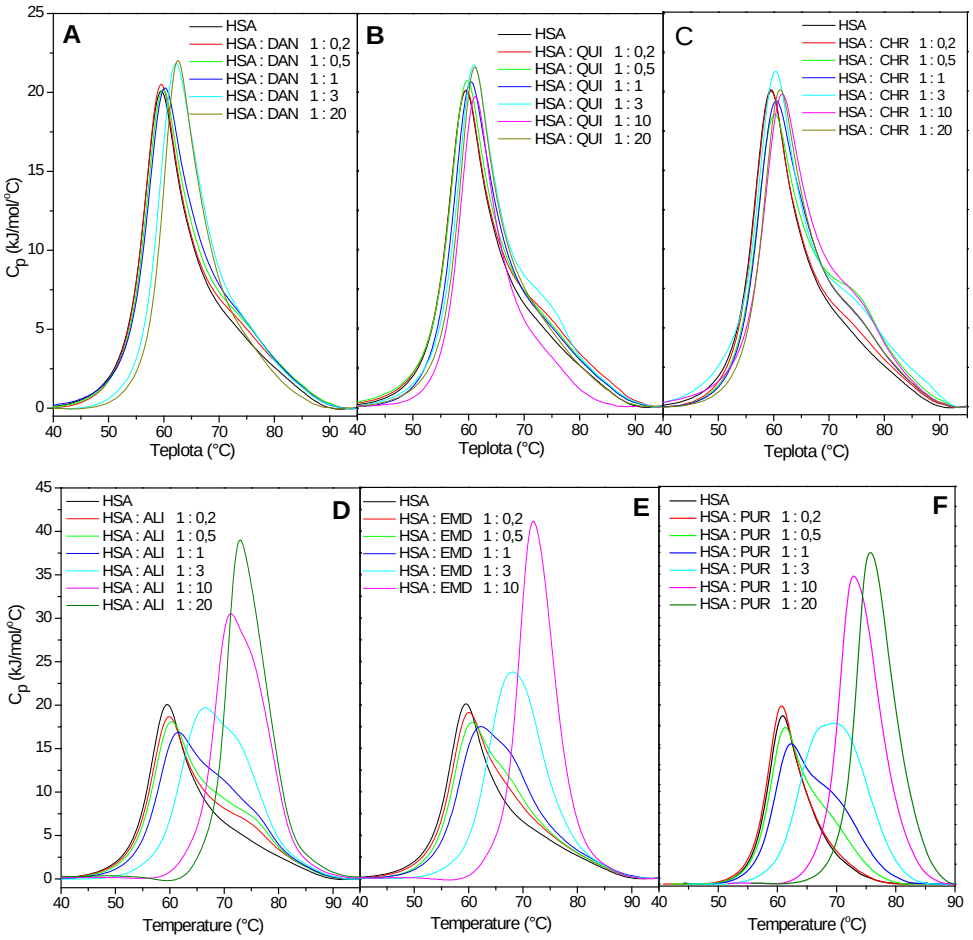

Fig. 2. DSC scans of HSA at various molar ratios: A) HSA : danthron, B) HSA : quinizarin, C) HSA : chrysophanol, D) HSA : alizarin, E) HSA : emodin and F) HSA : purpurin.

We suggest that the stabilizing effect on HSA structure can be attributed to the presence of two hydroxyl groups on one ring of the anthraquinone skeleton at positions 1,2 or 1,3.

Acknowledgment

This work was supported by the research grants from the Slovak Grant Agency APVV-15-0485, APVV-20-0340 and the project "Open scientific community for modern interdisciplinary research in medicine (OPENMED)", ITMS2014+: 313011V455 supported by the Operational Programme Integrated Infrastructure, funded by the ERDF

References

[1] B. Elsadek and F. Kratz, J. Controlled Release 157 (2012), 4-28.

[2] G. Bruylants, J. Wouters and C. Michaux, Current Medicinal Chemistry 12 (2005), 2011-2020.

Effect of Random Copolymer Nanosystems on Model Membranes and Whole Human Blood Rheological Properties

N. Naziris[1], S. Šutý[2], D. Selianitis[3], J. Jacko[2], Z. Garaiová[2], S. Pispas[3], M. Ionov[1], M. Bryszewska[1] and I. Waczulikova[2]

[1] *Department of General Biophysics, Faculty of Biology and Environmental protection, University of Lodz, 141/143 Pomorska, 90-236 Lodz, Poland.*
[2] *Department of Nuclear Physics and Biophysics, Faculty of Mathematics, Physics and Informatics, Comenius University, Mlynska Dolina F1, 84248 Bratislava, Slovakia.*
[3] *Theoretical and Physical Chemistry Institute, National Hellenic Research Foundation, 48 Vassileos Constantinou Avenue, 11635 Athens, Greece.*

e-mail: nikolaos.naziris@biol.uni.lodz.pl

Copolymers have attracted much attention lately as components of drug delivery nanosystems (DDnSs). They can be either used through their self-assembly or combined with other nanotechnological platforms, *e.g.*, lipids and liposomes, to produce mixed/chimeric nanosystems. Their unique morphologies and functionalities can aid the delivery of therapeutic and diagnostic molecules to target tissues [1,2].

The aim of the present work was to develop polymeric nanoparticles comprised of amphiphilic poly(lauryl methacrylate-co-2-(dimethylamino)ethyl methacrylate) P(LMA-co-DMAEMA) or poly(lauryl methacrylate-co-2-(dimethylamino)ethyl methacrylate-co-oligo(ethylene glycol) methyl ether methacrylate) P(LMA-co-DMAEMA-co-OEGMA) random/statistical copolymers and study their interactions with model membranes, as well as their effect on the rheological properties of human blood. These studies help to assess the biophysical profile and biocompatibility of these nanoparticles for their use as DDnSs [3].

The copolymers were synthesized by reversible addition−fragmentation chain-transfer (RAFT) polymerization and characterized by size-exclusion chromatography (SEC) and nuclear magnetic resonance (NMR). Polymeric nanostructures were prepared by the thin-film hydration method, while their physicochemical properties were assessed through dynamic and electrophoretic light scattering (DLS and ELS). The interactions between the nanoparticles and negatively charged DMPC:DMPG:cholesterol liposomes in Na-phosphate buffer (10 mM, pH 7.4) were then evaluated through DLS, ELS, and fluorescence anisotropy. Finally, the effect of the polymeric nanoparticles on the viscosity and flow of whole human blood was studied.

The polymeric nanoparticle size was in the nanoscale, around 110 nm with a polydispersity index (PDI) of 0.5-0.6, while their zeta potential was around 5 mV. The effect of the nanoparticles on the physicochemical properties of liposomes was concentration-dependent: the hydrodynamic diameter and PDI of liposomes were increased, while their zeta potential was decreased in absolute value. The fluidity of the membranes was also affected by both polymers. Blood rheology measurements showed an increase in blood viscosity at a polymer concentration of 5 μM. P(LMA-co-DMAEMA-co-OEGMA) appeared to have a greater effect on the model liposomes and blood.

The results indicate that amphiphilic copolymer nanoparticulate structures, depending on their composition, properties, and concentration, bring about considerable effects on model membranes and blood rheological properties, which should be taken into account for further utilization of such systems in biomedical applications.

Acknowledgment
Financed by NAWA International Academic Partnership Programme, project EUROPARTNER No. PPI/APM/2018/1/00007/U/001, by APVV, project No. SK-BY-RD-19-0019, and by VEGA, project No. 1/0756/20.

References

[1] E. Reimhult, M. M. Virk, J. Biomed. Res. 35 (2021), 301-309.
[2] L. Li, K. Raghupathi, C. Song, P. Prasad and S. Thayumanavan, Chem. Comm. 50 (2014), 13417-13432.
[3] U. Michalczuk, R. Przekop and A. Moskal, Bull. Pol. Acad. Sci. 70 (2022), e140437.

Deep learning in confocal microscopy of cardiomyocytes

A. Zahradnikova jr.[1] and P. Skrabanek[2]

[1] *Institute of Experimental Endocrinology, Biomedical Research Center of the Slovak Academy of Sciences, Bratislava, Slovakia.*
[2] *Institute of Automation and Computer Science, Brno University of Technology, Brno, Czech Republic.*

e-mail: ueensash@savba.sk

In the study of changes occurring in cardiomyocytes, quantitative analysis of the observed phenomena is necessary. Modern confocal microscopes can generate a large amount of image data quite automatically, but the analysis of the datasets is largely dependent on expertise and manhours put in by the researchers. Automatization of the analysis would be beneficial to not only decrease the time necessary for the evaluation of the image data but also to prevent bias or variability introduced by the individuals analyzing the images.

Our aim was to develop tools to analyze the image data automatically, including methods to enlarge the limited number of images available for the training of the proposed solution.

We concentrated on the classification of developmental stages of maturing cardiomyocytes based on the level of complexity and pattern of their t-tubule formation. We have built a system for the automatic assessment of cardiomyocyte development stages (SAACS) from confocal images [1]. For this purpose, we have proposed a densely connected convolutional network and designed an efficient data augmentation technique to extend the limited training data. We combined geometric transformations with manual image editing (Fig. 1).

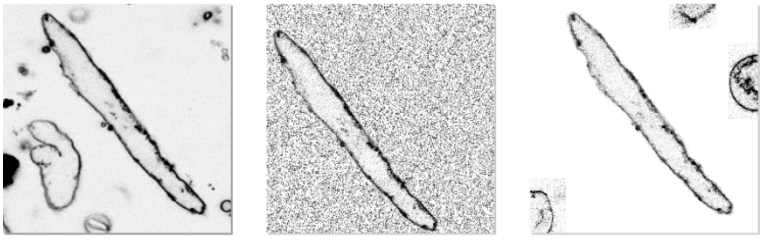

Fig. 1. Augmentation of source images by manually modified images. The cardiomyocyte in the source image (a) is manually cut while respecting its borders and pasted on different backgrounds (b) and (c). Image adapted from [1]

To simplify the evaluation of SAACS performance, we have implemented a class probability graph. The graph shows for each image in a test set its probabilities belonging to the recognized classes. The graph is capable to show the probabilities for various rotations of the image (Fig. 2).

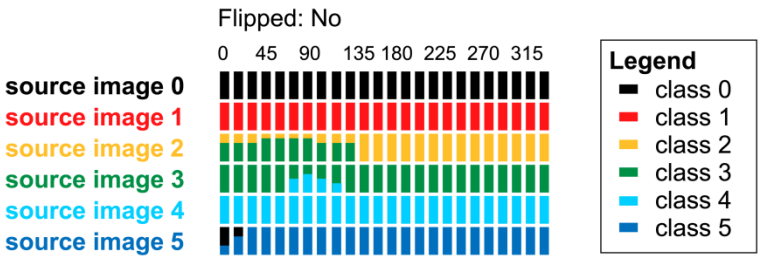

Fig. 2. Class probability graph. To increase the number of evaluation images, each source image was horizontally flipped (not shown here) and both forms were rotated (degrees of rotation in the first line). For each rotation of the source image (individual bars), the probability of belonging to a specific class is color-coded. Image adapted from [1].

The training subset included 15 images of each category of 6 categories. Using augmentation techniques, we expanded the dataset to a final 13050 images per category. The enhanced dataset was able to improve the performance of SAACS from per-class accuracy (acc) = 64.98%, macro-averaging precision (pr_M) = 63.88%, macro-averaging recall (re_M) = 64.01% to acc = 79.67%, pr_M = 72.08%, re_M = 71.29%. Class probability graph showed improvement in correct identification of images in all classes.

In conclusion, we have shown that deep learning can be successfully used for the quantification of confocal data even when trained on small datasets.

Acknowledgment
The work was supported by the project VEGA 2/0182/21 and by the Research and Development Operational Program ITMS 26230120006, co-financed by the European Regional Development Fund.

References
[1] P. Škrabánek and A. Zahradníková Jr., PLoS ONE 14 (2019), e0216720.

Robust estimation of parameters of calcium signals recorded from cardiac myocytes.

I. Baglaeva[1], B. Iaparov[1], A. Zahradníková jr.[1], I. Zahradník[1] and A. Zahradníková[1]

[1] *Department of Cellular Cardiology, Institute of Experimental Endocrinology, Biomedical Research Center, Slovak Academy of Sciences, Bratislava, Slovakia.*

e-mail: iuliia.baglaeva@savba.sk

The changes in cytoplasmic calcium concentration regulate the contraction of cardiac myocytes [1, 2]. Impairment of calcium fluxes together with structural changes of cardiomyocytes can lead to problems in excitation-contraction coupling and hence to various myocardial pathologies such as arrhythmias, hypertrophy, and heart failure. Changes in intracellular calcium concentration can be recorded in isolated cardiomyocytes using laser scanning fluorescence confocal microscopy as transient changes in the fluorescence of calcium-sensitive dyes. These calcium transients are the sum of brief local calcium signals emerging from individual calcium release sites in response to electrical stimulation. The time dependence of the calcium transients is characterized by specific parameters, namely, the amplitude, time to peak (*TTP*), duration at half maximum (*FDHM*), rise time, and decay time. The amplitude of the calcium transient characterizes the amount of calcium released to the myocyte cytoplasm. The other parameters characterize the kinetics of the calcium transient.

To find the parameters of calcium transients, the recorded signals have to be analyzed reliably and rapidly, which is not a trivial task due to the presence of excess noise, irregular time course, and random instabilities, and since a large number of events needs to be analyzed in prolonged recordings. The currently available software has inherent limitations, typically, requiring manual input or specific recording equipment, and insufficient ability to process noisy data. To analyze large datasets efficiently, and to eliminate user-dependent errors, we developed automatic software that can be instrumental for fast and complex analysis of transient signals. The algorithm was implemented as a module for Python (https://www.python.org/). The algorithm for transient analysis includes automatic detection of a transient, determination of its onset time (t_0) if the time of the stimulus is not provided, estimation of the basal signal level, approximation of the transient by a model-independent Gaussian process [3], determination of the amplitude at the time of the peak (A, t_p), and the half-amplitude duration of the best-fit transient. The time-to-peak was calculated as $TTP = t_p - t_0$, and the rise time and decay time were calculated between 20% and 80% of the amplitude.

For testing the performance of parameter estimation, we simulated calcium transients with known parameters using the model ToR-ORd [4]. A sequence of 100 identical calcium transients was generated and combined with various simulated Gaussian noise levels to set the signal-to-noise ratios (SNRs) to 2, 5, 7, 10, 15, 20, 40, 60, 80, and 100. An example of simulated calcium transients with an SNR of 10, a value typical for real experiments, is shown in Figure 1.

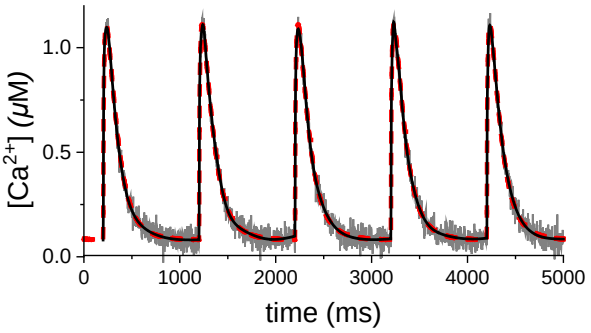

Fig. 1. A detail of a representative fit of simulated records with SNR = 10. The simulated sequence of calcium transients, the simulated sequence with added Gaussian noise, and the best fit curve are shown as a red, a grey, and a black line, respectively.

The algorithm fitted all simulated transients even at the very low SNR of 2. The best-fit curves approximated the simulated transients reliably. Estimation of parameters of 100 transients took 3 - 4 min on a PC. The

dependence of the estimated parameters on the value of SNR is shown in Fig. 2 for the parameter FDHM. The estimated parameters of individual transients were within 5% of the theoretical value for SNR > 5 in the case of FDHM, for SNR > 10 in the case of decay time, and within 10% of the theoretical value for SNR > 20 in the case of amplitude, TTP and rise time.

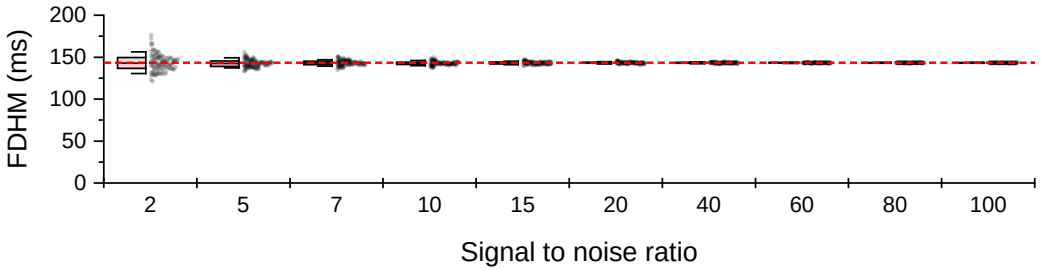

Fig. 2. Distribution of 100 FDHM estimates at different SNR values. The individual transient FDHM estimates (gray dots) are shown together with the half-box statistic (left to data). The black dashed line inside the half-box represents the median, whiskers show the 10% and 90% percentile, and the half-box shows the 25% and 75% percentile. The red dashed line shows the FDHM of the original model without the noise.

The simulated noisy transients were analyzed in batches of 20, imitating experiments on individual myocytes, and the average parameters of individual batches at different SNR values were compared with the parameters of the original model transient and expressed as a relative difference (Fig. 3). The relative deviation of the measured parameters from the true value was smaller than 5% at SNR = 5, with the rise time and the amplitude being the most sensitive to the noise. At SNR = 10, the relative deviations did not exceed 1%. Interestingly, the mean decay time was significantly different from the true value even at large SNR values ($p < 0.05$, one-sample t-test). The deviation was approximately 300 µs, which can be neglected in comparison with the line scan sampling rate of 400 Hz.

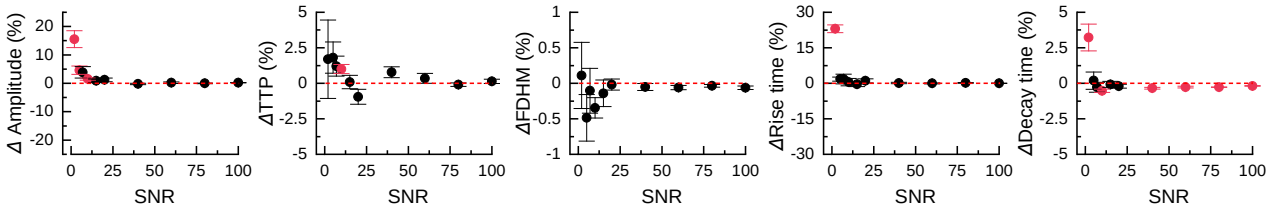

Fig. 3. The relative error of parameter estimation, i.e., the relative difference between the mean of estimates and the theoretical value at different signal-to-noise ratios. Values significantly different from 0 ($p < 0.05$, one-sample t-test) difference are shown as red circles.

In conclusion, our results show that, even in the presence of high levels of noise, the Gaussian process approach is convenient and can be used for the reliable estimation of kinetic parameters of transient signals that cannot be described by an explicit function.

Acknowledgment

The research was supported by the SAV-TUBITAK project JRP/2019/836/RyRinHeart, by the project VEGA 2/0182/21, and by the Operational Programme Integrated Infrastructure for the project: Long-term strategic research of prevention, intervention, and mechanisms of obesity and its comorbidities, IMTS: 313011V344, co-financed by the European Regional Development Fund.

References

[1] D. M. Bers, Nature 415 (2002), 198–205.
[2] D.A. Eisner, J.L. Caldwell, K. Kistamás and A.W. Trafford, Circ. Res, 121 (2017), 181–195.
[3] C. K. Williams, C. E. Rasmussen, Gaussian processes for machine learning. Cambridge, MA: MIT press. (2006).
[4] J. Tomek, A. Bueno-Orovio, E. Passini, X. Zhou, A. Minchole, O. Britton and C. Bartolucci, Elife 8 (2019), e48890.

Calcium transient alterations in cardiac myocytes of voluntarily running rats detected by calcium indicator Fluo-3

M. Cagalinec[1,2], I. Baglaeva[1], A. Zahradníková ml[1], B. Iaparov[1], I. Zahradník[1] and A. Zahradníková[1]

[1] *Dept. of Cellular Cardiology, Institute of Experimental Endocrinology, Biomedical Research Center, Slovak Academy of Sciences, Dúbravská cesta 9, 845 05 Bratislava.*
[2] *Centre of Excellence for Advanced Material Application, Slovak Academy of Sciences, Dúbravská cesta 9, 845 11 Bratislava.*

e-mail: michal.cagalinec@savba.sk

Introduction: Physical exercise is a well-known factor to improve cardiac performance by eliciting adaptations such as increased myocardial mass and ventricular chamber size. Various animal models of exercise have been developed, including voluntary exercise models where animals have free access to training regimes. While some studies demonstrated that training increases cardiomyocyte contractility [1], others demonstrated little change [2-4] or changes dependent upon experimental conditions [5]. Training does not seem to be associated with an increase in the amplitude of intracellular calcium ($[Ca^{2+}]_i$) transients [1-3]. However, an increase in myofilament Ca^{2+} sensitivity has been suggested as a mechanism for increased contractility in some [1,5,6] but not all [3] studies. Our group focuses on the early changes in the excitation-contraction coupling in models of pathological and physiological hypertrophy. We have shown that in both, pathological hypertrophy (induced by a single dose of isoproterenol) [7] and in the course of physiological hypertrophy (postnatal development) [8] remodeling occurs rapidly at both morphological and functional levels.

Aims: Since training produces physiological hypertrophy accompanied by changes in calcium signaling, the aim of this study was to analyze the parameters of calcium transients in isolated left ventricular myocytes derived from rats at the early stage of training, i.e., after two weeks of voluntary exercise.

Methods: Young adult male Wistar rats weighing ~ 260 g were individually placed in cages equipped with a voluntary running wheel, and the overall running distance was monitored daily. Sedentary rats were housed individually without access to a running wheel. After two weeks of this experimental protocol, left ventricular myocytes were isolated by retrograde perfusion of the heart with Tyrode solution containing collagenase/protease (Liberase, Roche) [9]. To record the calcium transients, myocytes were loaded with the fluorescent calcium indicator Fluo-3/AM at a concentration of 2.5 µmol/l at room temperature for 15 minutes. The cells were then gently centrifugated at 300 RPM for 1 minute and the supernatant was gradually replaced with a modified Tyrode solution containing 1.2 mmol/l $CaCl_2$. Myocytes were perfused with the same solution at a rate of 1 ml/min and electrically stimulated using the Myopacer current pulse generator at a rate of 1 Hz. Fluo-3 fluorescence (excitation at 488 nm, emission at 505 - 560 nm) was recorded by a Leica SP2 AOBS inverted confocal microscope equipped with a 63×/1.4 NA Planapochromat oil immersion objective. The signal was acquired using a line scan protocol at a rate of 0.4 Hz [9]. The confocal data were further transferred to an in-house developed automatic software for the determination of the basal signal level, signal amplitude at the time of the peak (A, t_p), and the signal duration at half-amplitude (*FDHM*). The time to peak was calculated as $TTP = t_p - t_0$, and the rise time and decay time were calculated between 20% and 80% of the amplitude. The data were processed and statistically analyzed in Origin software.

Results: After two weeks of voluntary exercise we have observed a significant decrease in the Ca^{2+} transient amplitude, *FDHM*, *TTP*, and 20-80% rise time in comparison with calcium transients from myocytes of sedentary rats. Of note is the reduced dispersion of these kinetic

parameters among exercising rats relative to sedentary ones. The decay time of the calcium transient was the only parameter not affected by the voluntary exercise (Fig. 1).

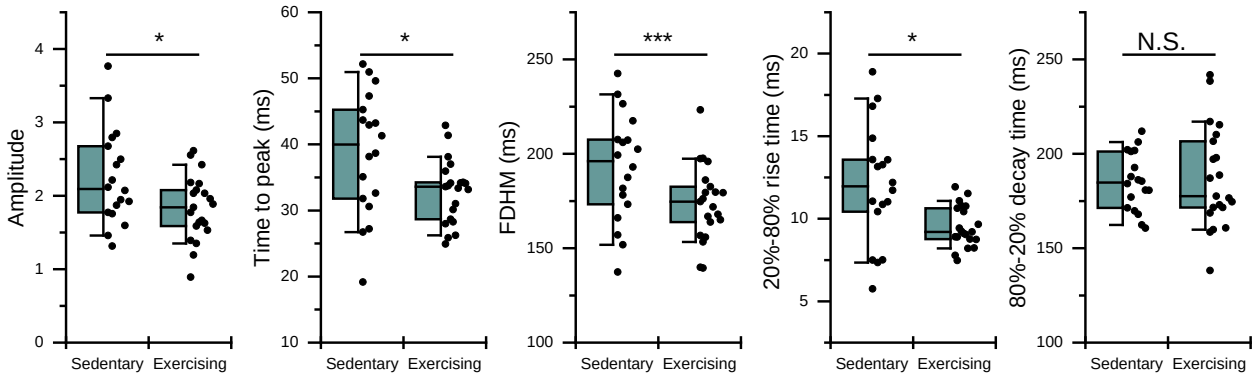

Fig. 1. Parameters of calcium transients of sedentary and exercising rats. Points show the average parameters of 15-20 transients recorded per cell. The box corresponds to the 25th-75th percentile and the whiskers to the 10th-90th percentile. The line shows the median of 18 myocytes of sedentary rates and 21 myocytes of exercising rats. The probability levels correspond to $p < 0.05$ (*) and $p < 0.005$ (***).

Conclusions: These results indicate that even two weeks of voluntary exercise may affect the kinetics of calcium transients in ventricular myocytes of rats. This indicates a positive effect of regular exercise on the activation of calcium signalling.

Acknowledgment

This work was supported by the projects VEGA 2/0121/19 and 2/0182/21 from the Scientific Grant Agency of the Ministry of Education, Science, Research and Sport of the Slovak Republic and the Slovak Academy of Sciences. This work was performed during the implementation of the project Building-up Centre for advanced materials application of the Slovak Academy of Sciences, ITMS project code 313021T081 supported by the Integrated Infrastructure Operational Programme funded by the ERDF.

References

[1] U. Wisloff, J. P. Loennechen, G. Falck, V. Beisvag, S. Currie, G. Smith, O. Ellingsen, Cardiovasc Res, 50 (2001), 495–508.
[2] M. H. Laughlin, M. E. Schaefer, M. Sturek, J Appl Physiol, 73 (1992), 1441–1448.
[3] B. M. Palmer, A. M. Trayer, S. M. Snyder, R. L. Moore, J Appl Physiol, 85 (1998), 2159–2168.
[4] A. J. Natali, D. L. Turner, S. M. Harrison, E. White, J Exp Biol, 204 (2001), 1191–1199.
[5] R. L. Moore, T. I. Musch, R. V. Yelamarty, J. R. C. Scaduto, A. M. Semanchick, M. Elensky, J. Y. Cheung, Am J Physiol, 264 (1993), C1180–1189.
[6] G. M. Diffee, E. A. Seversen, M. M. Titus, J Appl Physiol, 91 (2001), 309–315.
[7] M. Novotova, A. Zahradnikova, Jr, Z. Nichtova, R. Kovac, E. Kralova, T. Stankovicova, A. Zahradnikova and I. Zahradnik, Sci Rep 10 (2020) , 8076.
[8] K. Mackova, A. Zahradnikova, Jr, M. Hotka, B. Hoffmannova, I. Zahradnik and A. Zahradnikova. Eur Biophys J 46 (2017), 691-703.
[9] M. Cagalinec, A. Zahradnikova, A. Zahradnikova, Jr, D. Kovacova, L. Paulis, S. Kurekova, M. Hotka, J. Pavelkova, M. Plaas, M. Novotova and I. Zahradnik. Front Physiol 10 (2019), 172.

Inertial self-propelled particles in narrow channels

D. Horváth[1], C. Slabý[2], A. Hovan[2], Z. Tomori[3], P. Miškovský[1] and G. Bánó[2]

[1]*Center for Interdisciplinary Biosciences, TIP, P. J. Šafárik University, Jesenná 5, 041 54 Košice, Slovak Republic*
[2]*Department of Biophysics, Faculty of Science, P. J. Šafárik University, Jesenná 5, 041 54 Košice, Slovak Republic.*
[3]*Institute of Experimental Physics SAS, Department of Biophysics, Watsonova 47, 040 01 Košice, Slovak Republic*

e-mail: gregor.bano@upjs.sk

Self-propelled particles represent the basic building block of active matter. Many different systems can be mentioned here with scales covering few orders of magnitude. Self-propelled colloids, bacterial colonies, centimeter-sized vibrated granular particles or large-scale animal flocks and swarms are just few examples. The interesting features of active matter, including unique collective behavior, originate from: a) the propulsion of particles, b) the interactions of self-propelled particles with each other and c) the interactions of particles with their surroundings (potentials and/or constrictions). Self-propelled particles are also aimed to be utilized for drug delivery purposes [1].

In this work we study the motion of vibrated macroscopic toy-robots (hexbugs) confined in a narrow channel. Interestingly, the hexbug motion can be described with the physical model of active Brownian particles [2]. The corresponding Langevin equation needs to be completed by an inertial term, to account for the non-negligible mass of the macroscopic particles.

We identified two regimes of hexbug motion, depending on the frequency of the driving vibrations. At higher frequencies the particle periodically bounces off the ground and moves in a ballistic mode before hitting the ground again. Interesting phenomena are observed when the channel is closed with a hard wall. In this case, the hexbug reaches the channel end where it starts to bounce against the wall. We developed a mathematical description of the hexbug motion in the ballistic mode, which describes the dynamics of the bouncing oscillations very well. The power spectrum of the oscillations and the probability distribution of the hexbug position are analyzed in detail.

Acknowledgement
This publication is the result of the implementation of the project OPENMED (Open Scientific Community for Modern Interdisciplinary Research in Medicine) ITMS2014+: 313011V455 from the Operational Program Integrated Infrastructure funded by the ERDF.

References

[1] A. Ghosh, W. Xu, N. Gupta and D. Gracias, Nano Today, 31 (2020), 100836.
[2] O. Dauchot and V. Demery, Phys Rev Let., 122 (2019), 068002.

Characterization of Exosomes and their Interactions with Amphiphilic Dendrons Using Electron Microscopy

K. Čechová[1] , M. Velísková[1], D. Kosnáč[2], M. Bábelová[2], M. Kopáni[2], Š. Polák[2], M. Zvarík[1], L. Šikurová[1] and I. Waczulíková[1]

[1] *Department of Nuclear Physics and Biophysics, Faculty of Mathematics, Physics and informatics, Comenius University in Bratislava, Mlynská Dolina, 842 48 Bratislava, Slovakia.*
[2] *Institute of Histology and Embryology, Faculty of Medicine of the Comenius University, Sasinkova 4, 811 04 Bratislava, Slovakia*

e-mail: cechova60@uniba.sk

Introduction

Exosomes are extracellular vesicles secreted by body fluids and are known to represent the characteristics of the cells that secrete them. The content and morphology of exosomes reflect the behavior of cells or their physiological state. The size of exosomes ranges from 30 to 300 nm [1]. Exosomes can be used as targeted drug carriers [2].

To deliver the drug to the cell can be used synthetic polymers called dendrons. Their size depends on the number of repeated cycles called generations. They can interact with biological systems such as exosomes. The mode of this interaction is influenced by the generation of dendrons, their concentration, and environmental properties [3].

In this work were characterized the size and morphology of exosomes isolated from patients' urine and their interaction with 1st and 2nd generation amphiphilic dendrons. The listed properties of the exosomes were monitored by negative stain electron microscopy (EM). This technique allows relatively simple and fast observation of macromolecules and macromolecular complexes with a contrast-enhancing agent. Although the resolution is limited, negative stain EM provides a quick way to evaluate samples of macromolecular complexes [4].

Aim

The aim of this work was to characterize the size and morphology of exosomes isolated from the urine of a healthy patient and a patient with bladder cancer. Also observed was a change in the morphology of these exosomes after interaction with amphiphilic first- and second-generation dendrons. These characteristics were monitored by negative stain electron microscopy.

Methods

Approximately 5 ml of the exosome suspension was applied to a carbon dusted film. Subsequently, the sample was dried at room temperature for several minutes. A drop of 2% saturated uranyl acetate was then applied to the sample for contrast, and allowed to act for 20 minutes. After this time, the sample was washed several times in deionized water to wash the uranyl acetate well. After drying at room temperature, the exosomes were examined using a ZEISS EVO LS15 scanning electron microscope at 20 kV.

Representative Results

We studied the size and morphology of exosomes isolated from the urine of a healthy patient and a bladder cancer patient. Micrographs of negatively stained of exosomes were compared. Analysis of the micrographs revealed that all exosomes isolated from urine were approximately 30 to 100 nm in size and most of the exosomes had a typical shape and morphology [5] (Fig. 1a, Fig. 2a). We also monitored the interaction of first- and second-generation amphiphilic phosphorus dendrons with exosomes isolated from urine. The concentration of dendrons in the exosome suspension was 2 µl. We observed possible aggregation of exosomes in interaction with dendrons [6] (Fig. 1b-e; Fig. 2b-e).

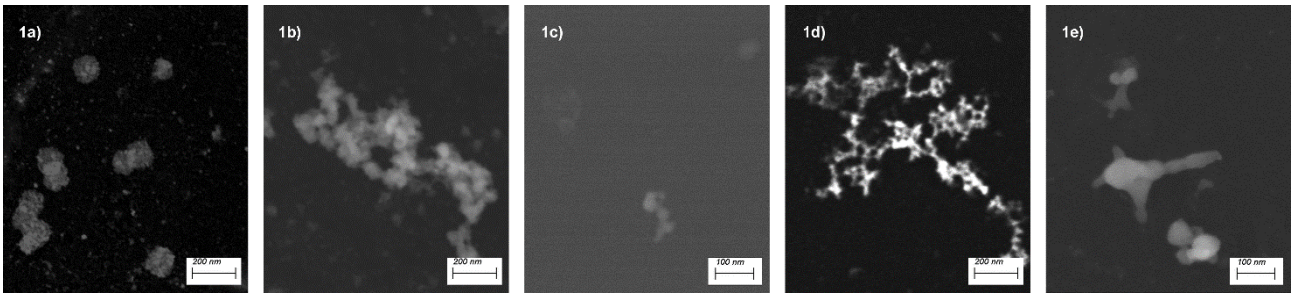

Fig. 1a) shows a micrograph of an exosome solution obtained by EM at x 100 000 magnification. This magnification was used to identify exosome-like particles isolated from the urine of a healthy patient based on size (30-100 nm), shape (round), and vesicle morphology. It seems that if the lattice were analyzed in more detail, other exosomes of different sizes could be found. **Fig. 1b)** shows exosomes isolated from the urine of a healthy patient with whom 1st generation amphiphilic dendrons interacted at a magnification of x 100,000. **Fig. 1c)** shows exosomes isolated from the urine of a healthy patient with whom 1st-generation amphiphilic dendrons interacted at a magnification of x 150,000. **Fig. 1d)** shows exosomes isolated from the urine of a healthy patient with whom 2nd generation amphiphilic dendrons interacted at a magnification of x 100,000. **Fig. 1e)** shows exosomes isolated from the urine of a healthy patient with whom 2nd generation amphiphilic dendrons interacted at a magnification of x 150,000. The color of the micrographs was inverted to obtain greater contrast.

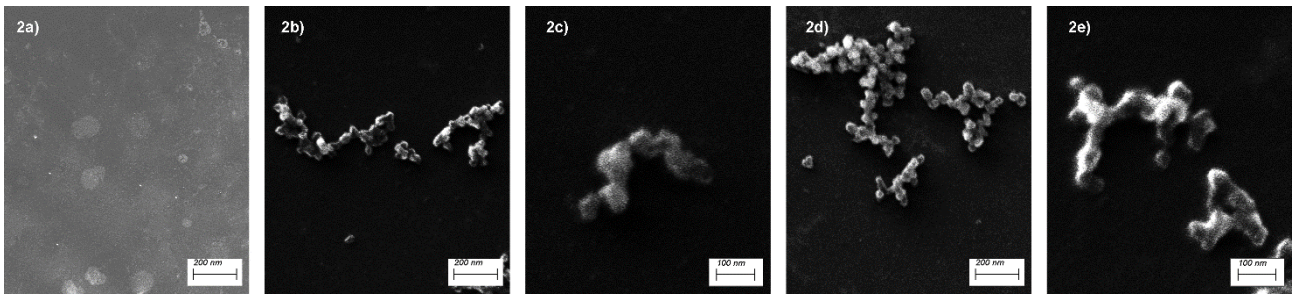

Fig. 2a) shows a micrograph of an exosome solution obtained by EM at x 100,000 magnification. This magnification was used to identify exosome-like particles isolated from the urine of a bladder cancer patient based on size (30-100 nm), shape (round), and vesicle morphology. It seems that if the lattice were analyzed in more detail, other exosomes of different sizes could be found. **Fig. 2b)** shows exosomes isolated from the urine of a bladder cancer patient with whom 1st generation amphiphilic dendrons interacted at a magnification of x 100,000. **Fig. 2c)** shows exosomes isolated from the urine of a bladder cancer patient with whom 1st-generation amphiphilic dendrons interacted at a magnification of x 150,000. **Fig. 2d)** shows exosomes isolated from the urine of a bladder cancer patient with whom 2nd generation amphiphilic dendrons interacted at a magnification of x 100,000. **Fig. 2e)** shows exosomes isolated from the urine of a bladder cancer patient who interacted with 2nd generation amphiphilic dendrons at a magnification of x 150,000. The color of micrographs was inverted to obtain greater contrast.

Discussion

In this work, we monitored the size and morphology of exosomes isolated from the urine, which interacted with amphiphilic dendrons, using the method of negative stain electron microscopy. The knowledge can be used to understand the specific relationships and interactions of amphiphilic dendrons in the biological systems under study and subsequent optimization for in vivo use. The experimental findings from these preliminary studies will be further used to clarify the basic understanding of the interactions of membrane structures with amphiphilic dendrons.

Acknowledgment

This work was supported by the NAWA International Academic Partnership Programme EUROPARTNER, PPI/APM/2018/1/00007/U/001, APVV SK-BY-RD-19-0019, and partly by KEGA 041UK-4/2020.

References

[1] M.K.Jung and J.Y.Mun, J Vis Exp. 131 (2018), 56482.
[2] G.Lugli, A.M.Cohen, D.A.Bennett, et al., PloS One. 10 (10), (2015), e0139233.
[3] A.Janaszewska, J.Lazniewska, P.Trzepiński, et al., Biomolecules. (2019), 9, 330.
[4] Ch.A.Scarff, M.J.G.Fuller, R.F.Thompson and M.G.Iadanza, J Vis Exp. 132, (2018), 1-8.
[5] J.Nillson, J.Skog, A.Nordstrand, et al., Br. J. Cancer. 100 (2009), 603-607.
[6] S.Michlewska, M.Ionov, D. Shcharbin, et al., Eur. Polym. J. 87 (2017), 39-47.

Modification of casein micelles by aptamers for targeted drug delivery purposes

Z. Garaiová[1], I. Kráľová[1] , M. Garaiová[2], R. Holič[2], and T. Hianik[1]

[1] *Faculty of Mathematics, Physics and Informatics, Department of Nuclear Physics and Biophysics, Comenius University, Mlynska dolina F1, Bratislava, 842 48 Slovakia*
[2] *Institute of Animal Biochemistry and Genetics, Centre of Biosciences, Slovak Academy of Sciences, Dubravska cesta 9, Bratislava 840 05, Slovakia*

e-mail: zuzana.garaiova@fmph.uniba.sk

Caseins – comprising about 80 % of milk total protein, are a family of proteins that can naturally self-organize in the aqueous solutions and form structures called micelles. These micelles gain a lot of interest as potential transporters of dietary supplements and pharmaceuticals including those with anticancer properties [1] into the human body. The effective transporters should provide targeted delivery of a load material into the desirable site of its therapeutical action. For this purpose - nucleic acid aptamers, especially DNA aptamers can be employed as targeting ligands [2].

We focused on the study of β-casein micelles (β-CN) and their modification by selective leukemia cell binding cholesteryl-linked aptamer (CHOL-sgc8c) (Fig.1). The β-CN micelles were prepared in Na-phosphate buffer (10mM, pH 7) at concentration 8 mg/ml, filtered (Millipore filters with a pore diameter of 0.2 μm) and combined with CHOL-sgc8c aptamers. The mixed solution of β-CN micelles (2 mg/ml) and CHOL-sgc8c aptamers (2 μM) was stirred (2h, at room temperature) and analyzed by agarose gel electrophoresis. The samples of free aptamers as controls were also included, loaded into 3% agarose gel supplemented with peqGREEN nucleic acid fluorescent dye followed by running the electrophoresis in Tris-acetate-EDTA buffer (pH 8) at 100 V for 15 min.

We observed, that in the combined casein/aptamer sample, the CHOL-sgc8c aptamers were partly present in unbound form. However, a significant portion of CHOL-sgc8c displayed a retarded migration profile, suggesting successful modification to β-CN micelles. The obtained data can be used for optimizing the modification protocol including purification steps to eliminate unbound material followed by testing the bound system for its target specific drug delivery properties.

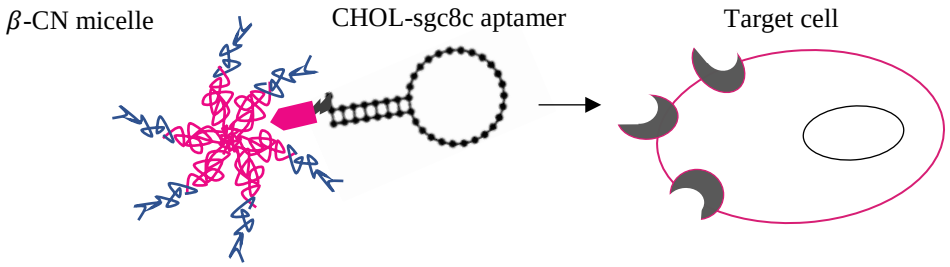

Fig. 1. Schematic illustration of β-casein micelles (β-CN) modified by cholesterol-linked aptamer (CHOL-sgc8c) for targeted drug delivery purposes

Acknowledgment
This work was supported by Science Grant Agency VEGA, project No. 1/0756/20; by Agency for Promotion Research and Development, project No. SK-BY-RD-19-0019; by KEGA, project No. 041UK-4/2020 and by NAWA International Academic Partnership Programme EUROPARTNER.

References

[1] J.C. Cuggino, M.L. Picchio, A. Gugliotta, M. Burgi, L.I. Ronco, M. Calderón, M. Etcheverrigaray, C.I. Alvarez Igarzabal, R.J. Minari, L.M. Gugliotta, Eur. Polym. J. 145 (2021), 110237
[2] M. Liu, L. Wang, Y. Lo, S.C-C, Shiu, A.B. Kinghorn, J.A. Tanner, Cells, 11 (2022), 159

Interactions of amphiphilic phosphorous dendrons with model membranes and whole human blood

Š. Šutý[1], P.Mydla[1],K. Ládiová[1] , P.Vitovič[2], M. Kopáni[3], D. Shcharbin[4] and I.Waczulíková[1]

[1] *Department of Nuclear Physics and Biophysics, Faculty of Mathematics, Physics and Informatics, Comenius University in Bratislava*
[2] *Department of simulation and virtual medical education, Faculty of Medicine, Comenius University in Bratislava*
[3] *Institute of Medical Physics, Biophysics, Informatics and Telemedicine, Faculty of Medicine, Comenius University in Bratislava*
[4] *Institute of Biophysics and Cell Engineering, National Academy of Sciences of Belarus*

e-mail: simon.suty@fmph.uniba.sk

Due to the unique physicochemical properties of nanoparticles (NPs) these has become of high interest in many fields including clinical and biomedical applications a promising diagnostic and/or therapeutic tool. One group of NPs widely studied for their theranostic potential is represented by dendritic assemblies, more specifically dendrimers and dendrons – synthetic hyperbranched polymers [1]. Depending on their physicochemical properties, these polymers can further arrange themselves into supramolecular assemblies, leading to various nanostructures characterized by their size (i.e. generation) and functional groups, which determine their function in vivo [2].

In this study we have investigated the interaction of amphiphilic phosphorous dendron of the first (D1) and second (D2) generation with liposomes using dynamic light scattering and Doppler velocimetry using Zetasizer-Nano ZS90 spectrophotometer (Malvern Instrument, Malvern, UK). In addition, we examined effects of D1 and D2 on selected blood and coagulation parameters determined with hematology analyzers. As a part of blood compatibility studies, we also searched for any abnormalities in blood smears after adding amphiphilic phosphorous dendrons. Increasing concentration and generation induced clumping of blood platelets as detected by the means of light microscopy (Fig. 1).

For investigation of blood viscosity changes upon interaction with D1 and D2, we used a rotational modular compact rheometer MCR 102 in the range of shear rate of 0,1 to 1000 s^{-1} and found an increased viscosity at the higher i.e, 10 µM concentration (Fig. 2). We also observed an increased shear stress at both concentrations which, together with increased viscosity, might have potentially serious consequences under *in vivo* conditions ranging from problems with perfusion in body tissues to thrombosis and embolism.

We can conclude that amphiphilic phosphorous dendrons interact with model membranes i.e. liposomes as well with platelets in whole human blood, and that those interactions are associated with alterations in blood flow and increase in viscosity. Physiological significance of these changes needs to be further investigated.

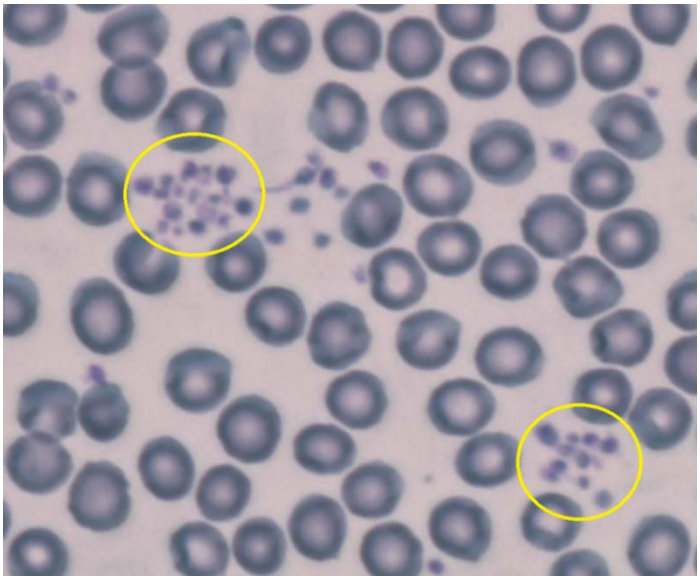

Fig. 1. The blood smear of the blood sample with added amphiphilic phosphorous dendrons. Clumps of the blood platelets are marked with yellow circles.

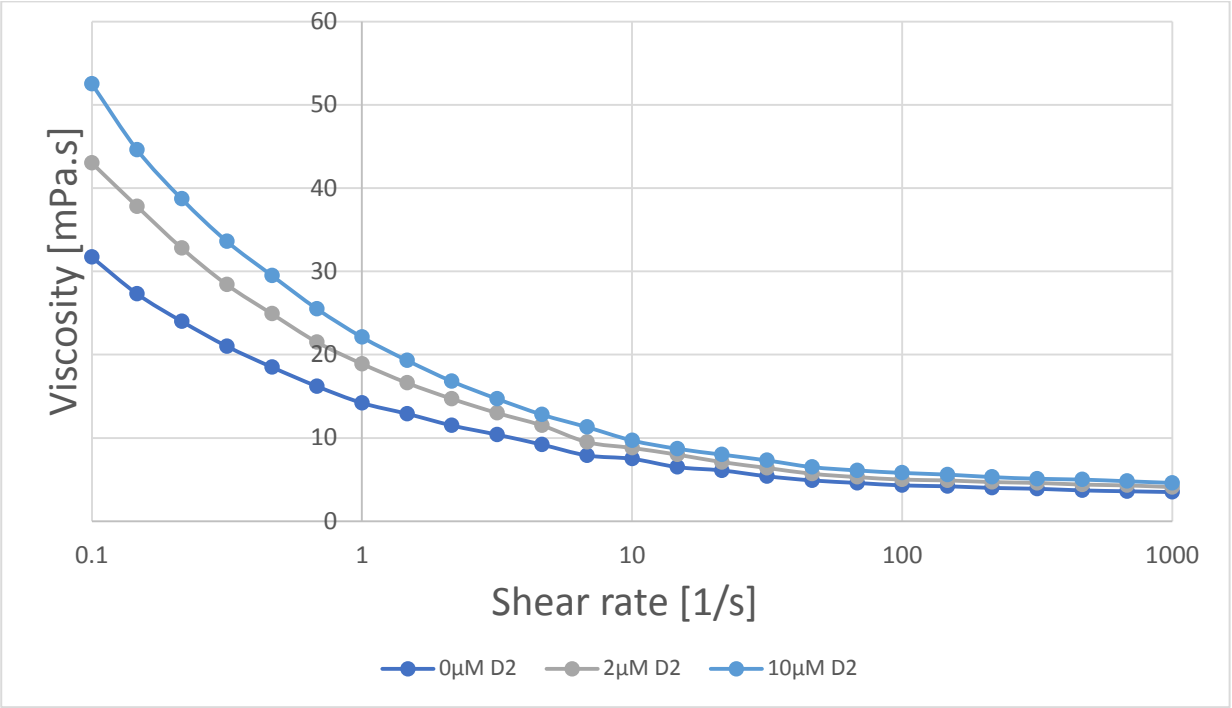

Fig. 2. Viscosity curves of whole human blood at 0 µM, 2 µM and 10 µM concentrations of D2

Acknowledgment

This work was supported by the grant agencies: NAWA International Academic Partnership Programme EUROPARTNER, PPI/APM/2018/1/00007/U/001; KEGA 041UK-4/2020; APVV SK-BY-RD-19-0019 and SK-PL-21-0073, and partly by the State Committee on Science and Technology of the Republic of Belarus (SCST RB) B20-SLKG-002 and Comenius University Grant UK/437/2021.

References

[1] K. Prashant; J. Keerti, J.K.Narendra, Prog. Polym. Sci. 39 (2014), 268–307.
[2] B. Ziemba G. Matuszko, M. Bryszewska, B. Klajnert, Cell. Mol. Biol. Lett. ,17 (2012), 21-35.

The viscoelastic parameters of photopolymer nanowires

C. Slabý[1], J. Kubacková[2], D. Horvath[3], A. Hovan[1], G. Žoldák[3], Z. Tomori[2] and G. Bánó[1]

[1]*Department of Biophysics, Faculty of Science, P. J. Šafárik University, Jesenná 5, 041 54 Košice, Slovak Republic*
[2]*Institute of Experimental Physics SAS, Department of Biophysics, Watsonova 47, 040 01 Košice, Slovak Republic*
[3]*Center for Interdisciplinary Biosciences, TIP, P. J. Šafárik University, Jesenná 5, 041 54 Košice, Slovak Republic*

e-mail: cyril.slaby@student.upjs.sk

Photopolymer nanowires are the building blocks of many microstructure systems. Such nanowires can be prepared by two-photon polymerization direct laser writing (TPP), one of the basic microstructure fabrication techniques used in biomedical and microfluidic applications [1]. Previously, we used a simple viscoelastic mechanical model to describe the bending recovery motion of deflected nanowire cantilevers in Newtonian liquids [2]. The inverse problem was targeted recently [3]. It was our goal to determine the nanowire physical characteristics based on the experimental recovery motion data. Explicit formulas were derived to calculate the nanowire viscoelastic material properties.

A holographic optical tweezer setup was used to deflect 16 µm long photopolymer nanowire cantilevers made of the Ormocomp photoresist. The measurements were repeated in different aqueous glucose solutions. After the initial deflection, the laser tweezer was switched off and the structure started to recover to the original, relaxed shape. In agreement with the model predictions, the recovery data (obtained by video-tracking) could be well fitted with a double-exponential time-dependence.

The effective elastic modulus of the studied nanowires was found to be two orders of magnitude lower than measured for the bulk material. Besides that, the intrinsic viscosity of the nanowire was obtained. Interestingly, this viscosity changes significantly with the glucose concentration, which indicates significant porosity of the nanowire material.

Acknowledgement

This work was funded by the Slovak Research and Development Agency (grant APVV-18-0285) and the Slovak Ministry of Education (grants VEGA 2/0094/21 and 2/0101/22). This publication is also the result of the implementation of the project OPENMED (Open Scientific Community for Modern Interdisciplinary Research in Medicine) ITMS2014+: 313011V455 from the Operational Program Integrated Infrastructure funded by the ERDF.

References

[1] A. Otuka, N. Tomazio, K. Paula and C. Mendonça. Polymers 13 (2021), 1994.
[2] J. Kubacková et al., Appl. Phys. Lett. ,117 (2020), 013701.
[3] J. Kubacková, C. Slabý, D. Horvath, A. Hovan, G. T. Iványi, G. Vizsnyiczai, L. Kelemen, G. Žoldák, Z. Tomori, G. Bánó Nanomaterials 11 (2021), 2961.

Interaction of amphiphilic phosphorous dendrons with lipid membranes studied by size exclusion chromatography

M. Velísková[1], M. Zvarík[1], K. Čechová[1] and I. Waczulíková[1]

[1]*Department od Nuclear Physics and Biophysics, Faculty of Mathematics, Physics and Informatics, Mlynská dolina F1, 842 48 Bratislava.*

e-mail: martina.veliskova@fmph.uniba.sk

Dendrons are branched synthetic polymers suitable for preparation of nanoscale molecular structures - dendrimers, which can be used to deliver drugs to cells. Due to the chemical structure, surface charge and number of branched layers (generations), they can interact with biological systems [1]. In addition to generation, the way they interact is affected by their concentration. Any compound intended for use in medicine must be safe and compatible with all systems in the body. We focused on investigating the interaction of first and second generation dendrons with liposomes and exosomes, which represent model structures of biological membranes [2,3]. We monitored aggregation propensity and stability of structures in the presence of dendrons using size exclusion chromatography. In the case of higher concentrations and higher generation of dendrons, we observed increased aggregation of liposomes as well as exosomes, which was consistent with previous findings by our group using various biophysical methods. In addition, our findings point out to destabilization of lipid bilayer, which needs further investigation. In general, the pattern of interaction can be explained by the electrostatic nature of the interaction of positively charged dendron and negatively charged membrane structures. The knowledge can be used to understand the specific relationships and interactions of dendrons on the biological systems under study and subsequent optimization for *in vivo* use.

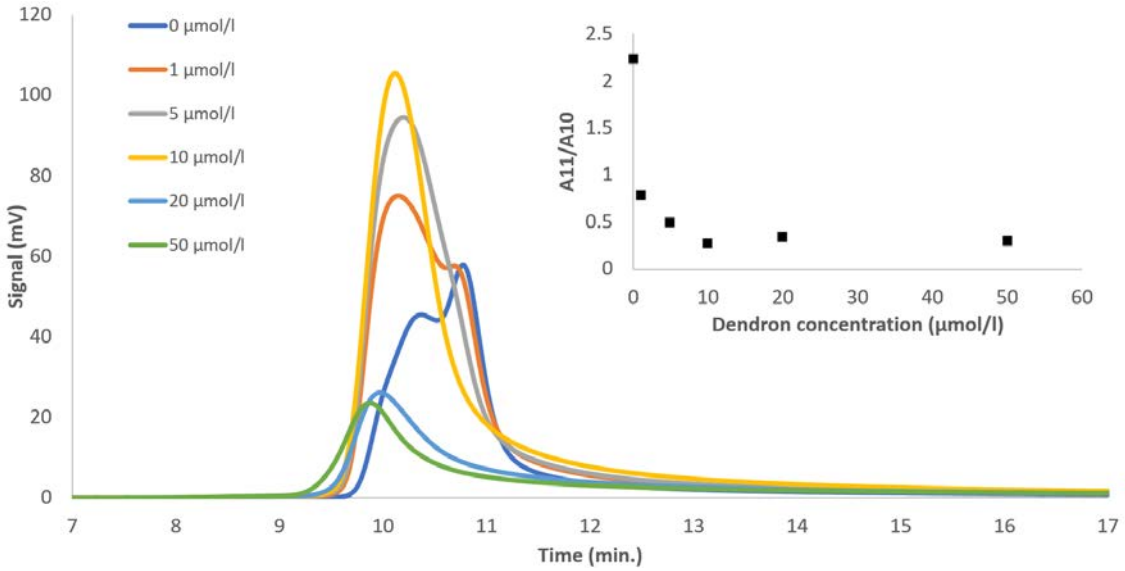

Fig. 2 Shift of absorption chromatograms of liposomes depending on the concentration of added dendron. The nested graph shows the ratio of absorbance at a retention time of 11 and 10 minutes depending on the concentration of dendrons.

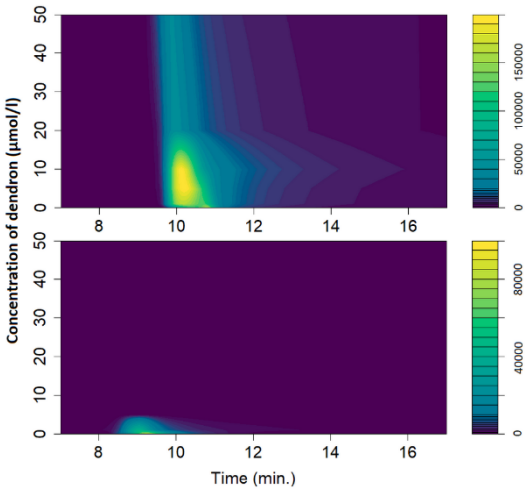

Fig. 3 Contour plots of liposome absorbance at different dendron concentrations, top – first-generation dendron, bottom – second-generation dendron.

Acknowledgment

This research was funded by the NAWA International Academic Partnership Programme EUROPARTNER, PPI/APM/2018/1/00007/U/001, Strengthening and spreading international partnership activities of the Faculty of Biology and Environmental Protection for Interdisciplinary Research and Innovation of the University of Lodz; by the Slovak Research and Development Agency (APVV), Project Nos. SK-BY-RD-19-0019; by the Cultural and Educational Grant Agency of the Ministry of Education, Science, Research, and Sport of the Slovak Republic (KEGA) 041UK-4/2020.

References

[1] S. Suty, V. Oravczova and Z. Garaiova, V. Subjakova, M. Ionov, D. Shcharbin, Z. Simonikova, P. Bartek, M. Zvarik, X. Shi, S. Mignani, J-P. Majoral, M. Bryszewska, T. Hianik, I. Waczulikova ., Biomedicines,9 (2021), 1672.
[2] S. Andrade, M. Ramalho, J. Loureiro and M. PereiraJ. Mol. Liq., 334(2021), 116141.
[3] D. Ha, N. Yang and V. Nadithe, Acta Pharm Sin B., 6 (2016), 287-296.

Interaction of potential SARS-CoV-2 antiviral GRL0617 with selected phospholipids

A. Čelková[1], A. Búcsi[1], J. Gallová[1], J.C. Martínez[2] and D. Uhríková[1]

[1]*Department of Physical Chemistry of Drugs, Faculty of Pharmacy, Comenius University in Bratislava, SK-832 32, Odbojárov 10, Bratislava, Slovakia.*
[2] *BL-11 NCD beamline, Alba Synchrotron, Carrer de la Llum 2-26, 08290 Cerdanyola del Vallès, Barcelona, Spain.*

e-mail: celkova20@uniba.sk

COVID-19 is great threat to global health and economy. The number of specific drugs for causal treatment of this disease is limited. Frequent and permanent mutations together with a resistance of the viruses add another level of difficulty, which forces us to look for new drugs. One of the promising antivirals is GRL0617 (Fig. 1), which inhibits viral PL^{PRO} (papain-like protease). This cysteine protease is necessary for viral maturation, dysregulation of host immune response and host inflammation process.

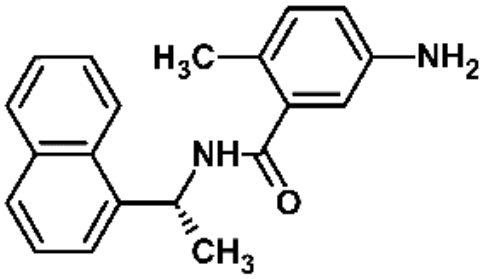

Fig. 1. Chemical structure of GRL0617.

Phospholipid aggregates of different structure are considered a promising drug formulation used for a targeted drug delivery.

In our work two types of phospholipids were examined as a potential phospholipid system for the drug delivery – DPPC and POPE. These phospholipids are biocompatible and biodegradable. We have followed the effect of GRL0617 on the structure and thermotropic behaviour of selected lipids. Small and wide-angle X-ray scattering (SAXS/WAXS) were employed to follow structural changes. Thermotropic behaviour was also examined by differential scanning calorimetry (DSC).

DPPC (1,2-dipalmitoyl-*sn*-glycero-3-phosphocholine) forms in contact with water phase spontaneously multilamellar vesicles – vesicular structures consisting of a large amount of concentric spheres of DPPC bilayers separated by water layers. Repeat distance *d* (the sum of the thickness of lipid bilayer plus the thickness of water layer) is a characteristic lattice parameter of lamellar phase. For DPPC, two transitions of lamellar phase have been observed with increasing temperature – from gel phase $L_{\beta'}$ to rippled gel phase $P_{\beta'}$ (T_p ~ 35°C) and to liquid-crystalline L_α (T_m ~ 41.3°C). Phase transitions temperatures were confirmed by SAXS and DSC.

POPE (1-palmitoyl-2-oleoyl-*sn*-glycero-3-phosphoethanolamine) shows in the temperature range 15–80°C phase transitions from L_β to L_α (T_m ~ 23°C) and to inverted hexagonal phase H_{II}. H_{II} phase is a two-dimensional periodic structure consisting of lipids arranged in the shape of cylinders with water enclosed inside the cylinders and hydrocarbon chains oriented to the outside, with cylinders hexagonally arranged. The lattice parameter *a* determines the distance between centres of

water cores of adjacent cylinders. SAXS patterns have shown the onset of a hexagonal phase at ~ 56°C for hydrated POPE. The enthalpy of L_α to H_{II} is too low to be detected by DSC.

GRL0617/DPPC mixtures form a lamellar phase. At molar ratios 0.005≤GRL0617/DPPC≤0.01, repeat distances d do not show any significant difference in comparison with the pure lipid in the entire studied temperature interval (20–60°C). At higher molar ratio GRL0617/DPPC = 0.05, we detected the coexistence of two lamellar phases in gel state of the mixture. Structural changes were obvious in the temperature range of rippled gel phase, however less visible in L_α phase. At molar ratios GRL0617/DPPC ≥0.1, WAXS patterns indicate the crystallization of the drug. Small changes in the phase transition temperature T_m were derived from DSC measurements. While in the molar range 0.005≤GRL0617/DPPC≤0.01 the phase transition temperature slightly increased from 41.3°C to 41.6°C; we found its decrease to 40.3°C at higher content of GRL0617 in the lipid mixture.

For POPE, we detected the effect of GRL0617 on lamellar – hexagonal phase transition: SAXS patterns of hydrated POPE show the coexistence of hexagonal (a ~ 7 nm) and lamellar phase (d ~ 5 nm) up to highest studied temperature, 80°C, in accord with [1]. SAXS patterns of GRL0617/POPE<0.1 mol/mol mixtures show that lamellar structures converted fully into H_{II} at this temperature. However, depending on the heating rate we observed the presence of a cubic phase in the mixture at the drug higher content. Unfortunately, the drug is not soluble at its higher content and WAXS detected its crystallization in the mixture.

In summary, GRL0617 is an effective antiviral agent at its micromolar concentrations (IC_{50} ~ 1.6 μM), however DMSO was used for the application in biological systems due to the drug poor solubility in water [2]. Our experiments revealed that both lipid systems could serve as a potential delivery system keeping the structural arrangement, however, the loading capacity for the drug is limited to GRL0617/lipid < 0.1 mol/mol.

Acknowledgement
SAXS and WAXS experiments were performed at BL11-NCD beamline at Alba Synchrotron, Barcelona with the collaboration of Alba staff. This work was supported by projects VEGA 1/0223/20; JINR 04-4-1142-2021/2025; APVV PP-COVID-20-0010 and FaF UK/17/2021.

References

[1] M. Rappolt, A. Hickel, F. Bringezu and K. Lohner, Biophys. J. 84 (2003), 3111–3122.
[2] K. Lopušná, S. Lenhartová and I. Nemčovičová, Eur. J. Immunol. 51 (Suppl. 1) (2021), P-1132.

Differences in membrane properties of sensitive and resistant yeast strains *Candida auris*

J. Jacko[1], M. Morvová Jr.[1], N. Toth-Hervay[2], L. Šikurová[1], Y. Gbelská[2]

[1] *Faculty of Mathematics, Physics and Informatics, Comenius University, Mlynská dolina F1, 842 48 Bratislava, Slovakia*

[2] *Faculty of Natural sciences, Comenius University, Ilkovičova 6, 842 48 Bratislava, Slovakia*

email: juraj.jacko@fmph.uniba.sk

Yeast has an irreplaceable place in science and industry. Especially in the food industry to produce baked goods, alcoholic beverages, and dairy products. In science, they are widely used as model eukaryotic organisms, and in the pharmaceutical industry as production organisms for various therapeutics. On another hand, certain yeast strains act as opportunistic pathogens. Yeast diseases are treated with antifungal drugs. The most widespread and effective class of antifungal agents are azole drugs. The growing level of yeast resistance to azole antifungals is a worldwide medical problem. Their main effect is the inhibition of sterol synthesis in yeast. At present, however, an increasing number of yeast strains resistant to azole antifungals present complications in the treatment of yeast infections. This is particularly important for the *Candida* genus. *Candida* infections are the most common cause of human opportunistic yeast infections worldwide, accounting for up to 96% of yeast infections. *Candida auris* is the 3rd most common cause of a yeast disease in the world (after *Candida albicans* and *Candida glabrata*) and the mortality rate varies from 30% to 60% [1].

The plasma membrane is an important cellular organelle and it plays a notable role in drug resistance mechanisms. Its properties depend on lipid and protein composition. Changes in membrane composition lead to changes in susceptibility to azole antifungals [2]. It has been shown that altered plasma membrane phospholipid and sterol composition can influence the membrane barrier function [3]. The aim of this work is to study the difference in the biophysical properties (namely membrane fluidity and transmembrane potential) between sensitive and resistant *Candida auris* yeast strains.

Differences in membrane fluidity were studied by measuring the fluorescence anisotropy of fluorescent probes. The DPH (1,6-diphenyl-1,3,5-hexatriene) probe is incorporated into hydrophobic and TMA-DPH (4-trimethyl-amino-1,6-diphenyl-1,3,5-hexatriene) probe is incorporated into hydrophilic part of cytoplasmic membrane. Differences in yeast transmembrane potential were studied by monitoring the shift in the position of emission maximum ($\Delta\lambda_{max}$) in the fluorescence spectrum of the DiS-C_3(3) probe in cells of the sensitive and resistant strain.

The results of our experiments show that there is a significant difference in membrane fluidity in the hydrophobic part of the cytoplasmatic membrane (0.269 ± 0.01 for sensitive and 0.293 ± 0.001 for resistant strain), but no difference in the hydrophilic part (0.356 ± 0.002 for sensitive and 0.357 ± 0.001 for resistant strain). There is a significant difference in the $\Delta\lambda_{max}$ value (2.35 ± 0.21 nm for sensitive and 6.25 ± 0.3 nm for resistant strain) that shows that the plasma membrane of the sensitive strain is depolarized compared to the resistant strain.

Acknowledgment

This work was supported by grants APVV-SK-BY-RD-19-0019, KEGA 041UK-4/2020, and UK/59/2021.

References

[1] https://www.cdc.gov/fungal/candida-auris/candida-auris-qanda.html, online, [17.3.2022].

[2] H. Van den Hazel, H. Pichler, M. A. Do Valle Matta, E. Leitner, A. Goffeau and G. Daum, J. Biol. Chem., 274(1999), 1934–1941.

[3] J. Loffler, H. Einsele, H. Hebart, U. Schumacher, C. Hrastnik and G. Daum, FEMS Microbiol. Lett., 185(2000), 59–63.

The effect of Budesonide on the bilayer of exogenous pulmonary surfactant

A. Keshavarzi[1], A. Asi Shirazi[1], A. Čelková[1], M. Klacsová[1], J.C. Martínez[2] and D. Uhríková[1]

[1]Faculty of Pharmacy, Comenius University Bratislava, Bratislava, Slovakia.
[2]Alba synchrotron, 08290 Cerdanyola del Vallès, Barcelona, Spain.

e-mail: Keshavarzi2@uniba.sk

The surface area for gas exchange in the lungs is mechanically dynamic, and this dynamic surface is stabilized by pulmonary surfactant, which is a complex composed of lipids (~90%) and proteins [1]. Pulmonary surfactant (PS) (Fig.1) not only eases the work of breathing by lowering the surface tension in the air-liquid interface and prevents atelectasis but also prevents the entry of pathogens. Produced by type II pneumocytes, PS is secreted from lamellar bodies in type II pneumocytes into the hypophase, forming a monolayer of lipid-protein in the air-liquid interface. Absence, deficiency, and inactivation of pulmonary surfactant is manifested as respiratory distress syndrome [1].

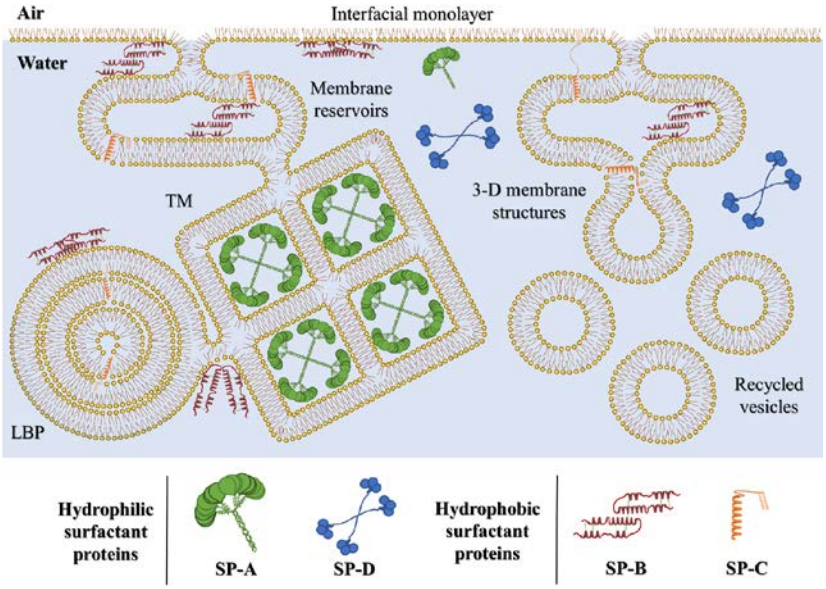

Fig. 1. Extracellular structure of pulmonary surfactant [3].

The only registered exogenous PS in Slovakia is Curosurf®, porcine PS. Due to its potential, further studies are conducted to utilize exogenous PS as a shuttle for other drug molecules. Patients can profit from the synergic effect of combination therapy in addition to the rapid onset of action due to local administration, limited systemic adverse effects, and better adsorption for drugs that are adsorbed poorly from the oral route of administration [2].

Budesonide is a glucocorticoid with an anti-inflammatory effect that is indicated for different pulmonary diseases. In the present work, the interaction of budesonide (BUD) and exogenous PS was studied. The thermotropic phase transition of PS was studied by differential scanning calorimetry (DSC). The size of the particles was determined by dynamic light scattering (DLS). The effect on the surface charge was followed by dynamic light scattering. Structural

changes were studied using synchrotron small-angle X-ray scattering (SAXS) at BL11-NCD beamline, Alba synchrotron, Barcelona.

Sample preparation: Curosurf® suspension was dried into lipid film by phosphorus pentoxide as a desiccant in vacuum. Dissolved BUD in methanol was then added to the Curosurf® film, and the organic solvent was evaporated and dried under the flow of nitrogen and in vacuum. Samples were hydrated with NaCl solution to reach physiological concentration (150 mM).

Fig. 2 shows selected DSC profiles of Curosurf - budesonide mixtures. The temperature of the main phase transition of pure Curosurf® was found at 27.78 ℃. A slight decrease in the temperature of phase transition was detected by increasing wt% of BUD.

Zeta potential measurement did not indicate a significant change in the negative surface charge of unilamellar vesicles (ULVs), which is typical for exogenous PS in physiological pH values. We did not detect changes in the size of ULVs due to the incorporation of BUD, as derived from the DLS.

For the structural study, 2 mM $CaCl_2$ was used in the hydration medium to screen the negative surface charge. SAXS patterns (Fig. 3) of pure Curosurf® in presence of different wt% of BUD show lamellar phase both at 20 and 50 ℃. We did not observe any significant structural changes.

In summary, our study of the physico-chemical properties of Curosurf® - budesonide mixtures indicates that the corticosteroid is localized in the hydrophobic region of the bilayer and well-tolerated due to the high content of polyunsaturated phospholipids in Curosurf®.

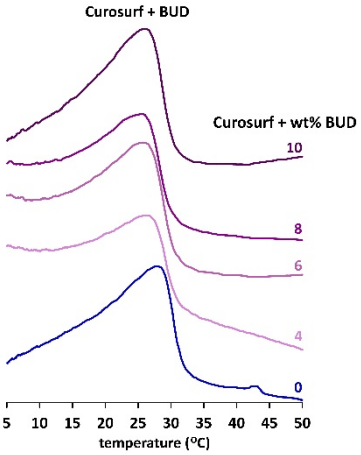

Fig. 2. DSC profiles of Curosurf® in presence of different wt% of BUD.

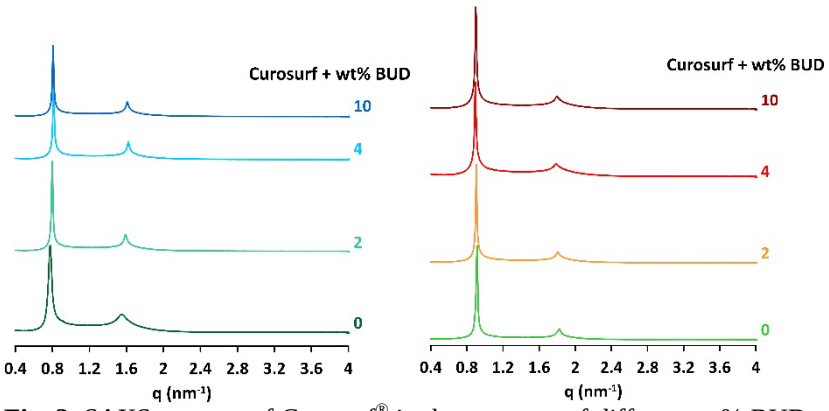

Fig. 3. SAXS patterns of Curosurf® in the presence of different wt% BUD at 20°C (left) and 50°C (right).

Acknowledgment

SAXD/WAXD experiments were performed at BL11-NCD beamline (proposal 2021025016) at Alba Synchrotron with the collaboration of Alba staff. This work was supported by grants VEGA 1/0223/20; JINR 04-4-1142-2021/2025; APVV 17-0250 and FaF UK/29/2021.

References

[1] E. Lopez-Rodriguez and J. Pérez-Gil, Biochim. Biophys. Acta Biomembr., 1838 (2014), 1568–1585.
[2] Aulton's Pharmaceutics, The design and manufacture of medicines, M. Aulton and K. Taylor (Eds.), Elsevier, Edinburgh (2018).
[3] J. C. Castillo-Sánchez, A. Cruz, and J. Perez-Gil, Arch. Biochem. Biophys., 703 (2021), 1–17.

The interaction of Cathelicidin LL-37 with exogenous pulmonary surfactant – Curosurf®

A. Asi Shirazi[1], A. Keshavarzi[1], N. Královič[1], M. Klacsová[1], J.C. Martínez[2] and D. Uhríková[1]

[1]*Faculty of Pharmacy, Comenius University Bratislava, Bratislava, Slovakia.*
[2]*Alba synchrotron, 08290 Cerdanyola del Vallès, Barcelona, Spain.*

e-mail: Shirazi1@uniba.sk

Stabilization of alveolar structure during cyclical changes of the lung volume is crucial for normal functioning of the respiratory system and eventually for normal breathing practice. The propensity of the alveolar sacs to collapse during expiration, also known as atelectasis, is due to the presence of relatively high surface tension caused by the presence of an aqueous layer lining the alveolar epithelium surface. To maintain alveolar stability, pulmonary surfactant (PS), which is a lipoprotein film, displaces water molecules at the air-liquid interface and reduces surface tension to extremely low levels as alveolar volume decreases [1].

PS is a phospholipid-rich complex, synthesized, assembled, and secreted onto the alveolar surface by type II alveolar epithelial cells (Fig.1). It is a proteolipidic surface-active complex, mainly comprised of an essential mixture of lipids (~90 wt%) and specific proteins (~10 wt%). Dipalmitoylphosphatidylcholine (DPPC) makes about 40% of the total surfactant mass, making it a key lipid molecule in acquiring very low surface tension values [2].

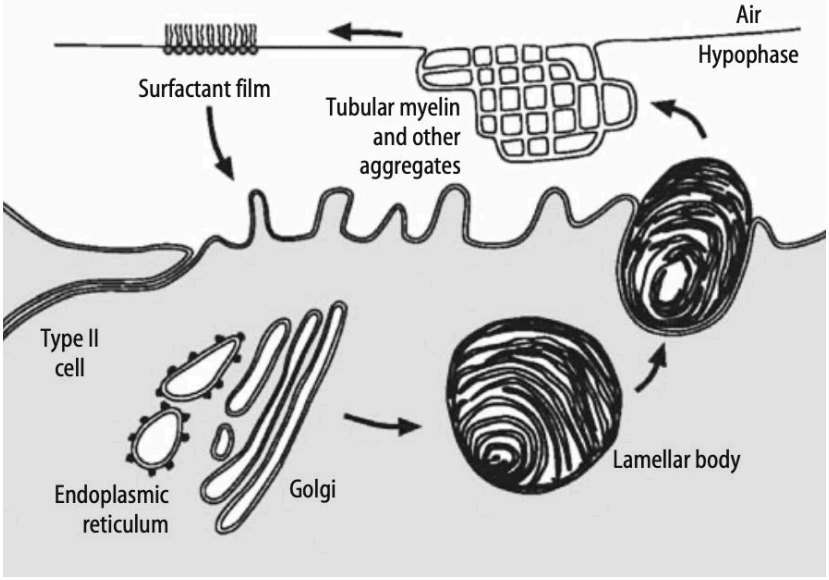

Fig.1. Schematic illustration of Pulmonary surfactant (PS) production and secretion system [3].

Lack or insufficient level of PS is linked with fatal conditions, especially in newborn babies, known as neonate respiratory distress syndrome (nRDS). Such a condition is clinically treated by endotracheopulmonary administration of exogenous PS. For instance, Curosurf® (Chiesi Farmaceutici SpA; Parma, Italy) is a porcine-derived exogenous PS used in surfactant replacement therapy. Curosurf® is composed of ~99 wt% of lipids and ~1–2 wt% of specific PS proteins and DPPC constitutes up to 50% of this fraction [4]. Utilizing exogenous PS preparations as a drug carrier to benefit from PS-drug synergic effect in therapy is an area of interest in recent research.

The rapid spread of antibiotic resistance increases demands for new therapeutical agents to ultimately avoid higher medical costs, prolonged hospitalization, and increased mortality. Cathelicidin (LL-37) is a cationic (+6 at physiological milieu), helically shaped host defense peptide that belongs to the group of antimicrobial peptides. LL-37 is highly expressed during infection, inflammation, and wound healing processes and possesses bactericidal activity against a broad spectrum of pathogens [5].

In the present work, we studied the interaction of LL-37 with exogenous PS Curosurf®. Physico-chemical properties of the complex system such as the effect of LL-37 on the surface properties and size of unilamellar vesicles (UVLs) have been studied using dynamic light scattering (DLS) and electrophoretic zeta potential (ELS). The effect of LL-37 on the temperature of gel to liquid-crystalline phase transition (T_m) has been studied using differential scanning calorimetry (DSC). The microstructure of the formed complex was examined using the synchrotron small-angle X-ray scattering (SAXS) at the BL-11NCD beamline of the Alba synchrotron, Barcelona, Spain.

For DSC studies, UVLs were prepared from Curosurf® suspension using freeze-thaw and extrusion technique (pore size 100 nm). Samples were prepared to contain various wt% of LL-37. Next, samples were incubated for one hour at 35°C and rested overnight before DSC measurements. The measurements were performed in a temperature range of 0–60°C and a temperature rate of 1°C/min under the constant pressure of 3 atm. We determined that T_m for pure Curosurf® is 26.93°C. T_m of the mixture increases as the content of LL-37 increases (Fig.2, left panel).

We found that cathelicidin LL-37 increases the surface charge of UVLs from ~ −9.1 mV detected for pure Curosurf® to ~ +5.0 mV at the highest studied LL-37 contents (4.8 wt%). Particle size measurement studies indicate that the size of UVLs increases with the addition of LL-37, and significant aggregation was detected at LL-37 > 1 wt%.

Fig. 2 (right panel) shows selected SAXS patterns taken at 50°C when the mixture is in a liquid-crystalline state. Curosurf® shows broad, weakly resolved peaks due to its negative surface charge. Cationic LL-37 neutralizes the surface charge and improves long-range order, showing a well-ordered lamellar phase. In summary, we found that LL-37 does not disturb the structure of PS, it helps to maintain multilamellar packing in a PS system, important for the proper function of pulmonary surfactant [6].

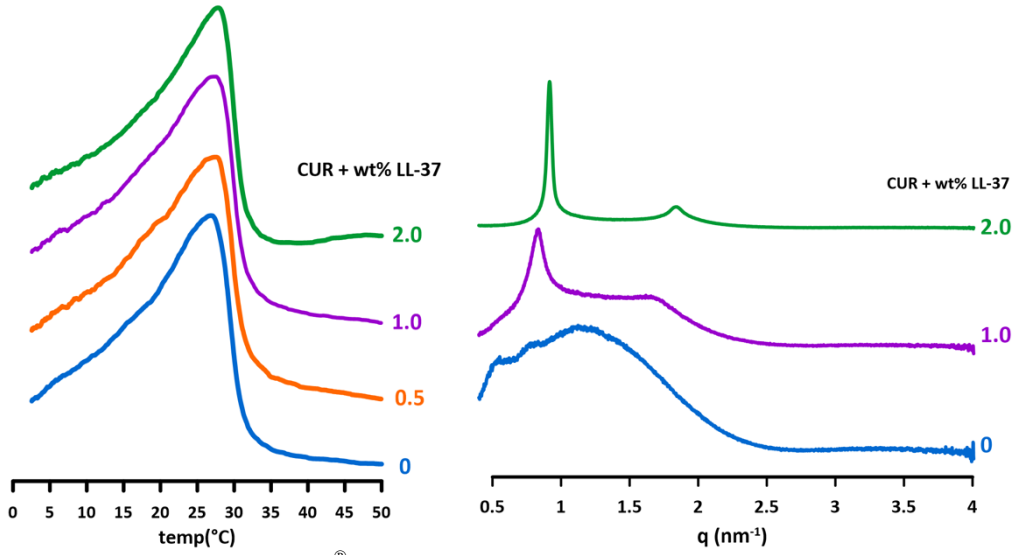

Fig.2. DSC thermograms of Curosurf® with different wt% of cathelicidin LL-37 (left panel). SAXS patterns of Curosurf® with different wt% of cathelicidin LL-37 at 50°C (right panel).

Acknowledgment

SAXD/WAXD experiments were performed at BL11-NCD beamline (proposal 2021025016) at Alba Synchrotron, Barcelona, Spain with the collaboration of Alba staff. This work was supported by grants VEGA 1/0223/20; JINR 04-4-1142-2021/2025; APVV 17-0250 and FaF UK/28/2021.

References

[1] J. Perez-Gil and T. E. Weaver, Physiology, 25 (2010), 132–141.
[2] M. Chakraborty and S. Kotecha,Breathe, 9 (2013), 476–488.
[3] The Respiratory Tract in Pediatric Critical Illness and Injury. D. Wheeler, H. Wong and T. Shanley, T. (Eds.), Springer, London (2009).
[4] O. Blanco and J. Pérez-Gil, Eur. J. Pharmacol., 568 (2007), 1–15.
[5] D. Xhindoli, S. Pacor, M. Benincasa, M. Scocchi, R. Gennaro, and A. Tossi, Biochim. Biophys. Acta - Biomembranes, 1858 (2016), 546–566.
[6] M. Kolomaznik, G. Liskayova, N. Kanjakova, L. Hubcik, D. Uhrikova, and A. Calkovska, Int. J. Mol. Sci., 19 (2018), 7.

α-lactalbumin amyloid fibrillization in the presence of chloride salts cations

A. Antosova[1], M. Gancar[1], E. Bystrenova[2], Z. Bednarikova[1], J. Marek[1] and Z. Gazova[1]

[1]Institute of Experimental Physics Slovak Academy of Sciences, Watsonova 47, 040 01 Kosice, Slovakia
[2]Consiglio Nazionale delle Ricerche - Istituto per lo Studio dei Materiali Nanostrutturati (CNR-ISMN) via P. Gobetti 101, 40129 Bologna, Italy

e-mail: antosova@saske.sk

The formation of protein amyloid fibrils, the intrinsic property of all polypeptide chains, is recently being intensively studied due to the possible application of amyloid fibrils as novel materials [1]. Therefore, knowledge regarding the fibrillization process of proteins in different conditions is of great interest. Using a multi-technique approach (ThT fluorescence, FTIR and CD spectroscopy, AFM microscopy), we have compared the effect of various cations (Mg^{2+}, Ca^{2+}, Na^{+}, K^{+}, NH_4^{+}, Cs^{+}) in the form of chloride salts at two different concentrations (100 mM and 300 mM) on the formation of α-lactalbumin (α-LA) amyloid fibrils at pH 2.0. We have observed that studied cations affect the kinetics of amyloid fibrillization, the morphology of prepared fibrils, and the secondary/tertiary structure of α-LA fibrils differently. The higher salt concentration significantly accelerated the aggregation process. Both salt concentrations stabilized the α-LA secondary structure compared to the α-LA structure at acidic pH 2.0 in the absence of salts. By adding salts, the distribution of secondary structures of α-LA at pH 2.0 obtained from FTIR is similar to the secondary structure of α-LA at pH 5.6. Interestingly, the presence of salts affected the tertiary structure of protein diversely.

In summary, the properties such as size and hydration of cations coupled with concentration profoundly affect the α-LA's amyloid aggregation propensity and the resulting morphology of the aggregates. Small and strongly hydrated cations (Ca^{2+} and Mg^{2+}) significantly accelerate the fibril assembly process, inducing the formation of shorter fibrils with less β-sheet content. Larger (excluding Na^{+}) and weakly hydrated cations (Na^{+}, K^{+}, NH_4^{+}, Cs^{+}) form morphologically more uniform, longer, and individual fibrils, however, at a slower rate.

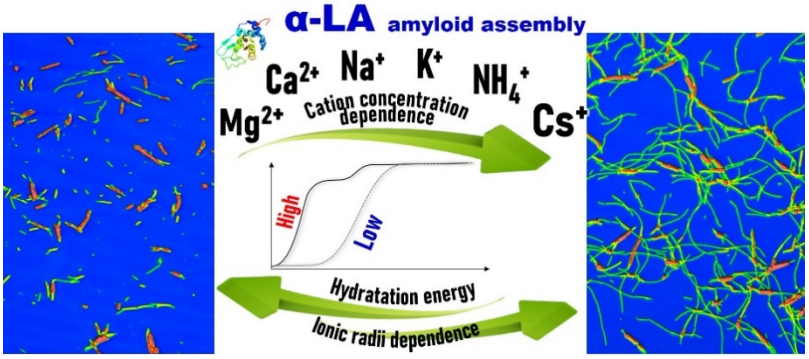

Fig.1: Schematic representation of cations' concentration, size, and free hydration energy affecting α-LA amyloid aggregation.

These findings are important to clarify the mechanism of α-LA fibrillation and the possible application of fibrils in biotechnology.

Acknowledgments
This work was supported by the Slovak Research and Development Agency under the Contract no. APVV-18-0284; Slovak Grant Agency VEGA 02/0176/21, VEGA 02/0164/22; Italian MIUR grant (PRIN 20173L7W8K); This work is also the result of the project implementation BIOVID-19 (ITMS2014+ 313011AVG3) and NANOVIR (ITMS2014+ 313011AUW7) supported by the Operational Programme Integrated Infrastructure (OPII) funded by the ERDF. Microscopy was carried out at the SPM@ISMN facility.

References
[1] F.Chiti, and M. Dobson, *Ann. Rev. Bioch*., 75 (2006), 333-366.

Protein amyloid self-assembly, polymorphism and biological significance

Z. Bednarikova[1], E. Bystrenova[2], M. Barbalinardo[2] and Z. Gazova[1]

[1] *Institute of Experimental Physics Slovak Academy of Sciences, Watsonova 47, Košice, Slovakia.*
[2] *Institute of Nanostructured Materials I.S.M.N – C.N.R., via Gobetti 101, Bologna, Italy.*

e-mail: bednarikova@saske.sk

The amyloid self-assembly is a hallmark of several neurodegenerative (Alzheimer's and Parkinson's disease) and systemic (lysozyme hereditary or insulin localized amyloidoses) amyloid-related disorders. A critical challenge in understanding the mechanism of amyloid species toxicity and the subsequent design of intervention strategies has been the correlation of a particular aggregate structure or size with biological effects, especially toxicity. Initially, fibrils were reported to be toxic, and inhibition of fibril formation or disruption of fibrils was considered to be a viable strategy for inhibiting amyloid toxicity [1, 2]. However, the majority of latter structural and toxicity studies suggest that protofibrils and prefibrillar intermediates exhibit stronger toxicity than monomeric and fibrillar amyloid species [3, 4].

Here we explore the effect of different amyloid species and types of fibrils on the human neuroblastoma (SH-SY5Y) cell line *in vitro*. Firstly, we have controlled the kinetics of human insulin and hen-egg white lysozyme (HEWL) by using various experimental conditions – modulation of pH, shaking and temperature or ultrasonic treatment. Ultrasonic treatment was used to break HEWL amyloid fibrils into fibrillar fragments – seeds. Thioflavin T assay, atomic force microscopy (AFM) and fluorescence microscopy were employed to characterize the morphology of the amyloid assemblies and neural cells–amyloid complexes. The number of cells and their morphology were correlated with the finer details of the amyloid species of studied proteins.

Insulin aggregates formed at different temperatures (37 °C, 50 °C and 65 °C) were deposited on neuroblastoma cells. Our results showed a progressive modification and decrease in the number of cells that correlates with the degree of fibrillization. The cells' exposure to protofilaments formed at 50 °C leads to a decrease in cells number below 50 % of the untreated SH-SY5Y cells (control) at 24 h. The presence of fibrils (65 °C) does not affect the number of cells at 24 h, whereas a drop down to 60 % is observed after 48 h of incubation.

The neuroblastoma cells were also exposed to various lysozyme amyloid species – native protein, seeds mimicking prefibrillar intermediates, the mixture of seeds and native protein and mature fibrils. Our results demonstrate that prefibrillar intermediates and their mixture with native proteins exhibit high cytotoxicity, although native lysozyme and HEWL fibrils do not affect the number of cells. Our findings confirm that innocuous hen lysozyme can be engineered to produce both cytotoxic fibrillar fragments and non-toxic mature amyloid fibrils.

Our work further strengthens the hypothesis that amyloid conformation, not the protein's identity, is key to cellular toxicity and the underlying specific cell death mechanism. In the case of insulin fibrils toxicity, our data unravels that the aggregates strongly interact with the cell membrane, forming a stiff encase that possibly leads to an increased cell membrane stiffness and deficit in the metabolic exchanges between the cells and their environment.

Acknowledgment
This work was supported by the Slovak Research and Development Agency under the Contract no. APVV-18-0284; Slovak Grant Agency VEGA 02/0176/21, Italian MIUR grant (PRIN 20173L7W8K). This work is also the result of the project implementation BIOVID-19 (ITMS2014+ 313011AVG3) supported by the Operational Programme Integrated Infrastructure (OPII) funded by the ERDF.

References
[1] B. Seilheimer *et al*. J. Struct. Biol. 119 (1997), 59–71.
[2] M. Wogulis *et al*. J. Neurosci. 25 (2005), 1071–1080.
[3] A. Jan, O. Gokce, R. Luthi-Carter, H.A. Lashuel. J. Biol. Chem. 283 (2008), 28176–28189.
[4] A. Jan, D. M. Hartley, H.A. Lashuel. Nature Protocols, 5(6) (2010), 1186–1209.

Dual activity of dipeptides on amyloid fibrils of insulin and Aβ$_{40}$

B. Borovská[1*], Z. Bednáriková[1], M. Tvrdoňová[2] and Z. Gažová[1]

[1]*Institute of Experimental Physics Slovak Academy of Sciences, Kosice, Slovakia.*
[2]*Institute of Chemistry, Faculty of Sciences, Pavol Jozef Safarik University in Kosice, Slovakia.*
e-mail: borovska@saske.sk

Self-assembly of proteins and peptides into amyloid aggregates and their accumulation in the human body is associated with more than 50 untreatable amyloid diseases. An increasing number of suffering patients and the socio-economic burden urged the importance of finding the compounds with anti-amyloid activity to prevent the formation of amyloid oligomers/fibrils or destroy mature amyloid fibrils to non-toxic protein species.

Several studies showed that peptide-based compounds mimicking the structure of amyloidogenic regions of proteins hold the anti-amyloid potential. *In silico* and *in vitro* studies showed that aromatic tripeptides have a high binding affinity to amyloid fibrils of Aβ peptide, leading to their intensive destruction [1]. Paul *et al.* [2] determined that not only aromatic amino acids but also a combination of amino acid and cyclic saccharide moiety have the potential to inhibit amyloid aggregation.

We studied the destructive potential of three dipeptides consisting of aromatic amino acids (Trp, Tyr, Phe) alone (MT compounds) or modified by the cyclic saccharide moiety (MT-S compounds) on amyloid fibrils of globular protein insulin and intrinsically disordered peptide (Aβ$_{40}$).

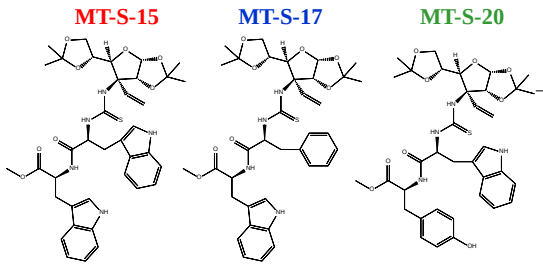

MT-S compounds	MT - compounds
MT-S-15 (OMe-Trp-Trp-ITK)	MT-15 (H-Trp-Trp-OMe.HCl)
MT-S-17 (OMe-Trp-Phe-ITK)	MT-17 (H-Trp-Phe-OMe.HCl)
MT-S-20 (OMe-Tyr-Trp-ITK)	MT-20 (H-Tyr-Trp-OMe.HCl)

Fig. 1. Structure of studied MT and MT-S compounds.

To determine the anti-amyloid potential of the studied compounds, we used the ThT binding assay. Matured amyloid fibrils of insulin and Aβ$_{40}$ were incubated with MT or MT-S compounds in a final concentration ratio of 1:10 (insulin amyloid fibrils) and 1:20 (Aβ$_{40}$ amyloid fibrils) for 24 h at 37 °C. The ThT fluorescence intensity decrease correlates with the degree of amyloid fibrils destruction.

The observed anti-amyloid activity of the MT and MT-S compounds is summarized in Fig. 2. While the destruction activity of both MT and MT-S compounds on amyloid fibrils of globular insulin was negligible (full bars), they showed increased destroying activity towards Aβ$_{40}$ fibrils (shredded bars). This effect was more significant in saccharide-modified dipeptides (MT-S-15, MT-S-17, and MT-S-20), decreasing ThT fluorescence intensity below 50 %. On the other hand, dipeptides containing only combinations of Trp with another amino acid (Phe or Tyr), MT-17 and MT-20, have weaker destroying potential to Aβ$_{40}$ peptide amyloid fibrils. The strongest anti-Aβ$_{40}$ fibrils potential was observed for dipeptide Trp-Trp (MT-15; shredded pink bar), which increased with saccharide moiety (MT-S-15; shredded red bar). The dual activity of the MT/MT-S compounds on insulin and Aβ$_{40}$ peptide amyloid fibrils was also studied by AFM, and the scans are shown in Fig. 3. In the presence of the most active MT-S-15 compound, a decrease in the number of

$A\beta_{40}$ amyloid fibrils was seen. However, neither morphological nor quantitative difference in insulin amyloid fibrils was seen after treatment with MT-S-15 compounds (Fig. 3), which is consistent with the ThT binding assay results.

Based on our results, we conclude that the aromatic dipeptides modified with cyclic saccharide moiety hold effective destruction potential for the $A\beta_{40}$ peptide while staying inactive towards amyloid fibrils of the globular protein insulin. The degree of the anti-amyloid activity depends on the amino acid composition of the studied saccharide-modified dipeptides – the most potent were the Trp-Trp and Tyr-Trp combinations, highlighting the importance of the presence of Trp in short peptide-based inhibitors.

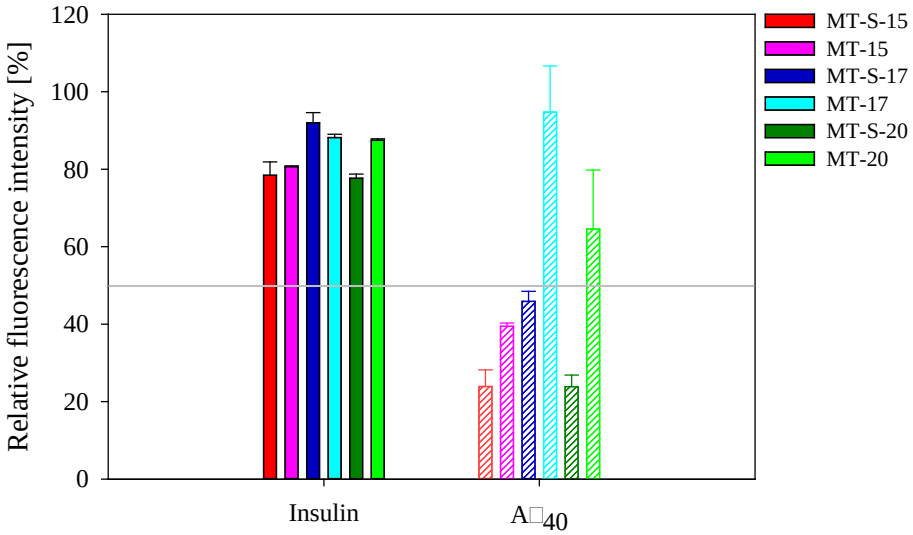

Fig. 2. ThT fluorescence intensity of the amyloid fibrils after 24 h incubation with MT and MT-S compounds. The concentration ratio of amyloid fibrils to MT/MT-S compounds was 1:10 (insulin) and 1:20 ($A\beta_{40}$). Data represent average values of three independent measurements of ThT fluorescence intensities normalized to 100 % (ThT fluorescence intensities of insulin/$A\beta_{40}$ amyloid fibrils alone). The silver line represents 50 % of the ThT fluorescence intensity, which correlates to a decrease in the number of amyloid fibrils by 50 %.

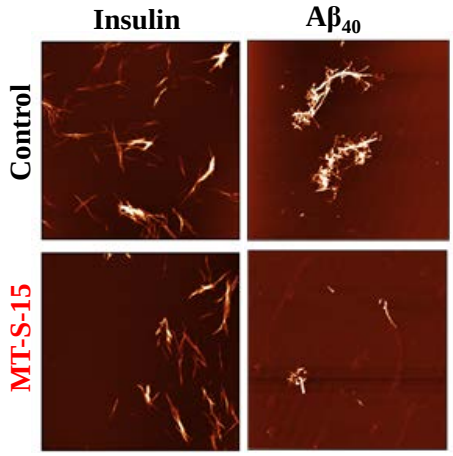

Fig. 3. AFM imaging – the amyloid fibrils of insulin and $A\beta_{40}$ alone (control) and after 24 h incubation with the MT-S-15 compound. The scanned area was 10 x 10 µm with 1024 x 1024 pixels resolution.

Acknowledgment

This work was supported by the Slovak Research and Development Agency under Contract no. APVV-18-0284; Slovak Grant Agency VEGA 02/0176/21, and Grant program for SAS PhD. Students APP0293. This work is also the result of the project implementation DIAGNAD (ITMS2014+ 313011T553) supported by the Operational Programme Integrated Infrastructure (OPII) funded by the ERDF.

References

[1] M. H. Viet, K. Siposova, Z. Bednarikova, A. Antosova, T. T. Nguyen, Z. Gazova, M. S. Li, *The Journal of Physical Chemistry B*, 119 (2015), 5145–5155.

[2] A. Paul, M. Frenkel-Pinter, D. Escobar Alvarez,. *et al. Commun Biol. 3* (2020), 484.

Modulation of insulin amyloid aggregation by amino acid-based ionic liquids: anion role

D. Fedunova[1], M. Guncheva [2], V. Vanik[1], Z. Bednarikova[1], M. Gancar[1] and Z. Gazova[1]

[1] *Institute of Experimental Physics, Slovak Academy of Sciences, Watsonova 47, 040 01 Kosice, Slovakia.*
[2] *Institute of Organic Chemistry with Centre of Phytochemistry, Bulgarian Academy of Sciences, Acad. G. Bonchev 9, Sofia 1113, Bulgaria.*

e-mail: fedunova@saske.sk

Introduction. Amyloid aggregates are insoluble fibrous structures with dominant β-sheet structure content, arising from non-native protein conformers. Nowadays, a substantial part of the research on amyloid aggregation is focused on exploring amyloid aggregates as potential biomaterials due to their specific properties such as high stability, strength, and elasticity or resistance against degradation. The fabrication of amyloid-based biomaterials requires strategies to control amyloid aggregation, namely structural and morphological characteristics of fibrils. One of the important tools for modulating amyloid aggregation is a variation of solvent properties.

Ionic liquids (ILs) represent a new class of solvents consisting of asymmetric organic cation and organic or inorganic anion. By selecting the type of ions, the ILs composition can be designed to match desired physicochemical properties (melting temperature, polarity, hydrophobicity, density, viscosity, solubility) for particular applications [1]. Amino acid-based ILs represent a comprehensive class of solvents with high biocompatibility potential. The presence of functional groups in their side chains incorporates a wide range of properties.

Aims. In this work, we have investigated the effect of the ILs series containing cholinium (Chol) and 1-ethyl-3-methyl imidazolium (EMIM) cations and non-polar (Gly, Val, Ile, Leu, Trp), and charged (Lys, Glu) amino acid anions on the structure and amyloid aggregation of human insulin. We have tested the potential of these compounds to inhibit amyloid aggregation or induce the formation of aggregation-prone protein conformers with the main focus on the formation of morphologically different fibrils for further potential biotechnological applications.

Methods. The effect of ILs on the kinetics of aggregation and morphology of amyloid fibrils of insulin were studied using Thioflavin T (ThT) fluorescence assay, FTIR spectroscopy, and atomic force microscopy (AFM) technique. The amyloid-inducing conditions were set to 50 ^{o}C, 1 200 rpm shaking, 10 mM KCl/HCl buffer, pH 1.6. The molar ratio of protein to IL was 1:500.

Results and Discussion. We have found that in the presence of both Trp-containing ILs, no fibrils were formed within the studied time interval in which mature insulin fibrils are accumulated in the ILs-free buffer solution. These results agree with previous findings that the presence of a planar aromatic ring is one of the crucial features of an effective amyloid aggregation inhibitor due to its ability to interfere with amyloid-aggregation-prone regions of the protein structure.

The kinetics of insulin amyloid aggregation in the presence of remaining ILs follows the nucleation-dependent model characterized by the sigmoidal kinetic curve with kinetic parameters: i) lag-time corresponding to the time necessary for nuclei formation; ii) aggregation half-time describing the time at which the polymerization of oligomers into fibrils reaches the midpoint. In the presence of amino-acid anions with additional charge (Lys, Glu), the lag-times and half-times of aggregation were shortened compared to conditions without ILs regardless of used cations. In the case of non-polar amino acids, the insulin aggregation kinetics were more complex. The lag-time and half-time of insulin amyloid aggregation kinetics increased in the following order: Chol-Ile < EMIM-Gly < ILs-free buffer < EMIM-Val < Chol-Gly < EMIM-Leu < EMIM-Ile. For the simple amino acid glycine with low hydrophobicity, the presence of chaotropic EMIM cation caused the promotion of insulin aggregation (Fig.1). In contrast, ILs with neutral Chol cation prolonged the

lag-time and half-time of insulin aggregation compared with ILs-free buffer solution. However, the effect of ILs with more complex amino acid Ile stand on the opposite sites of the order with chaotropic EMIM cation contributing as the stabilizing factor. These results indicate that the effect of ILs on insulin amyloid aggregation kinetics depends on the particular combination of used anions and cations, emphasizing the importance of specific interactions of ILs with insulin to modulate aggregation.

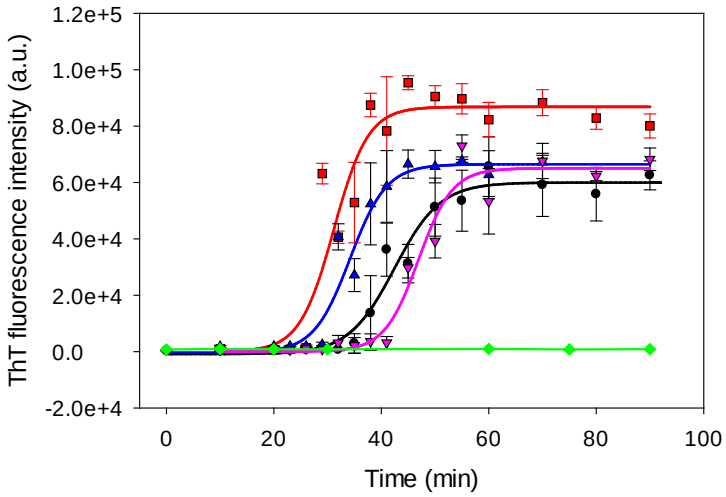

Fig. 1. Kinetics of insulin amyloid aggregation in ILs-free buffer (black circles) and presence of 10 mM ILs: Chol-Ile (red squares); EMIM-Gly (blue up triangles); EMIM-Leu (pink down triangles); EMIM-Trp (green diamonds). Insulin concentration was 20 μM.

The FTIR measurements also support this conclusion. All studied ILs induced conformational changes in the secondary structure of insulin at room temperature prior to aggregation; namely, the decrease of α-helix and the increase of β-sheet contents compared to the insulin structure in ILs-free buffer conditions. However, the extent of these conformational changes is not in direct correlation with the effect of ILs on aggregation lag-time or half-time. These results suggest that the local interactions of both - anionic and cationic - parts of ILs with aggregation-prone regions of insulin play an important role in promoting/inhibiting the amyloid aggregation process. For a better understanding ILs' interaction mechanism with insulin, docking calculations will be used.

AFM images showed that in the absence of ILs, the short insulin fibrils were detected, while EMIM-Val, Chol-Gly and Chol-Leu induced the formation of fibrils with the increasing length. In some cases (EMIM-Leu or Chol-Gly), a lateral association of fibrils was observed.

Our results show that the amyloid aggregation of insulin and morphology of insulin fibrils can be modulated by the presence of studied ILs which can be beneficial in utilizing amyloid aggregates as nanomaterials. Moreover, the work can contribute to a better understanding of the amyloid aggregation mechanism.

Acknowledgment
This work was supported by the Bilateral project "Stability and aggregation of globular proteins in the presence of biocompatible ionic liquids," funded by the Bulgarian Academy of Sciences (IC-SK/03/2021-2022) and Slovak Academy of Sciences (mobility grant BAS-SAS 21-02). The work was also supported by the Slovak Research and Development Agency under Contract no. APVV-18-0284 and Slovak research agency VEGA 2/0164/22 and 2/0176/21. This work is also the result of the project implementation BIOVID-19 (ITMS2014+ 313011AVG3) and NANOVIR (ITMS2014+ 313011AUW7) supported by the Operational Programme Integrated Infrastructure (OPII) funded by the ERDF. The authors thank D. Sedlakova for the ThT - assay measurements.

References
[1] D. Rogers and K. R. Seddon, Science 302 (2003), 792–793, 2003.

Amino acid-coated magnetite nanoparticles as potential inhibitors of α-lactalbumin amyloid aggregation

O. Parmar[1], A. Antosova[1], M. Gancar[1], Z. Bednarikova[1], E. Bystrenova[2], M. Kubovcikova[1], M. Koneracka[1], V. Zavisova[1] and Z. Gazova[1]

[1]*Institute of Experimental Physics, Slovak Academy of Sciences, Košice, Slovakia*
[2]*Institute of Nanostructured Materials, Bologna, Italy*

e-mail: parmar@saske.sk

There is an urge to develop a therapeutic strategy to inhibit the protein amyloid aggregation as it is associated with several amyloid-related diseases such as Alzheimer's disease, Parkinson's disease, diabetes mellitus type II, and many others [1]. Magnetic nanoparticles (MNPs) are already utilized in biomedicine [2] and have been found to affect amyloid aggregation [3]. Their surface properties enable their functionalization by various compounds, creating an opportunity for drug development.

In the present work, we have investigated *in vitro* interference of amino acid-coated MNPs (aa-MNPs) with α-lactalbumin (α-LA) amyloid aggregation, a small globular protein presented in the mammalian milk whey [4]. MNPs were coated by a cyclic non-polar proline (Pro-MNPs), polar cysteine (Cys-MNPs), or positively charged poly-lysine (PLL-MNPs).

The hydrodynamic diameter of aa-MNPs was determined by the dynamic light scattering (DLS), and zeta potential and isoelectric point (pI) were determined by laser Doppler velocimetry. Using the Thioflavin T (ThT) fluorescence assay, it was found that all studied nanoparticles are able to inhibit the α-LA amyloid fibrilization and destroy mature α-LA fibrils (α-LAF). The inhibitory and destroying effect of all studied nanoparticles was concentration-dependent.

The representative morphology of the α-LA mature fibrils obtained after 3h fibrillization of α-LA alone or in presence of aa-MNPs at two concentration ratios α-LA: aa-MNPs = 1:1 and 1:6 are shown in Figure 1. Compared to untreated α-LA aggregation (Figure 1, ratio 1:0), there is a significant reduction in the amount of fibrils at both concentration ratios. Very short fibrils or globular aggregates were observed after incubation with PLL-MNPs at ratios of 1:1 and 1:6 respectively. AFM images confirm that the ThT fluorescence decrease is due to the inhibition of the amyloid aggregation by aa-MNPs. Moreover, the destroying activity of aa-MNPs found from ThT and AFM correlates with the increasing hydrodynamic diameter of MNPs. The most significant destroying potential to α-LAF was observed for 40.8 nm Pro-MNPs, followed by PLL-MNPs with 70.3 nm diameter, and the weakest destroying activity has been shown for the biggest 85 nm Cys-MNPs.

The effect of studied nanoparticles at five concentrations (0.1, 1, 10, 50, 100, and 200 μg/ml of magnetite) on the viability of human kidney (HEK293) cells was investigated. All aa-MNPs exhibit some level of toxicity at 200 μg/ml, with the highest toxicity observed for PLL-MNPs at magnetite concentrations higher than 50 μg/ml after 24 hours of incubation. Although their inhibitory and destroying activities were observed, the possible toxicity of PLL-MNPs excludes them from being applicable as amyloid aggregation inhibitors.

Based on the results, we highlight that the size of the nanoparticle is an essential factor in determining the destroying activity of studied aa-MNPs, and the surface chemistry determines the cytotoxicity of aa-MNPs.

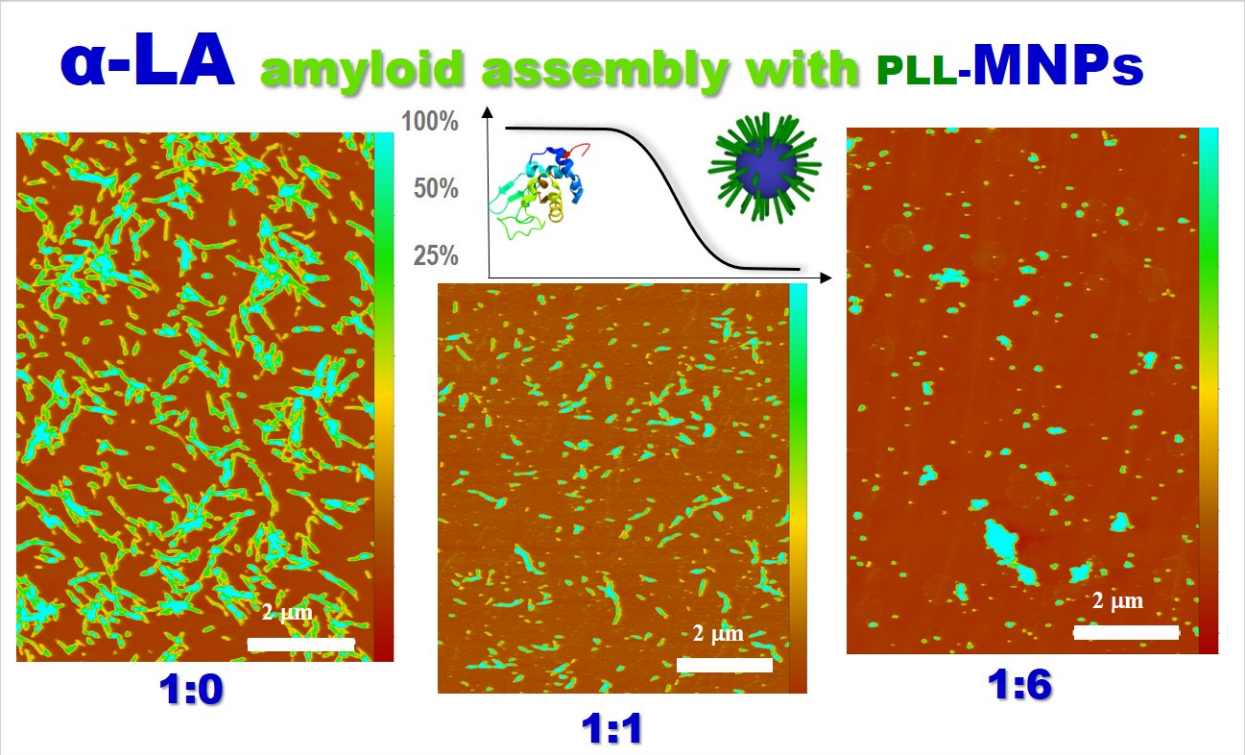

Fig 1. Representative AFM images of the fibrillization of α-LA alone (ratio of fibrils to magnetite contained in MNPs is 1:0) and fibrillization of α-LA in the presence of PLL-MNPs in concentration ratios 1:1 and 1:6.

Acknowledgments
This work was supported by the Slovak Research and Development Agency under the Contract no. APVV-18-0284; Slovak Grant Agency VEGA 02/0176/21, VEGA 02/0164/22, VEGA 02/0033/19; Italian MIUR grant(PRIN 20173L7W8K). This work is also the result of the project implementation DIAGNAD (ITMS2014+ 313011T553) and BIOVID-19 (ITMS2014+ 313011AVG3) supported by the Operational Programme Integrated Infrastructure (OPII) funded by the ERDF. Microscopy was carried out at the SPM@ISMN facility.

References
[1] T. P. J. Knowles, M. Vendruscolo and Ch. M. Dobson, Nature Reviews Molecular Cell Biology 15 (2014), 384–396.
[2] E. A. Permyakov, Biomolecules 10 (2020), 1–50.
[3] A. Antosova, Z. Bednarikova, M. Koneracka, I. Antal, V. Zavisova, M. Kubovcikova, J. W. Wub, S. S.-S. Wang, Z. Gazova, Journal of Magnetism and Magnetic Materials 471 (2019), 169–176.
[4] M. C. Daniel and D. Astruc, Chemical Reviews 104 (2004), 293–346.

AUTHOR INDEX

LIST OF PARTICIPANTS

1	Antošová Andrea	Department of Biophysics, Institute of Experimental Physics, Slovak Academy of Sciences, Watsonova 47, 040 01 Košice, Slovakia
2	Asi Shirazi Ali	Department of Physical Chemistry of Drugs, Faculty of Pharmacy, Comenius University in Bratislava, Odbojárov 10, 832 32 Bratislava, Slovakia
3	Baglaeva Iuliia	Department of Cellular Cardiology, Institute of Experimental Endocrinology, Biomedical Research Center, Slovak Academy of Sciences, Dúbravská cesta 9, 845 05 Bratislava, Slovakia
4	Bánó Gregor	Department of Biophysics, Faculty of Science, P.J. Šafárik University in Košice, Jesenná 5, 041 54 Košice, Slovakia.
5	Bednáriková Zuzana	Department of Biophysics, Institute of Experimental Physics, Slovak Academy of Sciences, Watsonova 47, 040 01 Košice, Slovakia
6	Borovská Barbora	Department of Biophysics, Institute of Experimental Physics, Slovak Academy of Sciences, Watsonova 47, 040 01 Košice, Slovakia
7	Cagalinec Michal	Department of Cellular Biophysics, Institute of Experimental Endocrinology, Biomedical Research Center, Slovak Academy of Sciences, Dúbravská cesta 9, 845 05 Bratislava, Slovakia
8	Čechová Katarína	Department of Nuclear Physics and Biophysics, Faculty of Mathematics, Physics and informatics, Comenius University in Bratislava, Mlynská Dolina, 842 48 Bratislava, Slovakia.
9	Cehlár Ondrej	Institute of Neuroimmunology of the Slovak Academy of Sciences, Dubravska cesta 9, 84510 Bratislava, Slovakia
10	Čelková Adriána	Department of Physical Chemistry of Drugs, Faculty of Pharmacy, Comenius University in Bratislava, Odbojárov 10, 832 32 Bratislava, Slovakia
11	Džupponová Veronika	Department of Biophysics, Faculty of Science, P.J. Šafárik University, Jesenná 5, 040 01 Košice, Slovakia
12	Dzurillová Veronika	Department of Biophysics, Faculty of Science, P.J. Šafárik University, Jesenná 5, 040 01 Košice, Slovakia
13	Fedunová Diana	Department of Biophysics, Institute of Experimental Physics, Slovak Academy of Sciences, Watsonova 47, 040 01 Košice, Slovakia
14	Felčíková Kristína	Department of Biophysics, Faculty of Science, P.J. Šafárik University, Jesenná 5, 040 01 Košice, Slovakia
15	Fuenzalida Sandoval Francisca Belén	Department of Biophysics, Faculty of Science, P.J. Šafárik University, Jesenná 5, 040 54 Košice, Slovakia
16	Gaburjáková Marta	Institute of Molecular Physiology and Genetics, Centre of Biosciences, Slovak Academy of Sciences, Dubravska cesta 9, 840 05 Bratislava, Slovakia

17	Gaburjáková Jana	Institute of Molecular Physiology and Genetics, Centre of Biosciences, Slovak Academy of Sciences, Dubravska cesta 9, 840 05 Bratislava, Slovakia
18	Gančár Miroslav	Department of Biophysics, Institute of Experimental Physics, Slovak Academy of Sciences, Watsonova 47, 040 01 Košice, Slovakia
19	Garaiová Zuzana	Department of Nuclear Physics and Biophysics, Faculty of Mathematics, Physics and informatics, Comenius University in Bratislava, Mlynská Dolina, 842 48 Bratislava, Slovakia.
20	Gažová Zuzana	Department of Biophysics, Institute of Experimental Physics Slovak Academy of Sciences, Watsonova 47, 040 01, Kosice, Slovakia
21	Golda Jan	Specion Ltd., Budějovická 55, 140 00 Praha 4, Czech Republic
22	Hoťka Matej	Center of Physiology and Pharmacology, Department of Neurophysiology and Neuropharmacology, Medical University of Vienna, Waehringerstrasse 13a, 1090, Vienna, Austria
23	Hovan Andrej	Department of Biophysics, Faculty of Science, P.J. Šafárik University, Jesenná 5, 040 54 Košice, Slovakia
24	Iaparov Bogdan	Department of Cellular Cardiology, Institute of Experimental Endocrinology, Biomedical Research Center, Slovak Academy of Sciences, Dúbravská cesta 9, 845 05 Bratislava, Slovakia
25	Jacko Juraj	Department of Nuclear Physics and Biophysics, Faculty of Mathematics, Physics and informatics, Comenius University in Bratislava, Mlynská Dolina, 842 48 Bratislava, Slovakia.
26	Jancura Daniel	Department of Biophysics, Faculty of Science, P.J. Šafárik University, Jesenná 5, 040 54 Košice, Slovakia
27	Jurašeková Zuzana	Department of Biophysics, Faculty of Science, P. J. Šafárik University, Jesenná 5, 040 01 Košice, Slovakia
28	Kania Pawel	NanoTemper Technologies GmbH, Flößergasse 4, 81369 München, Germany
29	Karhánek Miloslav	Specialized Bioinformatics Laboratory, Biomedical Research Center, Slovak Academy of Sciences, Dúbravská cesta 9, 845 05 Bratislava, Slovakia
30	Keshavarzi Atoosa	Department of Physical Chemistry of Drugs, Faculty of Pharmacy, Comenius University in Bratislava, Odbojárov 10, 832 32 Bratislava, Slovakia
31	Klacsová Mária	Department of Physical Chemistry of Drugs, Faculty of Pharmacy, Comenius University in Bratislava, Odbojárov 10, 832 32 Bratislava, Slovakia
32	Kučerka Norbert	Department of Physical Chemistry of Drugs, Faculty of Pharmacy, Comenius University in Bratislava, Odbojárov 10, 832 32 Bratislava, Slovakia

33	Lacinová Ľubica	Institute of Molecular Physiology and Genetics, Centre of Biosciences, Slovak Academy of Sciences, Dubravska cesta 9, 840 05 Bratislava, Slovakia
34	Májeková Magdaléna	Centre of Experimental Medicine SAS, Institute of Experimental Pharmacology and Toxicology, Dubravska cesta 9, 841 04, Bratislava, Slovakia
35	Marček Chorvátová Alžbeta	Department of Biophotonics, International Laser Center, Slovak Centre of Scientific and Technical Information, Ilkovičova 3, 814 04 Bratislava, Slovakia
36	Miskovsky Pavol	SAFTRA Photonics Ltd., Moldavská 51, 04011 Košice
37	Mydla Patrick	Department of Nuclear Physics and Biophysics, Faculty of Mathematics, Physics and informatics, Comenius University in Bratislava, Mlynská Dolina, 842 48 Bratislava, Slovakia.
38	Parmar Oľga	Department of Biophysics, Institute of Experimental Physics, Slovak Academy of Sciences, Watsonova 47, 040 01 Košice, Slovakia
39	Pevná Viktória	Department of Biophysics, Faculty of Science, P.J. Šafárik University, Jesenná 5, 040 01 Košice, Slovakia
40	Poliaček Ivan	Department of Medical Biophysics, Jessenius Faculty of Medicine in Martin, Comenius University in Bratislava, Mala Hora, 4 036 01, Bratislava, Slovakia
41	Sedlák Erik	Center for Interdisciplinary Biosciences, Technology and Innovation Park, P.J. Šafárik University in Košice, Jesenná 5, 041 54 Košice, Slovakia
42	Šimera Michal	Department of Medical Biophysics, Jessenius Faculty of Medicine in Martin, Comenius University in Bratislava, Mala Hora, 4 036 01, Bratislava, Slovakia
43	Škrabana Rostislav	Institute of Neuroimmunology of the Slovak Academy of Sciences, Dubravska cesta 9, 84510 Bratislava, Slovakia
44	Slabý Cyril	Department of Biophysics, Faculty of Science, P. J. Šafárik University, Jesenná 5, 041 54 Košice, Slovak Republic
45	Štroffeková Katarína	Department of Biophysics, Institute of Experimental Physics Slovak Academy of Sciences, Watsonova 47, 040 01, Kosice, Slovakia
46	Šubjaková Veronika	Department of Nuclear Physics and Biophysics, Faculty of Mathematics, Physics and informatics, Comenius University in Bratislava, Mlynská Dolina, 842 48 Bratislava, Slovakia.
47	Sztachová Tereza	Department of Biophysics, Faculty of Science, P.J.Šafárik University, Jesenná 5, 041 54 Kosice, Slovakia
48	Talafová Veronika	Department of Biophysics, Faculty of Science, P.J. Šafárik University, Jesenná 5, 040 01 Košice, Slovakia

49	Tatarko Marek	Department of Nuclear Physics and Biophysics, Faculty of Mathematics, Physics and informatics, Comenius University in Bratislava, Mlynská Dolina, 842 48 Bratislava, Slovakia.
50	Tomková Adriána	Department of Biophysics, Institute of Experimental Physics Slovak Academy of Sciences, Watsonova 47, 040 01, Kosice, Slovakia
51	Tomková Mária	Center for Interdisciplinary Biosciences, Technology and Innovation Park, P.J. Šafárik University in Košice, Jesenná 5, 041 54 Košice, Slovakia
52	Uličný Jozef	Faculty of Science, Department of Biophysics, Institute of Physics, P. J. Šafárik University, Jesenná 5, 04154 Košice, Slovakia
53	Velísková Martina	Department of Nuclear Physics and Biophysics, Faculty of Mathematics, Physics and informatics, Comenius University in Bratislava, Mlynská Dolina, 842 48, Bratislava, Slovakia
54	Waczulíková Iveta	Department of Nuclear Physics and Biophysics, Faculty of Mathematics, Physics and informatics, Comenius University in Bratislava, Mlynská Dolina, 842 48, Bratislava, Slovakia
55	Zahradník Ivan	Department of Cellular Cardiology, Institute of Experimental Endocrinology, Biomedical Research Center, Slovak Academy of Sciences, Dúbravská cesta 9, 845 05 Bratislava, Slovakia
56	Zahradnikova ml. Alexandra	Department of Cellular Cardiology, Institute of Experimental Endocrinology, Biomedical Research Center, Slovak Academy of Sciences, Dúbravská cesta 9, 845 05 Bratislava, Slovakia
57	Zahradníková Alexandra	Department of Cellular Cardiology, Institute of Experimental Endocrinology, Biomedical Research Center, Slovak Academy of Sciences, Dúbravská cesta 9, 845 05 Bratislava, Slovakia
58	Žoldák Gabriel	Center for Interdisciplinary Biosciences, Technology and Innovation Park, P.J. Šafárik University in Košice, Jesenná 5, 041 54 Košice, Slovakia

Book of Contributions, 10th Slovak Biophysical Symposium, May 3 – 5, 2022, Smolenice, Slovakia

Editors: M. Cagalinec, A. Zahradniková, B. Iaparov
Reviewers: A. Zahradniková, M. Gaburjáková, D. Jancura, Z. Gažová, J. Jakuš
Number of pages: 126

ISBN: 978-80-973719-4-4
EAN: 9788097371944